

001
002
003
004
005
006
007
008
009
010
011
012
013
014
015
016
017
018
019
020
021
022
023
024
025
026
027
028
029
030
031
032
033
034
035
036
037
038
039
040
041
042
043
044
045
046

Microbial symbionts buffer hosts from the demographic costs of environmental stochasticity

Joshua C. Fowler^{1,2*}, Shaun Ziegler³, Kenneth D. Whitney³,
Jennifer A. Rudgers³, Tom E.X. Miller¹

¹*Department of BioSciences, Rice University, Houston, 77005, TX, USA.

²Department of Biology, University of Miami, Miami, 33146, FL, USA.

³Department of Biology, University of New Mexico, Albuquerque, 87131, NM, USA.

*Corresponding author(s). E-mail(s): jcf221@miami.edu;

Contributing authors: shaun.ziegler@gmail.com; whitneyk@unm.edu;

jrudgers@unm.edu; tom.miller@rice.edu;

Phone: 719-359-2960

Author Contributions

J.C.F. contributed to data collection, data analysis, and led manuscript drafting. S.Z. contributed to data collection and manuscript revisions. K.D.W. contributed to research conception, data collection, and manuscript revisions. J.A.R. established transplant plots, contributed to research conception, data collection, and manuscript revisions. T.E.X.M. contributed to research conception, data collection, data analysis, and manuscript revisions.

Data and Code Accessibility

Data will be made accessible as an Environmental Data Initiative package online
DOI: [updated here when available](#). Code for all analysis is available through
<https://github.com/joshuacfowler/Grass-Endophyte-Stochastic-Demography>

Article Type: Letter

Running Title: Symbiont-mediated demographic buffering

Keywords: stochastic demography, plant-microbe interactions, environmental variability, symbiosis, mutualism, long-term data, life history, Epichloë, Poaceae

This file contains: Abstract (150 words), Main Text (5000 words), Figures (1-5); Supporting Information - Supplemental Methods, Supplemental Figures S1-S89, Supplemental Tables S1-S3, References (84)

047
048
049
050
051
052
053
054
055
056
057
058
059
060
061
062
063
064
065
066
067
068
069
070
071
072
073
074
075
076
077
078
079
080
081
082
083
084
085
086
087
088
089
090
091
092

Abstract

Species' persistence in increasingly variable climates will depend on resilience against the fitness costs of environmental stochasticity. Most organisms host microbiota that shield against stressors. Here, we test the hypothesis that, by limiting exposure to temporally variable stressors, microbial symbionts reduce hosts' demographic variance. We parameterized stochastic population models using data from a 14-year symbiont-removal experiment including seven grass species that host *Epichloë* fungal endophytes. Results provide novel evidence that symbiotic benefits arise not only through improved mean fitness, but also through damped inter-annual variance. Hosts with "fast" life history traits benefited most from symbiont-mediated demographic buffering. Under current climate conditions, contributions of demographic buffering were modest compared to benefits to mean fitness. However, simulations of increased stochasticity amplified benefits of demographic buffering and made it the more important pathway of host-symbiont mutualism. Microbial-mediated variance buffering is likely an important, yet cryptic, mechanism of resilience in an increasingly variable world.

	093
	094
Introduction	095
	096
Global climate change involves heterogenous changes in environmental variability, including increases in an increasing frequency of extreme weather events and in frequency of “whiplash events” that alternate between climate extremes (1; 3; 2). ¹	097
(1; 3; 4; 2). Yet, the ecological consequences of changing variability are less well understood than those of changing climate means, such as long-term warming or drying.	098
Incorporating environmental realistic variability into forecasts of population dynamics can improve predictions of the future (5)predictive ability (5).	099
Classic theory predicts that long-term population growth rates (equivalently, population mean fitness) will decline under increased environmental stochasticity because the costs of bad years outweigh the benefits of good years – a consequence of non-linear averaging (6; 7)(6; 7). For example, in unstructured populations, the long-term stochastic growth rate in a fluctuating environment (λ_S) will always be lower than the arithmetic mean growth rate ($\bar{\lambda}$) of annual growth rates ($\bar{\lambda}_t$) by an amount proportional to the environmental variance (σ^2):	100
$\log(\lambda_S) \approx \log(\bar{\lambda}_t) - \frac{\sigma^2}{2\bar{\lambda}_t}$	(1)
Populations structured by size or stage similarly experience similar costs of temporal variability (8; 9)(8; 9). There are accordingly two pathways to increase population viability in a variable environmentvariable environments: increase the arithmetic mean growth rate and/or dampen temporal fluctuation in growth rates, also called “demographic buffering”.	101
Both inherent characteristics of species and properties of the environments they experience their environments can buffer demographic fluctuations. Inherent characteristics include life history traits (10)(10), trade-offs among vital rates (12)(12), and transient shifts in population structure (13)(13). For example, theory predicts that long-lived species, those on the slow end of the slow-fast life history continuum, will to be less sensitive to environmental variability than short-lived species (14)(14), a pattern which has with empirical support across plants (15; 16) and animals (17; 11)(15; 16) and animals (17; 11). Demographic variance is also determined by external abiotic factors, such as the magnitude of environmental variability (18) or the degree of environmental autocorrelation (19; 20)(18) or environmental autocorrelation (19; 20). The complex interplay of these factors determines the risks of extinction faced by populations (21)–populations’ risk of extinction (21) and underlies management strategies promoting ecosystem resilience (22)(22). Yet, little is known about how inter-specific interactions influence demographic variability or contribute to demographic buffering (23)(23).	102
Most multicellular organisms host symbiotic microbes that affect growth and performance (24; 25), and many of these (24; 25), many of which are vertically transmitted from maternal hosts to offspring (26)(26). Vertical transmission links the fitness of	103
	104
	105
	106
	107
	108
	109
	110
	111
	112
	113
	114
	115
	116
	117
	118
	119
	120
	121
	122
	123
	124
	125
	126
	127
	128
	129
	130
	131
	132
	133
	134
	135
	136
	137
	138

¹Add citation — <https://www.nature.com/articles/s41558-018-0140-y>

hosts and symbionts in a feedback loop that selects for mutual benefits (27). Many vertically transmitted microbes are mutualistic and (27). These mutualistic microbes can protect hosts from stressful environmental conditions including drought, extreme temperatures, or natural enemies (28; 29). Some of the best (28; 29). Some well studied examples include bacterial symbionts of insects that provide their hosts with thermal tolerance through the production of heat-shock proteins (30)(30), and fungal symbionts of plants that produce anti-herbivore and drought-protective compounds (31; 32; 33) (31; 32; 33). However, these diverse protective symbioses are context-dependent: the magnitude of benefits depends on environmental conditions (34; 35)–(34; 35) and thus will vary temporally in a stochastic environment (36)stochastic environments (36). We hypothesized that context-dependent benefits from symbionts may buffer hosts-host populations against variability through strong benefits during harsh periods and neutral or even costly outcomes during benign periods, reducing the impacts of host exposure to extremes and dampening inter-annual variance relative to non-symbiotic hosts (Fig. ??¹A). Variance buffering is a previously unexplored mechanism by which symbionts may benefit their hosts instead of or in addition to elevating average fitness (Fig. ??¹C), the focus of most previous research.

To test the hypothesis that context-dependent benefits of symbiosis buffer hosts from the fitness effects of temporal environmental stochasticity dampen interannual variance in host fitness, we used a combination of long-term field experiments and stochastic demographic modeling. We used cool-season grasses and *Epichloë* fungal endophytes as a tractable experimental model in which non-symbiotic plants can be derived from naturally symbiotic plants through heat treatment, providing a contrast of symbiont effects that controls for the confounding influence of host genetic background. *Epichloë* endophytes are specialized symbionts growing intercellularly in the aboveground tissue of ~ 30% of *C₃* grass species (37)(37). These fungi are primarily transmitted vertically from maternal plants through seeds (38)(38). They produce a variety of alkaloids that can protect host plants from natural enemies (39)–(39) and drought stress (40)(40).

Over 14 years (2007–2021), we collected longitudinal demographic data on the survival, growth, reproduction, and recruitment of all plants within replicated endophyte-symbiotic and endophyte-free populations at our field site in southern Indiana, USA. Through taxonomic replication (seven host-symbiont species pairs) we aimed to understand whether host life history traits could explain inter-specific variation in the magnitude of demographic buffering through symbiosis. We used this long-term data to parameterize Bayesian stochastic population projection models in a hierarchical Bayesian framework. Specifically, we (1) quantified the effect of symbiosis on the mean and variance of host vital rates (survival, growth and reproduction) and fitness, (2) evaluated the relationship between host life history traits and the magnitude of symbiont-mediated variance buffering, (3) determined the relative contributions of symbiont-mediated mean and variance effects to host fitness, and (4) projected how increased environmental stochasticity (expected under future climates) changes the importance of variance buffering as a pathway of host-symbiont mutualism.

¹Reference new figure
¹Reference new figure

Materials and Methods	185
Study site and species	186
This study was conducted at Indiana University's Lilly-Dickey Woods Research and Teaching Preserve (39.238533, -86.218150) in Brown County, Indiana, USA. This site is part of the Eastern broadleaf forests of southern Indiana, where the ranges of many understory cool-season grass species overlap. The experiment We focused on seven of these grasses (<i>Agrostis perennans</i> , <i>Elymus villosus</i> , <i>Elymus virginicus</i> , <i>Festuca subverticillata</i> , <i>Lolium arundinaceum</i> , <i>Poa alsodes</i> , and <i>Poa sylvestris</i>), each of which hosts a unique species of <i>Epichloë</i> endophyte (Table S1). All are native to eastern North America except the Eurasian species <i>L. arundinaceum</i> .	187
Endophyte removal, plant propagation, and field set-up	188
Seeds from Seeds from local, naturally symbiotic populations of the seven focal host species were collected during summer-fall 2006 from Lilly-Dickey Woods and the nearby Bayles Road Teaching and Research Preserve (39.220167, -86.542683). To generate symbiotic (S+) and symbiont-free (S-) plants from the same genetic lineages, seeds from each species 2006. Seeds were disinfected with a heat treatment described in Table S1 or left untreated. The heat treatment created to generate symbiont-free plants by warming seeds to temperatures at which the fungus becomes inviable but the host seeds can still germinate. Both heat-treated and untreated seeds were surface sterilized with bleach to remove epiphyllous microbes, cold stratified for up to 4 weeks, then germinated in a growth chamber before transfer to the greenhouse at Indiana University where they grew for ~8 weeks. We confirmed endophyte status by staining thin sections of inner leaf sheath with aniline blue and examining tissue for fungal hyphae at 200X magnification (41). We established experimental populations with vegetatively propagated clones of similar sizes (ranging from one to six tillers). By starting the experiment with plants of similar sizes and the same number of unique genotypes, we aimed to limit any potential effects of heat treatments on initial plant growth (42). ¹	189
During the (S-) and symbiotic (S+) plants from the same genetic lineages. In fall of 2007 and spring of 2008, we established 10 3x3 m plots for <i>A. perennans</i>, <i>E. villosus</i>, <i>E. virginicus</i>, <i>F. subverticillata</i>, and <i>L. arundinaceum</i> and 18 plots for <i>P. alsodes</i> and <i>P. sylvestris</i>. Half of the plots were Each plot was randomly assigned to be planted with either 20 evenly spaced symbiotic (S+) or symbiont-free (S-) plants, and initiated with 20 evenly spaced individuals labeled with aluminum tags. In spring 2008, we placed plastic deer net fencing around each plot to limit deer herbivory and disturbance; damaged fences were regularly replaced. Full details of endophyte removal, plant propagation and field set-up are provided in Supporting Information - Supplemental Methods and Table S1.	190
Long-term demographic data collection	191
Each summer (2008–2021) we censused all individuals in each plot for survival, growth and reproduction, and added new recruits to the census. Plots contained 13.3	192
¹ I don't remember if this was always here but it actually makes no sense to me, and I think (?) a reviewer said something similar. I think nothing is lost if we cut this sentence.	193
	194
	195
	196
	197
	198
	199
	200
	201
	202
	203
	204
	205
	206
	207
	208
	209
	210
	211
	212
	213
	214
	215
	216
	217
	218
	219
	220
	221
	222
	223
	224
	225
	226
	227
	228
	229
	230

¹~~I don't remember if this was always here but it actually makes no sense to me, and I think (?) a reviewer said something similar. I think nothing is lost if we cut this sentence.~~

231 individuals/ m^2 on average over the course of the experiment during the study. Each cen-
232 sus year was a sample of inter-annual climatic variation ($n = 14$ years, comprising 13
233 demographic transition years). We censused each species during its peak fruiting stage
234 (May: *Poa alsodes*, *Poa sylvestris*; June: *Festuca subverticillata*; July: *Elymus villosus*,
235 *Elymus virginicus*, *Lolium arundinaceum*; September: *Agrostis perennans*), such
236 that the censuses were pre-breeding and new recruits came from the previous years'
237 seed production ¹-(Fig. S1 shows a generalized life cycle diagram). Leaf litter was
238 cleared out of each plot prior to before the census, to aid in locating plants. For each
239 plant remaining from the previous year tagged plant, we determined survival, measured
240 its size as a count of tillers, and collected reproductive data as counts of reproductive
241 tillers and seed-bearing spikelets on all reproductive tillers to a maximum of three up to
242 three reproductive tillers. We also tagged all unmarked individuals that were recruits
243 from the previous years' seed production and collected the same demographic data.
244 New recruits typically had one tiller and were non-reproductive. In 2008 through 2010,
245 we took additional counts of seeds per inflorescence for all reproducing individuals in
246 the plots to relate inflorescence and spikelet counts to seed production. In 2018, we
247 stopped collecting data for the exotic *L. arundinaceum*, which had very high survival
248 and low recruitment, and consequently very low variation low variation in population
249 size across years. In total across 14 years, the dataset included demographic information
250 for 16,789 individual host-plants and 31,216 transition-year observations.

251 We expected plots to maintain their endophyte status (S+ or S-) because these fungal
252 symbionts are almost exclusively vertically transmitted, and plots were spaced a minimum of
253 5 m apart, limiting seed dispersal or horizontal transmission of the symbiont between plots.
254 We regularly confirmed endophyte treatment throughout the lifetime of the experiment by
255 opportunistically taking subsets of seeds from reproductive individuals and scoring them
256 for their endophyte status with microscopy as above. Overall, these scores reflected 98%
257 faithfulness of recruits to their expected endophyte status across species and plots (Fig. S23;
258 Supplement data). Additionally, we have rarely observed fungal stromata, the fruiting bodies
259 by which *Epichloë* are potentially transmitted horizontally, provided the fly vector is also
260 present (43). For *A. perennans*, *F. subverticillata*, *L. arundinaceum*, and *P. alsodes*, we never
261 observed stromata. We observed stromata only infrequently for *E. villosus*, and even more
262 rarely for *E. virginicus* and *P. sylvestris* (Table S2). For these species, stromata have only
263 been observed irregularly across years on 35, 4, and 6 plants respectively, making up < 0.3%
264 of all censused plants.

265 **Vital rate modeling**

266 Equipped with these demographic data, we fit statistical models for adult survival, seedling
267 survival, adult growth, seedling growth, reproductive status (flowering or vegetative), fertility
268 of flowering plants (number of inflorescences), production of seed-bearing spikelets (number
269 per inflorescence), the average number of seeds per spikelet, and the recruitment of seedlings
270 from the preceding year's seed production. We fit these vital rates as generalized linear
271 mixed models in a hierarchical Bayesian framework using RStan (44) (44) which allowed us
272 to isolate endophyte effects on vital rate means and variances, borrow strength across species
273 for some variance components, and propagate uncertainty from the individual-level vital
274 rates to population projection models (45). Each (45). All size-structured vital rate model
275 included year effects specific to each species and endophyte status as well as random plot
276 variance shared across species. All models included the same linear predictor, including two
277 key parameters for each species: one which described the effect of endophyte symbiosis on
278 the mean of that vital rate, and another which described the inter-annual variance in the
279 vital rate for symbiotic and symbiont-free plants. The, estimated using random year effects
280 specific to each species and endophyte status. This species- and endophyte status- specific

281 ¹ Could reference life cycle figure here.

random year effects effect allowed us to quantify the effect effects of endophytes on inter-
annual variance for each vital rate. Other parameters accounted for size structure in the
data (defined as the number of tillers) as well as the difference differences between originally
transplanted plants (raised-started in a greenhouse) and those which recruited naturally into
the plots. Preliminary analyses indicated similar model fits between models including linear
and quadratic terms, and so we proceeded with only linear effects. Full details of the vital
rate modeling are included in the Each vital rate model included a random effect for plot
variance shared across species. Full statistical analyses are detailed in *Supporting Information*
- *Supplemental Methods*. All parameters were given vague priors (46). We ran each vital rate
model for 2500 warm-up and 2500 MCMC sampling iterations with three chains. We assessed
model convergence with trace plots of posterior chains and checked for \hat{R} values less than 1.01,
indicating low within-and-between chain variation (47; 48). For those models that showed
poor convergence, we extended the MCMC sampling to include 5000 warm-up and 5000
sampling iterations, which was only necessary for seedling growth. We graphically checked
vital rate model fit with posterior predictive checks comparing simulated and observed data
(Fig. S29-S30).

Stochastic population model

We parameterized-a-built stochastic matrix projection model for each host species. We parameterized the models using the fitted statistical vital rate models -in a manner similar to continuous IPM models (?), while accounting for the discrete data representing our focal species' growth (?). Each matrix projection model included two state variables: r_t (the number of newly recruited individuals in year t which we assume to be non-reproductive), and n_t (a vector including all non-seedling individuals of discrete sizes $x \in \{1, 2, \dots, U\}$ ranging from one to the maximum number of tillers U). We use these two state variables to avoid having to-assume-assuming demographic equivalence between seedling and non-seedling one-tiller plants. We used the same model structure, corresponding to a pre-breeding census, for each species and endophyte status (not shown in model notation for readability). See Fig. S21 for a-generalized-life-cycle graph; Fig. S1).

The number of recruits in year $t+1$ is given by:

$$r_{t+1} = \sum_{x=1}^U P(x; \tau_P) F(x; \tau_F) K(x; \tau_K) D R(\tau_R) n_t^x \quad (2)$$

The total number of seeds produced by a maternal plant of size x is the product of the size-specific probability of flowering P , the number of inflorescences conditional on flowering F , the number of spikelets per inflorescence K , and the number of seeds per spikelet D . Multiplying by the probability of transitioning from seed to seedling R gives a per-capita rate of seedling production-seedling production rate, which is multiplied by the number of plants of size x (n_t^x , the x^{th} element of n_t) and summed over all sizes. Each function also depends on the species- and endophyte-specific year random effects for that vital rate (τ , a vector of year-specific values derived from the statistical models).

The number of y -sized plants in year $t+1$ is given by:

$$n_{t+1}^y = Z(y; \tau_Z) B(\tau_B) r_t + \sum_{x=1}^U S(x; \tau_S) G(x, y; \tau_G) n_t^x \quad (3)$$

where n_{t+1}^y is the y^{th} element of vector n_{t+1} . The first term on the right hand side of Eqn. 3 represents growth (Z) and survival (B) of seedling recruits. The second term includes the survival of previously x -sized plants and the growth of survivors from size x to y , summed over all x . To avoid predictions of unrealistic growth outside of the observed size distribution, we set a ceiling on capped the growth function for plants at the 97.5th percentile of observed sizes for each host species (49)-(49). We analyzed projection models constructed from parameters representing the dynamics of naturally recruited plants.

Each of the vital-rate functions-vital rate function in Eqns. 2 and 3 have-has separate intercepts and year random effects for symbiotic and symbiont-free populations, allowing

323 us to calculate the effect of endophyte symbiosis on the mean, variance, and coefficient of
324 variation (CV) of λ_t , the dominant eigenvalue of the year- and endophyte-specific projection
325 matrix. This model treats climate drivers implicitly through year-specific random effects. We
326 also developed a climate-explicit version with the addition of additional parameters defining
327 the relationship between either annual or growing season drought index and each vital rate
328 . A full description of climate-explicit methods can be found in the *Supporting Information*
Supplemental Methods.

328 (Supporting Information - Supplemental Methods).

329 To calculate stochastic population growth rates (λ_S) for each host species and endo-
330 phyte status we simulated population dynamics for 1000 years by randomly sampling from
331 the 13 annual transition matrices, discarding the first 100 years to minimize the influence
332 of initial conditions. Sampling observed transition matrices (rather than independently sam-
333 pling regression coefficients) produces models that realistically capture inter-annual variation
334 by preserving correlations between vital rates (50) vital rate correlations (50). We tallied the
335 total population size at each time step as $N_t = r_t + \sum_{x=1}^U n_t^x$ and calculated the stochastic
336 growth rate as $\log(\lambda_S) = E[\log(\frac{N_t}{N_{t+1}})]$ (51; 52) $\log(\lambda_S) = E[\log(\frac{N_t}{N_{t+1}})]$ (51; 52). We calcu-
337 lated the total effect total effects of endophyte symbiosis as the difference in $\lambda_S - \lambda_S$ between
338 S+ and S- populations. We propagated uncertainty from the vital rate models rates to the cal-
339 culation of $\lambda_S - \lambda_S$ using 500 draws from the posterior distribution of model parametersmodel
340 posteriors.

340

340 Life History Analysis

341 We collected metrics describing each host species' life history to test the relationship between
342 pace of life and variance buffering (Table S2). Using the Rage package (53), we calculated R_0 ,
343 longevity, generation time, Keyfitz entropy, and Demetrius entropy from the mean transition
344 matrix for symbiont-free populations.¹ We recorded seed size as the average lemma length
345 from the Flora of North America (54). We also (54). We calculated the 99th percentile
346 of maximum observed age for symbiont-free plants from the census data for each species.
347 Using the Rage package (53), we calculated generation time, longevity, net reproductive
348 rate R_0 , Keyfitz entropy (describing survivorship across lifespan), and Demetrius entropy
349 (describing reproduction across lifespan) from the mean transition matrix for symbiont-free
350 populations. Next, we fit Bayesian phylogenetic mixed-effects models using the brms package
351 (55)-(55) to test the relationship between each life history trait and the effect of symbio-
352 sis on the CV of λ_t (a measure of variance buffering) while controlling for phylogenetic
353 non-independence between host and symbiont species. We pruned species-level phylogenies of
354 plants (56) and *Epichloë* fungi (57)-(57) to include the focal species *A. perennans*
355 was not included in the tree, and so we used the congener *A. hyemalis*. We (or a congener for
356 one host), and defined separate phylogenetic covariance matrices for each pruned treefrom
357 these pruned trees for host and symbiont species. We propagated uncertainty in the estimated
358 variance buffering effect V with a measurement error model.

359 Here, V_{EST} is the variance buffering effect for host species h , estimated from the posterior
360 mean (V_{MEAN}) and standard deviation (V_{SD}), propagating uncertainty associated with
361 the effect of symbiosis. The model includes an intercept (α) and a slope (β) defining the
362 relationship between the variance buffering effect and the life history trait. The residual
363 standard deviation is given by (σ). We used weakly informative priors to aid model
364 convergence. Each prior was centered at zero, except for the residual standard deviation,
365 which we centered at the standard deviation of the estimated variance buffering effect, .04.
366 The phylogenetic random effect (π), which is modeled as a multivariate normal distribution,
367 has a between-species standard deviation (σ_π) structured by the phylogenetic covariance
368 matrix A . We ran each MCMC sampling chain for 8000 warmup iterations and 2000 sampling
369 iterations. We assessed model convergence as described for the vital rate models, described
370 in full in the *Supporting Information - Supplemental Methods*.

371

372 ¹I think a brief description of each of these is necessary, especially the two entropies, which
373 most readers will not have seen before.

374

375

Mean-variance decomposition	369
We decomposed the total endophyte effect on λ_S —total endophyte effects on λ_S into contributions from effects on vital rate means, variances, and their interaction and variances.	370
Specifically, we repeated the calculation of S+ and S- λ_S described above for two additional “treatments”: (1) endophyte effects on mean vital rates only, with inter-annual variances shared between S+ and S- at the S- reference level for all vital rates, and (2) endophyte effects on vital rate variances only, with vital rate means shared between S+ and S- at the S- reference level. The combination of all four λ_S - λ_S treatments (S+ vital rate means and variances, S- means and variances, S+ means with S- variances, S- means with S+ variances) allowed us to quantify to what extent the overall effect of symbiosis derives the extent that overall effects of symbiosis derive from changes in vital rates means, variances, and their interaction.	371
The interaction occurs because the variance penalty to stochastic growth is proportional to the arithmetic mean of annual growth rates (as in Eq. 1, for example) such that variance is more detrimental for populations with lower average growth rates. To quantify how mean and variance effects of symbionts arise through effects on different vital rates, we performed an additional decomposition described in the <i>Supporting Information Supplemental Methods</i> that isolates symbiont effects on growth and survival from their effects on fertility and recruitment.	372
We simulated scenarios of increased variance relative to that observed during the study period—our study by sampling subsets of the 13 observed annual transition matrices. We created two scenarios of increased environmental variance by sampling the transition matrices associated with the set of either six or two most extreme λ -values λ_t values for S- populations. These extreme λ - λ_t values represent the best and worst years for S- populations, the reference condition, experienced by symbiont-free populations. By sampling away from an average year in both directions, the six- and two- years scenarios increased the standard deviation of annual host growth rates by 1.3 and 2.1 times, respectively, without changing mean growth rates ($<2.3 < 2.1\%$ difference in $\bar{\lambda}$ - $\bar{\lambda}_t$ between simulation treatments, Fig. S50-S80). We performed the same mean-variance decomposition for these scenarios as for the ambient conditions (all 13 years sampled) for all host species described above.	373
Results	378
Symbionts buffer host demographic variance	379
Across the 14 census years, endophytes reduced inter-annual variance for 66% (37/56) of host species-vital rate combinations (average Cohen’s D for effects on vital rate standard deviation: -0.15) (Fig. 2A; Fig. S6-Figs. S22 - Fig. S18-S29). Endophytes also increased mean vital rates for the majority (36/56) of host species-vital rate combinations (average Cohen’s D for effects on vital rate mean: 0.15), and benefits were particularly strong for host survival, plant growth and recruitment (Fig. 2A; Fig. S1-S2 - Fig. S5-S11). The magnitude of mean and variance effects differed among host species-hosts and vital rates. Symbiont effects on vital rate variance were as large and even exceeded effects on vital rate means-mean effects for certain species. For example, endophytes modestly increased mean adult survival (Fig. 2C) and strongly reduced variance in survival (Fig. 2D) for <i>Festuca subverticillata</i> , while for <i>Poa alsodes</i> , variance buffering was more apparent in seedling growth and inflorescence production (Fig. 2E). Additionally, some vital rates showed costs of endophyte-symbiosis. Symbiotic individuals of <i>A. perennans</i> grew larger than those without endophytes symbiont-free hosts (Fig. 2B), yet endophytes also reduced this species’ mean recruitment rates (Fig. 2A). Similarly, endophytes increased variance for certain species’ vital rates, such as in including seedling growth for <i>Elymus villosus</i> and <i>Festuca subverticillata</i> (Fig. 2A).	380
Because not all vital rates contribute equally to fitness, we used stochastic matrix models to integrate the diverse effects on vital rates—diverse vital rate effects described above into comprehensive measures for the arithmetic mean and variance of year-to-year fitness (λ_t). ¹ On average across host species, the mean fitness of S+ populations increased by more than 10% ($> 92\%$ confidence that endophytes increased $\bar{\lambda}\bar{\lambda}_t$) and inter-annual variability in fitness	381
¹ The methods and results sections are inconsistent in their use of λ vs λ_t . I think we could use either but either way tighten this up.	382
	383
	384
	385
	386
	387
	388
	389
	390
	391
	392
	393
	394
	395
	396
	397
	398
	399
	400
	401
	402
	403
	404
	405
	406
	407
	408
	409
	410
	411
	412
	413
	414

415 was 26% lower ($> 86\%$ confidence that endophytes decreased the coefficient of variation of
416 λ_t) than S- populations (Fig. 3). For some host species, the CV of λ_t declined by more
417 than 62% (*P. alsodes*, *F. subverticillata*), while for others, endophyte effects on variance were
418 substantially smaller (5% lower for *E. villosus*, 13% lower for *A. perennans*), or even positive
419 (37% increase for *E. virginicus*). When Considering mean and variance effects of symbionts
420 were considered together, none of the host-symbiont pairings were antagonistic (i.e., with
421 endophytes that both decreased mean fitness and increased variance) (Fig. 3C)

421 **Faster life histories predict stronger symbiont-mediated 422 variance buffering**

423 Hosts with trait values representing slower life history strategies slow life history trait values
424 experienced weaker variance buffering from endophytes than those with fast life histories
425 (Fig. 4). Bayesian phylogenetic mixed-effects models, controlling for species' relatedness,
426 indicated that variance buffering was stronger for host species with shorter lifespan
427 (Fig. 4A; 75.67% probability of positive relationship with empirically observed maximum
428 plant age) and smaller seeds (Fig. 4B; 73.65% probability of positive relationship with seed
429 length). Other life history traits similarly had positive, but weaker, weak, positive support
430 for the prediction that faster life history traits correlate with stronger variance buffering
431 (Fig. S57-S59S83-S85). Models indicate moderate phylogenetic signal in the effect of variance
432 buffering (average Pagel's λ of 0.26 and of 0.63–0.22 (90% CI: 0–0.8) and of 0.56 (90% CI: 0–
433 0.9) from models including host and symbiont phylogenetic covariance respectively phylogeny
434 respectively (Table S2)).

435 **Contributions from variance buffering are weak relative to 436 mean effects**

437 To evaluate the relative importance of mean fitness benefits and variance buffering as alter-
438 native pathways of mutualism, we decomposed the overall effect of the symbiosis on the
439 stochastic growth rate stochastic growth rates λ_S using simulations that included includ-
440 ing either the full symbiosis effect (both mean and variance buffering effects), mean effects
441 alone, variance effects alone, or neither mean nor variance effects. Overall, the full effect of
442 symbiosis on λ_S , averaged across host species, provided strong evidence of grass-endophyte
443 mutualism (99% certainty of a positive total effect on λ_S) (Fig. 5; see Fig. S52–S81 for
444 individual host species). Contributions to this full effect derived from both mean and var-
445 iance buffering effects, as well as a slightly negative interaction (i.e., the combined influence of
446 mean and variance effects was smaller than the sum of their individual effects). Endophytes'
447 contributions to λ_S from mean effects were four times greater, averaged across species, than
448 contributions from variance buffering (Fig. 5), suggesting that, under the regime of envi-
449 ronmental variability represented by our 14-year study, damped fluctuations in fitness via
450 variance buffering was a far less important element of the benefits of symbiosis symbiont ben-
451 efits than increased mean fitness. Decomposing this result further into contributions through
452 endophytes effects on different vital rates demonstrated that demographic buffering arose
453 primarily from symbionts' effects on host survival and growth, rather than from effects on
454 reproduction (Fig. S53S82). Results for individual host species were largely consistent with
455 the cross-species trends (Fig. S22, S81). The full effect of symbiosis on λ_S was positive for
456 seven out of eight five out of seven host species, with statistical confidence ranging from 66%
457 to > 99% certainty. The one exception was the host species exceptions were *P. sylvestris*
458 and *A. perennans*, for which our analysis indicated that fungal endophytes were effectively
459 neutral effectively neutral symbionts in their overall fitness effect (45% and 55.42% and 57%
460 posterior probability of positive and negative effects ; Fig. S22 effects respectively; Fig. S81).

456 **Variance buffering strengthens under increased environmental 457 variability**

458 To simulate increased variability, we repeated the decomposition of λ_S for two alternative
459 forecast scenarios, randomly sampling transition matrices that represented either the six or
460 two most extreme years, subsets of the thirteen transition matrices across the 14-year study

period. Increased variability elicited stronger mutualistic benefits of endophyte symbiosis than ambient variability (Fig. 5; overall effect of the symbiosis increased by >130%, a 2.3 fold increase~ 2fold). This increase was driven by increased contributions from the variance buffering mechanism variance buffering (from a 24% 16% contribution in the ambient scenario to a 6654% contribution in the most variable scenario) rather than from greater mean effects. In the most variable scenario, the relative importance of mean and variance effects reversed, with variance buffering contributions that were 1.5-1.2 times greater than contributions from mean benefitsmean contributions, averaged across species (Fig. 5).	461 462 463 464 465 466 467 468 469 470 471 472 473 474 475 476 477 478 479 480 481 482 483 484 485 486 487 488 489 490 491 492 493 494 495 496 497 498 499 500 501 502 503 504 505 506
Discussion	468
Across seven host species, eight vital rates, 14 years, and 16,789 individuals, our analysis provided the first empirical evidence, to our knowledge, of demographic buffering conferred by microbial symbionts. Our taxonomically-replicated, long-term field experiments that manipulated the presence/absence of fungal symbionts in plants revealed that heritable microbes can commonly benefit hosts not only through improved mean fitness – the focus of most previous research – but also through buffering against environmental variance -(Fig. 1). Benefits to mean fitness dominated the overall fitness advantage of endophyte symbiosis under the observed regime of environmental variability, but observed environmental variability. However, the strongest symbiotic benefits derived from the combination of both mean effects and variance buffering (Fig. 1B), and simulation experiments point to a dominant an increasing role for demographic buffering under increased temporal environmental stochasticity -(Fig. 5; Figs. S81-S82). There is growing interest in demographic buffering as a potential source of resilience against the increased stochasticity that is expected increased stochasticity under global change (eite)(23). Our results suggest that biotic interactions, and microbial mutualisms in particular, may be an under-appreciated mechanism of demographic buffering. In fact, any interaction that is subject to context-dependence – where the magnitude magnitudes of cost or benefit depends on harshness of the environment – holds potential to modify demographic variance across years(Figure 1). However, the long-term experimental data required to detect such an influence is are rarely available.	469
Taxonomic replication of host-symbiont pairs enabled us to generalize beyond the focal taxa and facilitated inference about the <i>types</i> of species in which demographic buffering may be more or less likely. Because host taxa with “slow” life history traits, such as long lifespan, may be intrinsically buffered from environmental variability (61; 62; 11)(61; 62; 11), we predicted that the buffering effects of endophyte symbiosis would be stronger in hosts with a fast faster pace of life. In support of Supporting this prediction, we found that shorter-lived and smaller-seeded host species experienced stronger reductions in demographic variance through endophyte symbiosis. Thus, microbial symbiosis may compensate for the lack of intrinsic tolerance of variability conferred by slow life history traits. Considering Future studies may consider fungal life history traits, the three such as diversity in biologically-active alkaloids, or the production of stromata - fruiting bodies capable of horizontal (contagious) transmission. The host species for which the net mutualism benefit was weakest greatest (<i>Elymus villosus</i> , <i>Elymus virginicus</i> , and <i>F. subverticillata</i> and <i>Poa sylvestris</i> L. <i>arundinaceum</i>) (Fig. 2C) were the only hosts for which we observed fungal stromata, fruiting bodies capable of horizontal (contagious) transmission (S79) were among those never observed to produce fungal stromata (Table S2). This result supports the theoretical expectation-, supporting theoretical expectations that strict vertical transmission drives the evolution of strong host-symbiont mutualism (27; 63)(27; 63). We caution that our inferences on trait correlates of demographic buffering were subject to large uncertainties (FigureFig. S85), reflecting the relatively narrow range of taxonomic breadth that we were able to consider relatively narrow taxonomic breadth (closely related grass species in the sub-family Pooideae and their co-evolving symbionts). Our understanding Understanding of how life history variation modulates the fitness consequences of microbial symbiosis would profit from tests across a wider span of plant and animal groups (64)(64). We also found relatively consistent, positive effects of endophyte symbiosis on stochastic fitness (eite supp figure—is this true?Fig. S78-S79), suggesting that variation across host species and vital rates in mean and variance effects (Fig2,3, 3C) may reflect alternative strategies that yield similar net benefitsof endophyte symbiosis.	470
While our results highlight symbiont-mediated demographic buffering as a potential source of resilience against increased environmental stochasticity, much work remains to connect endophyte symbiont effects on mean and variance to quantitative forecasts of	471

host-symbiont dynamics under global change. Like most temporally stochastic population projection models, our approach quantified demographic variance across years (and simulated increasing variance) without attributing its cause(s). Realistic forecasts for host-symbiont dynamics under environmental change will require explicit connections between driver variables and demographic responses. Reduced sensitivity to drought, as has been reported for some¹ in *Epichloë* symbioses (40¹(31; 32; 33; 40), is a candidate mechanism that could generate a signature of variance buffering: drought conditions may have weaker fitness effects be less costly for S+ hosts, dampening the cost effects of drought years and reducing fluctuations in fitness through time (Figure Fig. 1). Our preliminary climate-explicit analyses indicated that symbionts reduced sensitivity to annual or growing-season drought indices for five of seven host taxa (Supporting InformationText; Fig. S24-S25S88-S89; Table S3). However, we did not find a strong relationship between the-magnitude of variance buffering and relative drought sensitivities, suggesting that other climatic factors or other-temporally-varying aspects of the environment may elicit benefits of endophyte-symbiosis, including documented resistance to herbivory for six of these host taxa (59; 60)(59; 60). Identifying the type and timescale of relevant drivers would allow more direct connections between demographic models and outputs from global climate models.

Symbiont-mediated demographic buffering is a potential target of selection for improved holobiont fitness (65)–(65) and carries implications for the evolution of bet-hedging strategies in variable environments. Demographic buffering may be considered a bet-hedging strategy if reduced temporal variance comes at the cost of arithmetic mean fitness (eite Childs, Metcalf). This is likely not the case in our (66). This may be unlikely in this system, where most host species exhibited both reduced variance and elevated mean fitness through symbiosis (supp FigureFig. 3C). However, the context-dependent fitness effects that underlie demographic buffering may favor other forms of evolutionary bet-hedging. Theory suggests that imperfect transmission (the production of S- offspring from an S+ maternal individual parent) may be an adaptive host strategy in spatially or temporally varying environments when the-fitness effects of symbionts are environment-dependent , because it extends by extending phenotypic variance of offspring and improves improving the odds of some having the symbiont status that is optimal-optimal symbiont status for their environment (67; 68; 69)(67; 68; 69). Imperfect vertical transmission is well-documented in grass-endophyte symbioses (CITE)(63), including our focal taxa (Table S2), and could be incorporated into our modeling-framework-model by dynamically linking S+ and S- populations (eite Yule et al., Chung et al.) (70; 71). A further step could incorporate diverse symbiont partners (e.g. different strains of *Epichloë* fungi or multiple species within the microbiome) to understand how microbial diversity contributes to host genotypic and phenotypic variance (?).

Several limiting features of our study point to new directions and valuable next steps. We focused explicitly on temporal variation and intentionally averaged over spatial heterogeneity. We speculate that endophytes Endophytes may dampen spatial heterogeneity in host fitness in ways that parallel their effects on temporal variance, and this hypothesis could be explored by leveraging the plot replication of our experimental designin our experiment. At larger spatial scales, it may be important to consider how-buffering effects of symbionts may vary across the broad geographic distributions of these eastern North American grass species, especially since historical and projected trends in climate variability are geographically heterogeneous (3)(3). Finally, our demographic modeling framework could be further “unpacked” to explore other elements of fitness in stochastic environments. Our analyses assumed that the environmental state is independently distributed , but We identified damping variance in survival and growth as the key avenue by which symbionts' variance effects contributed to host fitness (Fig. S82). Elasticity analyses could explore the selection that drives diverse symbiont effects across host vital rates. Small changes in variance of vital rates that are highly important to population growth (i.e. those with high elasticities) may be more strongly selected for than larger changes in less important vital rates (?), and symbionts may even provide an adaptive advantage by increasing temporal variance in certain vital rates (i.e. demographic lability) (?). Further, our simulations assumed an independently distributed environmental distribution through time, but environmental auto-correlation of the environment can be an important component of stochastic population projections (72)–(72) and might modify the fitness consequences of symbiont-mediated variance buffering. Similarly, correlated responses of multiple vital rates could amplify or dampen demographic variance (9; 73; 12)(9; 73; 12)

551

552 ¹eite a bunch more

. Our “matrix sampling” approach accounted for vital rate correlations implicitly (50)–(50)	553
but exploring whether and how endophyte symbiosis alters the correlation structure of host	554
vital rates could add nuance to our understanding of how symbiontsecontribute understanding	555
of symbionts’ contributions to variance buffering.	556
	557
Conclusion	558
Ecologists increasingly recognize the importance of symbiotic microbes for host organisms	559
and the populations, communities, and ecosystems in which their hosts reside (74; 75; 76; 77)	560
(74; 75; 76; 77). Despite awareness of these ubiquitous interactions, long-term studies of	561
microbial symbiosis are very rare. Our results provide an important advance to improve fore-	562
casts of the responses of populations (and symbionts) to increasing environmental stochasticity	563
under global change. We found that, relative to mean fitness benefits, symbiont-mediated vari-	564
ance buffering made weak contributions to host-symbiont mutualism under the current regime	565
of observed environmental variability. However, demographic buffering is likely to become the	566
dominant benefit that fungal endophytes confer to grass hosts in more variable future envi-	567
ronments. Thus, demographic buffering – a cryptic microbial influence that manifests only	568
over long time scales – is poised to become the dominant way in which grasses benefit from	569
symbiosis with fungal endophytes in more variable climates of the futurebenefit of symbio-	570
sis. This result emerges from the context-dependent nature of grass-endophyte interactions,	571
combined with the observation that environmental stochasticity generates fluctuation in con-	572
tect. These key ingredients, and thus the potential for symbiont-mediated variance buffering,	573
similarly apply to the diverse host-microbe symbioses across the tree of life.	574
	575
	576
	577
	578
	579
	580
	581
	582
	583
	584
	585
	586
	587
	588
	589
	590
	591
	592
	593
	594
	595
	596
	597
	598

599 **Acknowledgments** We thank Mark Sheehan, Ali Campbell, Kyle Dickens, Blaise Willis,
600 and Sar Lindner for contributions to field data collection. We also thank Volker Rudolf, Daniel
601 Kowal, Lydia Beaudrot and Judie Bronstein for helpful comments on and discussion of this
602 project. This research was supported by the National Science Foundation (grants 1754468
603 and 2208857).

603 **Supplementary information** Supplementary information for this paper includes
604 Supplementary Methods, Figs. A1 to A28S1 to S89, and Tables A1 to A3S1 to S3.

605

606 **References**

607

- 608 [1] Seneviratne, S. *et al.* *Changes in climate extremes and their impacts on the*
609 *natural physical environment* (Cambridge University Press, 2012).
- 610
- 611 [2] IPCC. Climate change 2021: The physical science basis (2021). URL <https://www.ipcc.ch/report/ar6/wg1/>.
- 612
- 613 [3] Bathiany, S., Dakos, V., Scheffer, M. & Lenton, T. M. Climate models predict
614 increasing temperature variability in poor countries. *Science advances* **4**, eaar5809
615 (2018).
- 616
- 617 [4] Swain, D. L., Langenbrunner, B., Neelin, J. D. & Hall, A. Increasing precipitation
618 volatility in twenty-first-century California. *Nature Climate Change* **8**, 427–433
619 (2018).
- 620
- 621 [5] Clark, J. S. Why environmental scientists are becoming bayesians. *Ecology letters*
622 **8**, 2–14 (2005).
- 623
- 624 [6] Lewontin, R. C. & Cohen, D. On Population Growth in a Randomly Varying Envi-
625 ronment. *Proceedings of the National Academy of Sciences* **62**, 1056–1060 (1969).
626 URL <https://www.pnas.org/content/62/4/1056>. Publisher: National Academy of
627 Sciences Section: Biological Sciences: Zoology.
- 628
- 629 [7] Tuljapurkar, S. D. Population dynamics in variable environments. III. Evolution-
630 ary dynamics of r-selection. *Theoretical Population Biology* **21**, 141–165 (1982).
631 URL <http://www.sciencedirect.com/science/article/pii/0040580982900107>.
- 632
- 633 [8] Cohen, J. E. Comparative statics and stochastic dynamics of age-structured
634 populations. *Theoretical population biology* **16**, 159–171 (1979).
- 635
- 636 [9] Tuljapurkar, S. *Population dynamics in variable environments* Vol. 85 (Springer
637 Science & Business Media, 2013).
- 638
- 639 [10] Pfister, C. A. Patterns of variance in stage-structured populations: evolutionary
640 predictions and ecological implications. *Proceedings of the National Academy of
641 Sciences* **95**, 213–218 (1998).
- 642
- 643 [11] Morris, W. F. *et al.* Longevity can buffer plant and animal populations against
644 changing climatic variability. *Ecology* **89**, 19–25 (2008).

- [12] Compagnoni, A. *et al.* The effect of demographic correlations on the stochastic population dynamics of perennial plants. *Ecological Monographs* **86**, 480–494 (2016). 645
646
647
648
- [13] Ellis, M. M. & Crone, E. E. The role of transient dynamics in stochastic population growth for nine perennial plants. *Ecology* **94**, 1681–1686 (2013). 649
650
- [14] Murphy, G. I. Pattern in life history and the environment. *The American Naturalist* **102**, 391–403 (1968). 651
652
653
- [15] Davison, R., Stadman, M. & Jongejans, E. Stochastic effects contribute to population fitness differences. *Ecological Modelling* **408**, 108760 (2019). 654
655
656
- [16] Compagnoni, A. *et al.* Herbaceous perennial plants with short generation time have stronger responses to climate anomalies than those with longer generation time. *Nature communications* **12**, 1–8 (2021). 657
658
659
660
- [17] Le Coeur, C., Yoccoz, N. G., Salguero-Gómez, R. & Vindenes, Y. Life history adaptations to fluctuating environments: Combined effects of demographic buffering and lability. *Ecology Letters* **25**, 2107–2119 (2022). 661
662
663
664
- [18] Rodríguez-Caro, R. C. *et al.* The limits of demographic buffering in coping with environmental variation. *Oikos* **130**, 1346–1358 (2021). 665
666
- [19] Tuljapurkar, S. & Orzack, S. H. Population dynamics in variable environments i. long-run growth rates and extinction. *Theoretical Population Biology* **18**, 314–342 (1980). 667
668
669
670
- [20] Fieberg, J. & Ellner, S. P. Stochastic matrix models for conservation and management: a comparative review of methods. *Ecology letters* **4**, 244–266 (2001). 671
672
673
- [21] Menges, E. S. Applications of population viability analyses in plant conservation. *Ecological Bulletins* **73**–84 (2000). 674
675
676
- [22] Kuparinen, A., Boit, A., Valdovinos, F. S., Lassaux, H. & Martinez, N. D. Fishing-induced life-history changes degrade and destabilize harvested ecosystems. *Scientific reports* **6**, 22245 (2016). 677
678
679
680
- [23] Hilde, C. H. *et al.* The Demographic Buffering Hypothesis: Evidence and Challenges. *Trends in Ecology & Evolution* **0** (2020). URL [https://www.cell.com/trends/ecology-evolution/abstract/S0169-5347\(20\)30050-1](https://www.cell.com/trends/ecology-evolution/abstract/S0169-5347(20)30050-1). Publisher: Elsevier. 681
682
683
684
- [24] Rodriguez, R., White Jr, J., Arnold, A. E. & Redman, a. R. a. Fungal endophytes: diversity and functional roles. *New phytologist* **182**, 314–330 (2009). 685
686
- [25] McFall-Ngai, M. *et al.* Animals in a bacterial world, a new imperative for the life sciences. *Proceedings of the National Academy of Sciences* **110**, 3229–3236 (2013). 687
688
689
690

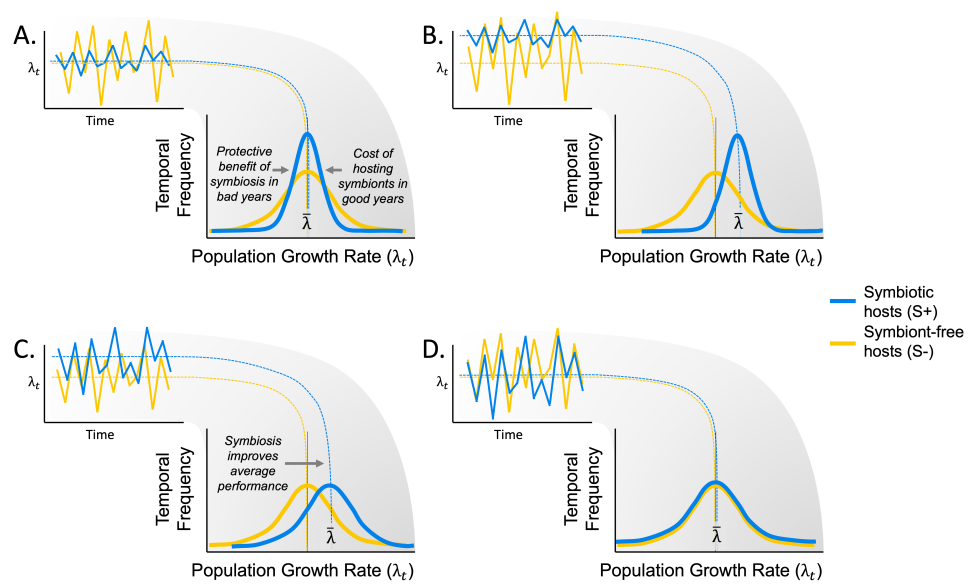
- 691 [26] Funkhouser, L. J. & Bordenstein, S. R. Mom knows best: the universality of
692 maternal microbial transmission. *PLoS biology* **11**, e1001631 (2013).
- 693
- 694 [27] Fine, P. E. Vectors and vertical transmission: an epidemiologic perspective.
695 *Annals of the New York Academy of Sciences* **266**, 173–194 (1975).
- 696
- 697 [28] Russell, J. A. & Moran, N. A. Costs and benefits of symbiont infection in aphids:
698 variation among symbionts and across temperatures. *Proceedings of the Royal
699 Society B: Biological Sciences* **273**, 603–610 (2006).
- 700
- 701 [29] Kivlin, S. N., Emery, S. M. & Rudgers, J. A. Fungal symbionts alter plant
702 responses to global change. *American Journal of Botany* **100**, 1445–1457 (2013).
- 703
- 704 [30] Dunbar, H. E., Wilson, A. C. C., Ferguson, N. R. & Moran, N. A. Aphid thermal
705 tolerance is governed by a point mutation in bacterial symbionts. *PLoS biology*
706 **5**, e96 (2007).
- 707
- 708 [31] Reyna, R., Cooke, P., Grum, D., Cook, D. & Creamer, R. Detection and local-
709 ization of the endophyte *undifilum oxytropis* in locoweed tissues. *Botany* **90**,
710 1229–1236 (2012).
- 711
- 712 [32] Saikkonen, K., Gundel, P. E. & Helander, M. Chemical ecology mediated by
713 fungal endophytes in grasses. *Journal of chemical ecology* **39**, 962–968 (2013).
- 714
- 715 [33] Neyaz, M., Gardner, D. R., Creamer, R. & Cook, D. Localization of the
716 swainsonine-producing chaetothyriales symbiont in the seed and shoot apical
717 meristem in its host *ipomoea carnea*. *Microorganisms* **10**, 545 (2022).
- 718
- 719 [34] Chamberlain, S. A., Bronstein, J. L. & Rudgers, J. A. How context dependent
720 are species interactions? *Ecology letters* **17**, 881–890 (2014).
- 721
- 722 [35] Catford, J. A., Wilson, J. R., Pyšek, P., Hulme, P. E. & Duncan, R. P. Address-
723 ing context dependence in ecology. *Trends in Ecology & Evolution* **37**, 158–170
724 (2022).
- 725
- 726 [36] Jordano, P. Spatial and temporal variation in the avian-frugivore assemblage of
727 *prunus mahaleb*: patterns and consequences. *Oikos* 479–491 (1994).
- 728
- 729 [37] Leuchtmann, A. Systematics, distribution, and host specificity of grass endo-
730 phytes. *Natural toxins* **1**, 150–162 (1992).
- 731
- 732 [38] Cheplick, G. P., Faeth, S. & Faeth, S. H. *Ecology and evolution of the grass-*
733 *endophyte symbiosis* (OUP USA, 2009).
- 734
- 735 [39] Brem, D. & Leuchtmann, A. Epichloë grass endophytes increase herbivore resis-
736 tance in the woodland grass *brachypodium sylvaticum*. *Oecologia* **126**, 522–530

- [40] Decunta, F. A., Pérez, L. I., Malinowski, D. P., Molina-Montenegro, M. A. & Gundel, P. E. A systematic review on the effects of epichloë fungal endophytes on drought tolerance in cool-season grasses. *Frontiers in plant science* **12**, 644731 (2021). 737
738
739
740
741
742
743
744
745
746
747
748
749
750
751
752
753
754
755
756
757
758
759
760
761
762
763
764
765
766
767
768
769
770
771
772
773
774
775
776
777
778
779
780
781
782
- [41] Bacon, C. W. & White, J. F. in *Stains, media, and procedures for analyzing endophytes* 47–56 (CRC Press, 2018).
- [42] Rudgers, J. A. & Swafford, A. L. Benefits of a fungal endophyte in *elymus virginicus* decline under drought stress. *Basic and Applied Ecology* **10**, 43–51 (2009).
- [43] Bultman, T. L., White Jr, J. F., Bowdish, T. I., Welch, A. M. & Johnston, J. Mutualistic transfer of epichloë spermatia by phorbis flies. *Mycologia* **87**, 182–189 (1995).
- [44] Stan Development Team. RStan: the R interface to Stan (2022). URL <https://mc-stan.org/>. R package version 2.21.7.
- [45] Elderd, B. D. & Miller, T. E. Quantifying demographic uncertainty: Bayesian methods for integral projection models. *Ecological Monographs* **86**, 125–144 (2016).
- [46] Gabry, J., Simpson, D., Vehtari, A., Betancourt, M. & Gelman, A. Visualization in bayesian workflow. *Journal of the Royal Statistical Society Series A: Statistics in Society* **182**, 389–402 (2019).
- [47] Brooks, S. P. & Gelman, A. General methods for monitoring convergence of iterative simulations. *Journal of computational and graphical statistics* **7**, 434–455 (1998).
- [48] Gelman, A. & Hill, J. *Data analysis using regression and multilevel/hierarchical models* (Cambridge university press, 2006).
- [49] Williams, J. L., Miller, T. E. & Ellner, S. P. Avoiding unintentional eviction from integral projection models. *Ecology* **93**, 2008–2014 (2012).
- [50] Metcalf, C. J. E. et al. Statistical modelling of annual variation for inference on stochastic population dynamics using integral projection models. *Methods in Ecology and Evolution* **6**, 1007–1017 (2015).
- [51] Caswell, H. Matrix population models: Construction, analysis, and interpretation. 2nd edn sinauer associates. Inc., Sunderland, MA (2001).
- [52] Rees, M. & Ellner, S. P. Integral projection models for populations in temporally varying environments. *Ecological Monographs* **79**, 575–594 (2009).

- 783 [53] Jones, O. R. *et al.* Rcompadre and rage—two r packages to facilitate the use of
784 the compadre and comadre databases and calculation of life-history traits from
785 matrix population models. *Methods in Ecology and Evolution* **13**, 770–781 (2022).
- 786
- 787 [54] .
- 788
- 789 [55] Bürkner, P.-C. brms: An R package for Bayesian multilevel models using Stan.
790 *Journal of Statistical Software* **80**, 1–28 (2017).
- 791
- 792 [56] Zanne, A. E. *et al.* Three keys to the radiation of angiosperms into freezing
793 environments. *Nature* **506**, 89–92 (2014).
- 794
- 795 [57] Leuchtmann, A., Bacon, C. W., Schardl, C. L., White Jr, J. F. & Tadych,
796 M. Nomenclatural realignment of neotyphodium species with genus epichloë.
797 *Mycologia* **106**, 202–215 (2014).
- 798
- 799 [58] Vicente-Serrano, S. M., Beguería, S. & López-Moreno, J. I. A multiscalar drought
800 index sensitive to global warming: the standardized precipitation evapotranspi-
801 ration index. *Journal of climate* **23**, 1696–1718 (2010).
- 802
- 803 [59] Rudgers, J. A. & Clay, K. An invasive plant–fungal mutualism reduces arthropod
804 diversity. *Ecology Letters* **11**, 831–840 (2008).
- 805
- 806 [60] Crawford, K. M., Land, J. M. & Rudgers, J. A. Fungal endophytes of native
807 grasses decrease insect herbivore preference and performance. *Oecologia* **164**,
808 431–444 (2010).
- 809
- 810 [61] Rees, M. Evolutionary ecology of seed dormancy and seed size. *Philosophical
Transactions of the Royal Society of London. Series B: Biological Sciences* **351**,
811 1299–1308 (1996).
- 812
- 813 [62] Moles, A. T. & Westoby, M. Seedling survival and seed size: a synthesis of the
814 literature. *Journal of Ecology* **92**, 372–383 (2004).
- 815
- 816 [63] Afkhami, M. E. & Rudgers, J. A. Symbiosis lost: imperfect vertical transmission
817 of fungal endophytes in grasses. *The American Naturalist* **172**, 405–416 (2008).
- 818
- 819 [64] Jeschke, J. M. & Kokko, H. The roles of body size and phylogeny in fast and
820 slow life histories. *Evolutionary Ecology* **23**, 867–878 (2009).
- 821
- 822 [65] Vandenkoornhuyse, P., Quaiser, A., Duhamel, M., Le Van, A. & Dufresne, A.
823 The importance of the microbiome of the plant holobiont. *New Phytologist* **206**,
824 1196–1206 (2015).
- 825
- 826 [66] Childs, D. Z., Metcalf, C. & Rees, M. Evolutionary bet-hedging in the real world:
827 empirical evidence and challenges revealed by plants. *Proceedings of the Royal
828 Society B: Biological Sciences* **277**, 3055–3064 (2010).

- [67] Brown, A. & Akçay, E. Evolution of transmission mode in conditional mutualisms with spatial variation in symbiont quality. *Evolution* **73**, 128–144 (2019). 829
830
831
- [68] Bruijning, M., Henry, L. P., Forsberg, S. K., Metcalf, C. J. E. & Ayroles, J. F. Natural selection for imprecise vertical transmission in host–microbiota systems. *Nature ecology & evolution* **6**, 77–87 (2022). 832
833
834
- [69] Lange, C. *et al.* Impact of intraspecific variation in insect microbiomes on host phenotype and evolution. *The ISME journal* **17**, 1798–1807 (2023). 835
836
837
- [70] Yule, K. M., Miller, T. E. & Rudgers, J. A. Costs, benefits, and loss of vertically transmitted symbionts affect host population dynamics. *Oikos* **122**, 1512–1520 (2013). 838
839
840
841
- [71] Chung, Y. A., Miller, T. E. & Rudgers, J. A. Fungal symbionts maintain a rare plant population but demographic advantage drives the dominance of a common host. *Journal of Ecology* **103**, 967–977 (2015). 842
843
844
845
- [72] Tuljapurkar, S. & Haridas, C. Temporal autocorrelation and stochastic population growth. *Ecology Letters* **9**, 327–337 (2006). 846
847
848
- [73] Davison, R., Nicole, F., Jacquemyn, H. & Tuljapurkar, S. Contributions of covariance: decomposing the components of stochastic population growth in cypripedium calceolus. *The American Naturalist* **181**, 410–420 (2013). 849
850
851
- [74] Afkhami, M. E. & Strauss, S. Y. Native fungal endophytes suppress an exotic dominant and increase plant diversity over small and large spatial scales. *Ecology* **97**, 1159–1169 (2016). 852
853
854
855
- [75] Smith, E., Vaughan, G., Ketchum, R., McParland, D. & Burt, J. Symbiont community stability through severe coral bleaching in a thermally extreme lagoon. *Scientific Reports* **7**, 2428 (2017). 856
857
858
859
- [76] Dallas, J. W. & Warne, R. W. Captivity and animal microbiomes: potential roles of microbiota for influencing animal conservation. *Microbial Ecology* 1–19 (2022). 860
861
862
- [77] Wu, L. *et al.* Reduction of microbial diversity in grassland soil is driven by long-term climate warming. *Nature Microbiology* **7**, 1054–1062 (2022). 863
864
865
- [78] Ehrlén, J. & Morris, W. F. Predicting changes in the distribution and abundance of species under environmental change. *Ecology letters* **18**, 303–314 (2015). 866
867
868
- [79] Chamberlain, S., Hocking, D. & Anderson, B. Package ‘rnoaa’ (2022). 869
- [80] Beguería, S. & Vicente-Serrano, S. M. Spei: calculation of the standardised precipitation-evapotranspiration index. *R package version* **1** (2013). 870
871
872
873
874

875 **Figures**



897 **Fig. 1:** Hypothesized effects of symbiosis on the mean and variance of annual popula-
 898 tion growth rates. (A) Context-dependent symbiosis may provide benefits to hosts
 899 during harsh years while being neutral or costly during benign years. Temporal vari-
 900 ance in populations growth rates of symbiotic host populations (S+; blue lines)
 901 is expected to decrease relative to symbiont-free hosts (S-; yellow lines). (B) Symbiosis
 902 may improve average performance across years in addition to reducing temporal vari-
 903 ance. (C) Consistent benefits of symbiosis could improve average performance across
 904 years with no influence on temporal variance. (D) Symbiosis may have an effectively
 905 neutral effect on population growth rates.

921
 922
 923
 924
 925
 926
 927
 928
 929
 930
 931
 932
 933
 934
 935
 936
 937
 938
 939
 940
 941
 942
 943
 944
 945
 946
 947
 948
 949
 950
 951
 952
 953
 954
 955
 956
 957
 958
 959
 960
 961
 962
 963
 964
 965
 966

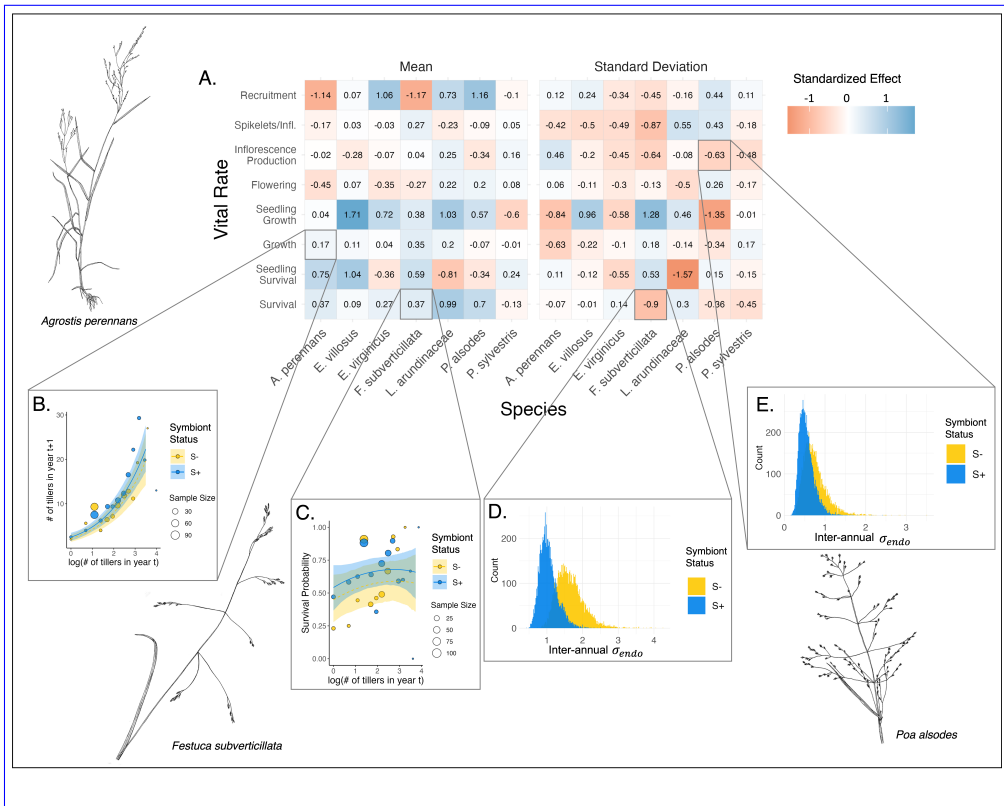


Fig. 2: Endophyte symbiosis altered host vital rates. (A) Shading represents the posterior mean standardized effect size (Cohen's D) of endophyte symbiosis on mean or standard deviation of host vital rates (blue indicates that symbiosis increased the mean or standard deviation and red indicates a reduction). Endophytes' diverse vital rate effects include increased (B) mean growth of *A. perennans* and (C) mean survival probability of *F. subverticillata*. Endophyte presence also reduced inter-annual standard deviation in (D) the survival of *F. subverticillata* and (E) the fertility of *P. alsodes*. In panels B-C, expected mean vital rate estimates rates that average across years and plots are shown with 80% credible intervals along with points representing data binned by size for symbiotic (S+) and symbiont-free (S-) plants, while panels D-E show estimated posterior distributions of endophyte-status specific inter-annual standard deviation ($\sigma_{\tau_{e,h}}^2$) for each vital rate for S+ (blue) and S- (beige) populations. Organism silhouettes modified from "Festuca subverticillata" by Cindy Roché and "Agrostis hyemalis" and "Poa alsodes" by Sandy Long ©Utah State University.

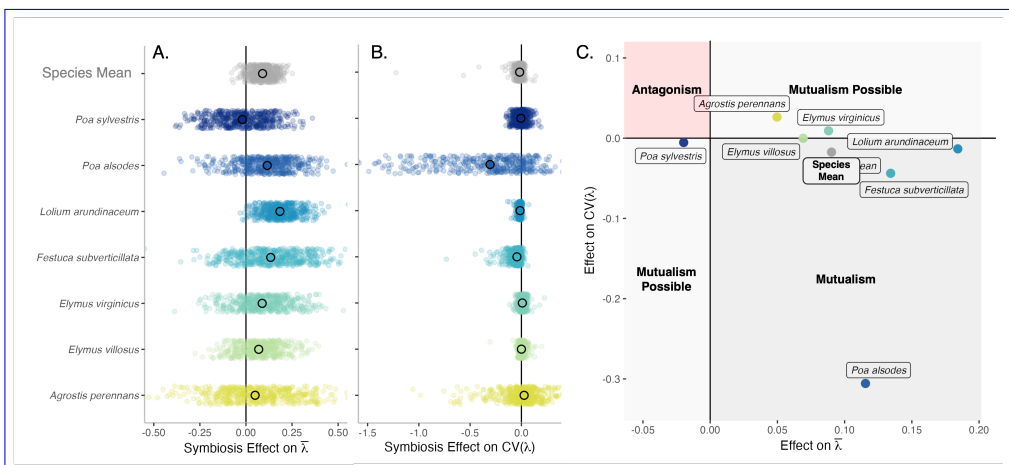


Fig. 3: Mean and variance-buffering effects on fitness. Black circles indicate the **average posterior median** effect of endophytes along with 500 posterior draws (smaller colored circles) on the (A) mean and (B) coefficient of variation in λ_t for each host species as well as a cross species mean. (C) For all hosts, endophytes either reduce variance, increase the mean, or both, and consequently when considering stochastic environments, the interactions are always at least potentially mutualistic.

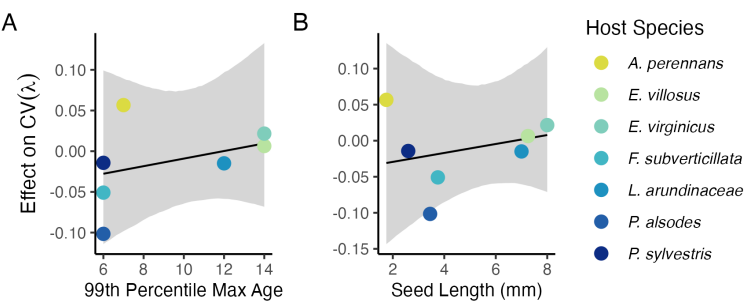
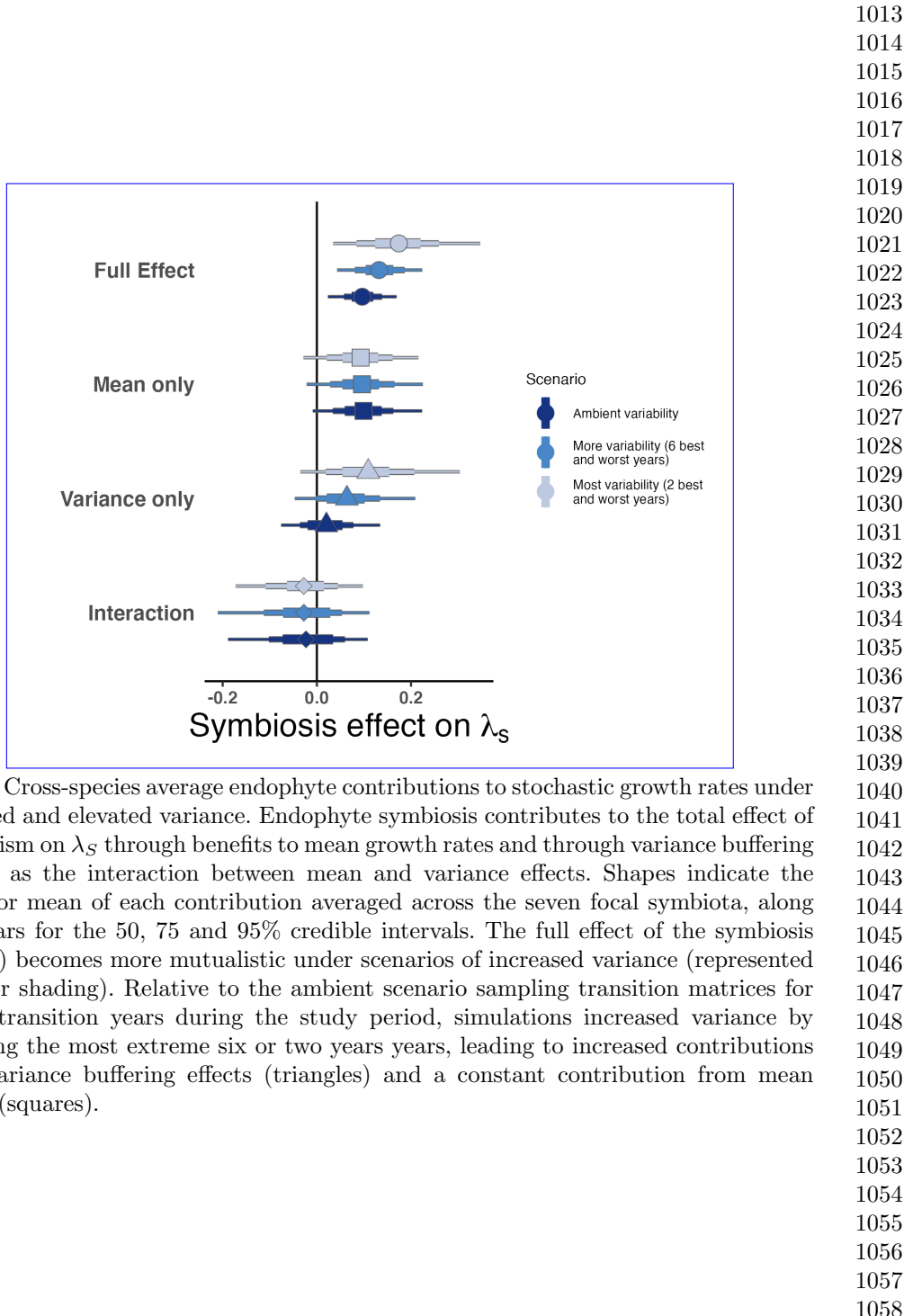


Fig. 4: Host species with faster life history traits experience stronger effects of symbiont-mediated variance buffering. Regressions between life history traits describing the fast-slow life history continuum ((A) 99th percentile maximum age observed during long term censuses in years; (B) Seed size) and the effect of endophyte symbiosis on the coefficient of variation in annual population growth rate (λ_t). Each panel shows the fitted mean relationship (line) along with the 95% credible interval.



1059 **Supporting Information**

1060

1061 **Supplemental Methods**

1062

1063

1064 Supporting Information

1065

1066 **Detailed vital rate modeling**

1067

1068 List of Supp. Figures

1069

1070	1	Life cycle diagram depicting the generalized structure of matrix population model	31
1071	2	Effect of endophyte symbiosis on mean adult survival - Original	32
1072	3	Effect of endophyte symbiosis on mean adult survival - Recruits	33
1073	4	Effect of endophyte symbiosis on mean adult growth - Original	34
1074	5	Effect of endophyte symbiosis on mean adult growth - Recruits	35
1075	6	Effect of endophyte symbiosis on mean flowering - Original	36
1076	7	Effect of endophyte symbiosis on mean flowering - Recruits	37
1077	8	Effect of endophyte symbiosis on mean fertility - Original	38
1078	9	Effect of endophyte symbiosis on mean fertility - Recruits	39
1079	10	Effect of endophyte symbiosis on mean spikelet production - Original	40
1080	11	Effect of endophyte symbiosis on mean spikelet production - Recruits	41
1081	12	Effect of endophyte symbiosis on yearly adult survival - Original	42
1082	13	Effect of endophyte symbiosis on yearly adult survival - Recruits	43
1083	14	Effect of endophyte symbiosis on yearly adult growth - Original	44
1084	15	Effect of endophyte symbiosis on yearly adult growth - Recruits	45
1085	16	Effect of endophyte symbiosis on yearly flowering - Original	46
1086	17	Effect of endophyte symbiosis on yearly flowering - Recruits	47
1087	18	Effect of endophyte symbiosis on yearly fertility - Original	48
1088	19	Effect of endophyte symbiosis on yearly fertility - Recruits	49
1089	20	Effect of endophyte symbiosis on yearly spikelet production - Original	50
1090	21	Effect of endophyte symbiosis on yearly spikelet production - Recruits	51
1091	22	Posterior distributions of the standard deviations of inter-annual year effects for survival	52
1092	23	Posterior distributions of the standard deviations of inter-annual year effects for seedling survival	52
1093	24	Posterior distributions of the standard deviations of inter-annual year effects for growth	53
1094	25	Posterior distributions of the standard deviations of inter-annual year effects for seedling growth	53
1095	26	Posterior distributions of the standard deviations of inter-annual year effects for flowering probability	54
1096	27	Posterior distributions of the standard deviations of inter-annual year effects for fertility	54
1097	28	Posterior distributions of the standard deviations of inter-annual year effects for spikelets per inflorescence	55
1098	29	Posterior distributions of the standard deviations of inter-annual year effects for recruitment	55
1099	30	Graphical posterior predictive check for mean and higher moments of <i>A. perennans</i> growth model across size	56
1100	31	Graphical posterior predictive check for mean and higher moments of <i>E. villosus</i> growth model across size	57
1101	32	Graphical posterior predictive check for mean and higher moments of <i>E. virginicus</i> growth model across size	58
1102	33	Graphical posterior predictive check for mean and higher moments of <i>F. subverticillata</i> growth model across size	59

34	Graphical posterior predictive check for mean and higher moments of <i>L. arundinacea</i> growth model across size	60	1105
35	Graphical posterior predictive check for mean and higher moments of <i>P. alsodes</i> growth model across size	61	1106
36	Graphical posterior predictive check for mean and higher moments of <i>P. sylvestris</i> growth model across size	62	1107
37	Graphical posterior predictive check for mean and higher moments of <i>A. perennans</i> survival model across size	63	1108
38	Graphical posterior predictive check for mean and higher moments of <i>E. villosus</i> survival model across size	64	1109
39	Graphical posterior predictive check for mean and higher moments of <i>E. virginicus</i> survival model across size	65	1110
40	Graphical posterior predictive check for mean and higher moments of <i>F. subverticillata</i> survival model across size	66	1111
41	Graphical posterior predictive check for mean and higher moments of <i>L. arundinacea</i> survival model across size	67	1112
42	Graphical posterior predictive check for mean and higher moments of <i>P. alsodes</i> survival model across size	68	1113
43	Graphical posterior predictive check for mean and higher moments of <i>P. sylvestris</i> survival model across size	69	1114
44	Graphical posterior predictive check for mean and higher moments of <i>A. perennans</i> inflorescence production model across size	70	1115
45	Graphical posterior predictive check for mean and higher moments of <i>E. villosus</i> inflorescence production model across size	71	1116
46	Graphical posterior predictive check for mean and higher moments of <i>E. virginicus</i> inflorescence production model across size	72	1117
47	Graphical posterior predictive check for mean and higher moments of <i>F. subverticillata</i> inflorescence production model across size	73	1118
48	Graphical posterior predictive check for mean and higher moments of <i>L. arundinacea</i> inflorescence production model across size	74	1119
49	Graphical posterior predictive check for mean and higher moments of <i>P. alsodes</i> inflorescence production model across size	75	1120
50	Graphical posterior predictive check for mean and higher moments of <i>P. sylvestris</i> inflorescence production model across size	76	1121
51	Graphical posterior predictive check for mean and higher moments of <i>A. perennans</i> spikelet model across size	77	1122
52	Graphical posterior predictive check for mean and higher moments of <i>E. villosus</i> spikelet model across size	78	1123
53	Graphical posterior predictive check for mean and higher moments of <i>E. virginicus</i> spikelet model across size	79	1124
54	Graphical posterior predictive check for mean and higher moments of <i>F. subverticillata</i> spikelet model across size	80	1125
55	Graphical posterior predictive check for mean and higher moments of <i>L. arundinacea</i> spikelet model across size	81	1126
56	Graphical posterior predictive check for mean and higher moments of <i>P. alsodes</i> spikelet model across size	82	1127
57	Graphical posterior predictive check for mean and higher moments of <i>P. sylvestris</i> spikelet model across size	83	1128
58	Graphical posterior predictive check for mean and higher moments of <i>A. perennans</i> flowering model across size	84	1129
59	Graphical posterior predictive check for mean and higher moments of <i>E. villosus</i> flowering model across size	85	1130
60	Graphical posterior predictive check for mean and higher moments of <i>E. virginicus</i> flowering model across size	86	1131
61	Graphical posterior predictive check for mean and higher moments of <i>F. subverticillata</i> flowering model across size	87	1132
62	Graphical posterior predictive check for mean and higher moments of <i>L. arundinacea</i> flowering model across size	88	1133
63	Graphical posterior predictive check for mean and higher moments of <i>P. alsodes</i> flowering model across size	89	1134

1151	64	Graphical posterior predictive check for mean and higher moments of <i>P. sylvestris</i> flowering model across size	90
1152	65	Graphical posterior predictive check for statistical model of Seedling Survival	91
1153	66	Graphical posterior predictive check for statistical model of Seedling Growth	92
1154	67	Graphical posterior predictive check for statistical model of Mean Seeds/Spikelet	93
1155	68	Graphical posterior predictive check for statistical model of Recruitment	94
1156	69	Posterior distributions of the vital rate regressions for Adult Survival	95
1157	70	Posterior distributions of the vital rate regressions for Seedling Survival	96
1158	71	Posterior distributions of the vital rate regressions for Adult Growth	97
1159	72	Posterior distributions of the vital rate regressions for Seedling Growth	98
1160	73	Posterior distributions of the vital rate regressions for Flowering Probability .	99
1161	74	Posterior distributions of the vital rate regressions for Inflorescence Production .	100
1162	75	Posterior distributions of the vital rate regressions for Spikelets/Inflorescence .	101
1163	76	Posterior distributions of the vital rate regressions for Seeds/Spikelet	102
1164	77	Posterior distributions of the vital rate regressions for Recruitment	103
1165	78	Annual growth rate values (λ_t) over thirteen years	104
1166	79	Stochastic population growth rates (λ_S) for symbiotic and symbiont-free populations	105
1167	80	Mean and standard deviation of annual growth rate values during simulation scenarios	106
1168	81	Endophyte contributions to stochastic growth rates under observed and elevated variance across species	107
1169	82	Vital rate decomposition of endophyte contributions to stochastic growth rates under observed and elevated variance across species	108
1170	83	Relationship between variance buffering and life history traits describing the fast-slow life history continuum accounting for phylogenetic covariance between <i>Epichloë</i> symbionts	109
1171	84	Relationship between variance buffering and life history traits describing the fast-slow life history continuum accounting for phylogenetic covariance between <i>Epichloë</i> symbionts	110
1172	85	Posterior estimates of life history trait effects on variance buffering	111
1173	86	Posterior distributions of the life history trait regressions	112
1174	87	Faithfulness of experimental plots to assigned endophyte status	113
1175	88	Weather station time-series for Bloomington, IN	114
1176	89	Predicted population growth rates across drought indices	115
1177			

1178 **List of Supp. Tables**

1180	S1	Summary of host-endophyte propragation and transplant methods	117
1181	S2	Summary of focal life history traits	118
1182	S3	Summary of host-endophyte drought sensitivities	119
1183			
1184			
1185			
1186			
1187			
1188			
1189			
1190			
1191			
1192			
1193			
1194			
1195			
1196			

Supplemental Methods	1197
Endophyte removal, plant propagation, and field set-up	1198
Seeds from naturally symbiotic populations of the seven focal host species were collected during summer-fall 2006 from Lilly-Dickey Woods and the nearby Bayles Road Teaching and Research Preserve (39.220167, -86.542683). To generate symbiotic (S+) and symbiont-free (S-) plants from the same genetic lineages, seeds from each species were disinfected with a heat treatment described in Table S1 or left untreated. The heat treatment created symbiont-free plants by warming seeds to temperatures at which the fungus becomes inviable but the host seeds can still germinate.	1199
Both heat-treated and untreated seeds were surface sterilized with bleach to remove epiphyllous microbes, cold stratified for up to 4 weeks, then germinated in a growth chamber before transfer to the greenhouse at Indiana University where they grew for ~ 8 weeks. We confirmed endophyte status by staining thin sections of inner leaf sheath with aniline blue and examining tissue for fungal hyphae at 200X magnification (41). We established experimental populations with vegetatively propagated clones of similar sizes (ranging from one to six tillers).	1200
During the fall of 2007 and spring of 2008, we established 10 3x3 m plots for <i>A. perennans</i> , <i>E. villosus</i> , <i>E. virginicus</i> , <i>F. subverticillata</i> , and <i>L. arundinaceum</i> and 18 plots for <i>P. alsodes</i> and <i>P. sylvestris</i> . Half of the plots were randomly assigned to be planted with either symbiotic (S+) or symbiont-free (S-) plants, and initiated with 20 evenly spaced individuals labeled with aluminum tags. In spring 2008, we placed plastic deer net fencing around each plot to limit deer herbivory and disturbance; damaged fences were regularly replaced.	1201
We expected plots to maintain their endophyte status (S+ or S-) because these fungal symbionts are almost exclusively vertically transmitted, and plots were spaced a minimum of 5 m apart, limiting seed dispersal or horizontal transmission of the symbiont between plots. We regularly confirmed endophyte treatment throughout the lifetime of the experiment by opportunistically taking subsets of seeds from reproductive individuals and scoring them for their endophyte status with microscopy as above. Overall, these scores reflected 98% faithfulness of recruits to their expected endophyte status across species and plots (Fig. S87; Supplement data). Additionally, we have rarely observed fungal stromata, the fruiting bodies by which <i>Epichloë</i> are potentially transmitted horizontally, provided the fly vector is also present (43). For <i>A. perennans</i> , <i>F. subverticillata</i> , <i>L. arundinaceum</i> , and <i>P. alsodes</i> , we never observed stromata. We observed stromata only infrequently for <i>E. villosus</i> , and even more rarely for <i>E. virginicus</i> and <i>P. sylvestris</i> (Table S2). For these species, stromata have only been observed irregularly across years on 35, 4, and 6 plants respectively, making up < 0.3% of all censused plants.	1202
Detailed vital rate modeling	1203
We fit vital rates models in a Bayesian hierarchical framework. Statistical models for adult survival, seedling survival, adult growth, seedling growth, flowering (yes or no), fertility of flowering plants (number of flowering tillers), production of seed-bearing spikelets (number per inflorescence), the average number of seeds per spikelet, and the recruitment of seedlings from the preceding year's seed production, were constructed as follows:	1204
<i>Survival</i> - We modeled survival as a Bernoulli process, where the survival (<i>S</i>) of an individual <i>i</i> in plot <i>p</i> and census year <i>t</i> was predicted by the plot-level endophyte status (<i>e</i>), host species (<i>h</i>), size in the preceding census, and the plant's origin status (<i>o</i> ; whether it was initially transplanted or naturally recruited into the plot).	1205
$S_{i,p,e,h,t} \sim Bernoulli(\hat{S}_{i,p,e,h,t})$	(S4a)
$logit(\hat{S}_{i,p,e,h,t}) = \beta_{0_{h,o}} + \beta_{1_h} * endoe$	(S4b)
$+ \beta_{2_{h,o}} * size_{i,t-1} + \beta_{3_{h,o}} * size_{i,t-1}^2 + \tau_{e,h,t} + \rho_p$	(S4c)
$\tau_{e,h,t} \sim Normal(0, \sigma_{\tau_{e,h}}^2)$	(S4d)

$$1243 \quad \rho_p \sim Normal(0, \sigma_\rho^2) \quad (S4e)$$

1244

1245 Here, \hat{S} is the survival probability, $\beta_{0_h} - \beta_{0_{h,o}}$ is an intercept specific to each host species ;
 1246 β_1 is the effect of the plant's and recruitment origin, $\beta_{2_h} - \beta_{1_h}$ is the endophyte effect, β_{3_h} is
 1247 the size effect $\beta_{2_{h,o}}$ is the effect of plant size specific to each species and recruitment origin, $\beta_{3_{h,o}}$ is
 1248 a quadratic plant size effect specific to each species and recruitment origin, $\tau_{e,h,t}$
 1249 is a normally distributed year effect for each species and endophyte status with variance
 1250 $\sigma_{\tau_{e,h}}^2$, and ρ_p is a normally distributed plot effect with variance σ_ρ^2 ($p(e)$ indicates that plot
 1251 identity is uniquely associated with an endophyte status). We assume that origin effect β_1
 1252 and the plot-to-plot variance σ_ρ^2 are was shared across host species, allowing us to “borrow
 1253 strength” across the multi-species dataset; other model parameters are unique to host species.
 1254 We separately modeled the survival of newly recruited seedlings with a similar model but
 1255 omitting previous size dependence and origin status.

1255 *Growth* - We modeled plant size in census year t (G) with the same linear predictor
 1256 for the mean as described for survival. Because we measured size as positive integer-valued
 1257 counts of tillers, we modeled it with a zero-truncated Poisson-inverse Gaussian distribution.
 1258 This distribution includes a shape parameter λ_G to account for overdispersion in the data.
 1259 We additionally modeled the growth of newly recruited seedlings separately with a Poisson-
 1260 inverse Gaussian model omitting size structure and the plants' origin status as with seedling
 1261 survival.

1260 *Flowering* - We modeled whether or not a plant was flowering during the census (P) as a
 1261 Bernoulli process, with the same linear predictor for the mean as described above for survival
 1262 except that size dependence for reproductive vital rates was determined by the individual's
 1263 size during the same census year as opposed to its size during the previous year.

1263 *Fertility* - For a plant that was flowering during the census, its fertility was the number
 1264 of reproductive tillers produced (F), which we modeled as a function of size in the same
 1265 census period with a zero-truncated Poisson-Inverse Gaussian distribution, with the same
 1266 linear predictor for the mean as described above.

1266 *Spikelets per Inflorescence* - Spikelet production (K) was recorded as integer counts on
 1267 up to three inflorescences per reproducing plant. We modeled these data with a negative
 1268 binomial distribution, with the same linear predictor for the mean as described above.

1268 *Seed Production per Spikelet* - For individuals with recorded counts of seed production,
 1269 we calculated the number of seeds per spikelet from our counts of seeds and spikelets per
 1270 inflorescence, and then modeled seeds per spikelet (D) as means of a Gaussian distribution
 1271 for each species and endophyte status. Because we had less detailed data across years and
 1272 plants for seed production than for other reproductive vital rates, we omitted both plot and
 1273 year random effects.

1273 *Seedling Recruitment* - We used a binomial distribution to model the recruitment of new
 1274 seedlings (R) into the plots from seeds produced in the preceding year, assuming no long-
 1275 lived seed bank. We included an intercept specific to each host and endophyte status and the
 1276 same random effects structure as in other models. We estimated the number of seeds per plot
 1277 in the preceding year by multiplying the total number of reproductive tillers per plant by the
 1278 mean number of spikelets per inflorescence and mean number of seeds per spikelet (D). For
 1279 plants with missing fertility or spikelet data, we used the expected number of reproductive
 1280 tillers (F) or of spikelets per inflorescence from (K), drawing from the full posteriors of our
 1281 models. We rounded this value to get the estimated seed production for each individual, and
 1282 finally summed across all reproductive plants in each year and plot to get the total number
 1283 of seeds produced.

1281

1282 **Estimating climate drivers of environmental context-dependence**

1283 To connect the variance buffering effects of endophytes with inter-annual variability in
 1284 climate, we built climate-explicit stochastic matrix population models from the vital rate
 1285 data in addition to the climate-implicit model described in the main text. Identifying the
 1286 potentially complex relationships between vital rates and environmental drivers remains a
 1287 key challenge for accurate forecasts of the ecological impacts of environmental stochasticity
 1288 (78). We first downloaded temperature and precipitation data from a weather station
 1289 in Bloomington, IN, approx. 27 km from our study site, using the rnoaa package (79)

. Compared to other weather stations in the area, the measurements from Bloomington contain the most complete climate record across the study period and are correlated with more local measurements from Nashville, IN for years in which local data are available (total daily precipitation: $R^2 = .76$; mean daily temperature: $R^2 = .94$). The mean annual temperature across the study period was $11.9^\circ C$ ($SD: 1.05^\circ C$) and the average annual precipitation was 1237.9 mm/year ($SD: 204.89$ mm/year) (Fig. S24). Given the known role of endophytes in promoting host drought tolerance, we calculated the Standardised Precipitation-Evapotranspiration Index (SPEI) for 3 and 12 months preceding each annual censuses, reflecting drought during the growing season and across the year (58). To calculate SPEI, we used the Thornthwaite equation to model potential evapotranspiration as implemented in the SPEI R package

We repeated the process of fitting statistical models for each vital rate as described in Materials and Methods with the inclusion of a parameter describing the influence of SPEI. We fit separate vital rate models incorporating either the growing season or annual drought index for each vital rate, except for the model describing the mean number of seeds per inflorescence. This model was fit without climate effects because the data came from only a few years. Initial analyses indicated similar fits for models including only a linear term and those with both linear and quadratic terms describing the relationship between the climate driver and the vital rate response, and so we proceeded with models including only the linear term. We expected that including climate predictors into the models would explain some inter-annual variance in vital rates, shrinking the variance associated with the fitted year random effects. We assessed model fit with graphic posterior predictive checks and convergence diagnostics as described for the climate-implicit analysis. Finally, we next built matrix projection models incorporating the climate-dependent vital rate functions to assess the response of symbiotic (S+) vs symbiont-free (S-) populations to drought. The model is as described in Materials and Methods with the inclusion of parameters describing the slope of the relationship with SPEI. We compared the sensitivity of λ to either annual or seasonal SPEI of S+ populations ($\frac{\Delta\lambda^+}{\Delta SPEI}$) with those of S- populations ($\frac{\Delta\lambda^-}{\Delta SPEI}$) (Fig. S25; Table S).

Most species were slightly more responsive to growing season rather than annual drought conditions, and for most species symbiotic populations were less sensitive to SPEI than symbiont-free populations (Fig. S25; Table S3). However, these drought indices did not explain the full extent of inter-annual variability in demographic vital rates. For example, flowering in *A. perennans* had one of the strongest climate signals (82% probability of a positive relationship with SPEI), yet the estimated inter-annual variance $\sigma_{\tau_P}^2$ for symbiont-free plants shrank from 6.7 to 6.1 after including 3-month SPEI as a covariate, suggesting that other factors contribute to inter-annual variability.

Model assessment

All parameters were given vague priors (46). We ran each vital rate model for 2500 warm-up and 2500 MCMC sampling iterations with three chains. We assessed model convergence with trace plots of posterior chains and checked for \hat{R} values less than 1.01, indicating low within- and between-chain variation (47; 48). For those models that showed poor convergence, we extended the MCMC sampling to include 5000 warm-up and 5000 sampling iterations, which was only necessary for seedling growth. We visualized the interactions between plant size, origin status, and endophyte status for both the interannual mean expected value for each vital rate (averaging over year and plot variance) (Fig. S2 - S11) and for the expected vital rate values specific to each year (averaging over plot variance) (Fig. S12 - S21). We graphically checked vital rate model fit with posterior predictive checks comparing simulated and observed data (Fig. S30-S68). Initial analyses including only linear effects of size produced estimates of endophytes' effects on vital rate means and inter-annual variances that were similar to those from the more flexible quadratic models, but provided worse fit to size-structure in the data in some cases. We therefore proceeded with the more flexible quadratic models. Results from subsequent matrix model analyses were qualitatively similar regardless of this choice.

Vital rate mean-variance decomposition

We repeated the mean-variance decomposition to quantify the extent that mean and variance effects on stochastic population growth rates arise through different vital rates. Specifically,

1335 we repeated the calculation of λ_s as described in the main text for symbiotic populations
1336 as well as symbiont-free populations, as well as for four additional “treatments”. These
1337 treatments differentiate between mortality and growth related vital rates (adult survival,
1338 adult growth, seedling survival, and seedling growth) and reproductive vital rates (probability
1339 of flowering, inflorescence production, spikelet production, seed production, and recruitment).
1340 Each treatment held vital rate mean and interannual variances at the S reference level across
1341 vital rates while introducing (1) endophyte effects on the vital rate means for survival and
1342 growth vital rates only, (2) endophyte effects on the vital rate variances for survival and
1343 growth vital rates only, (3) endophyte effects on the vital rate means for reproductive vital
1344 rates only, and (4) endophyte effects on the vital rate variances for reproductive vital rates
1345 only.

1346 The combination of all six λ_s treatments allowed us to quantify to what extent the overall
1347 effect of symbiosis derives from changes in mean and variance of mortality and growth versus
1348 in reproductive vital rates. To explore how these contributions could be expected to change
1349 under increased variability relative to that observed during the study period, we repeated this
1350 decomposition under the scenarios of increased variance described in the main text, sampling
1351 transition matrices associated with the set of either six or two most extreme λ values.

1352 This analysis revealed that both mean and variance buffering effects are driven primarily
1353 by symbiont effects on survival and growth rather than on reproduction (Fig S53).

1354

1355 **Estimating climate drivers of environmental 1356 context-dependence**

1357 To connect the variance buffering effects of endophytes with inter-annual variability in cli-
1358 mate, we built climate-explicit stochastic matrix population models from the vital rate data
1359 in addition to the climate-implicit model described in the main text. Identifying the poten-
1360 tially complex relationships between vital rates and environmental drivers remains a key
1361 challenge for accurate forecasts of the ecological impacts of environmental stochasticity (78)
1362 . We first downloaded temperature and precipitation data from a weather station in Bloom-
1363 ington, IN, approx. 27 km from our study site, using the rnoaa package (79). Compared to
1364 other weather stations in the area, the measurements from Bloomington contain the most
1365 complete climate record across the study period and are correlated with more local measure-
1366 ments from Nashville, IN for years in which local data are available (total daily precipitation:
1367 $R^2 = .76$; mean daily temperature: $R^2 = .94$). The mean annual temperature across the
1368 study period was $11.9^\circ C$ (SD: $1.05^\circ C$) and the average annual precipitation was 1237.9
1369 mm/year (SD: 204.89 mm/year) (Fig. S88). Given the known role of endophytes in promot-
1370 ing host drought tolerance, we calculated the Standardised Precipitation-Evapotranspiration
1371 Index (SPEI) for 3 and 12 months preceding each annual censuses, reflecting drought during
1372 the growing season and across the year (58). To calculate SPEI, we used the Thornthwaite
1373 equation to model potential evapotranspiration as implemented in the SPEI R package (80)

1374 We repeated the process of fitting statistical models for each vital rate as described
1375 above with the inclusion of a parameter describing the influence of SPEI. We fit separate
1376 vital rate models incorporating either the growing season or annual drought index for each
1377 vital rate, except for the model describing the mean number of seeds per inflorescence. This
1378 model was fit without climate effects because the data came from only a few years. Initial
1379 analyses indicated similar fits for models including only a linear term and those with both
1380 linear and quadratic terms describing the relationship between the climate driver and the
1381 vital rate response, and so we proceeded with models including only the linear term. We
1382 expected that including climate predictors into the models would explain some inter-annual
1383 variance in vital rates, shrinking the variance associated with the fitted year random effects.
1384 We assessed model fit with graphic posterior predictive checks and convergence diagnostics
1385 as described for the climate-implicit analysis. Finally, we next built matrix projection models
1386 incorporating the climate-dependent vital rate functions to assess the response of symbiotic
1387 (S+) vs symbiont-free (S-) populations to drought. The model is as described in **Materials**
1388 and **Methods** with the inclusion of parameters describing the slope of the relationship with
1389 SPEI. We compared the sensitivity of λ to either annual or seasonal SPEI of S+ populations
1390 ($\frac{\Delta\lambda^+}{\Delta SPEI}$) with those of S- populations ($\frac{\Delta\lambda^-}{\Delta SPEI}$) (Fig. S89; Table S).

1391 Most species were slightly more responsive to growing season rather than annual drought
1392 conditions, and for most species symbiotic populations were less sensitive to SPEI than

symbiont-free populations (Fig. S89; Table S3). However, these drought indices did not explain the full extent of inter-annual variability in demographic vital rates. For example, flowering in *A. perennans* had one of the strongest climate signals (82% probability of a positive relationship with SPEI), yet the estimated inter-annual variance $\sigma_{\tau_{e,h}}^2$ for symbiont-free plants shrank from 6.7 to 6.1 after including 3-month SPEI as a covariate, suggesting that other factors contribute to inter-annual variability.

Detailed statistical analysis of life history traits

We fit Bayesian phylogenetic mixed-effects models using the brms package (55) to test the relationship between each life history trait and the effect of symbiosis on the CV of λ_t (a measure of variance buffering) while controlling for phylogenetic non-independence. We pruned species-level phylogenies of plants (56) and *Epichloë* fungi (57) to include the focal species. *Agrostis perennans* was not included in the published tree, and so we used the congener *A. hyemalis*. We defined separate phylogenetic covariance matrices for the pruned tree for host and symbiont species.

We propagated uncertainty in the estimated variance buffering effect V with a measurement error model:

$$\begin{aligned}
 V_{MEAN,h} &\sim Normal(V_{EST,h}, V_{SD,h}) & (S5a) \\
 V_{EST,h} &\sim Normal(\mu_h, \sigma) & (S5b) \\
 \mu &= \alpha + \beta * trait + \pi_j & (S5c) \\
 \alpha &\sim Normal(0, .1) & (S5d) \\
 \beta &\sim Normal(0, .1) & (S5e) \\
 \sigma &\sim Half - Normal(.05, .01) & (S5f) \\
 \pi_h &\sim MVN(0, \sigma_\pi \mathbf{A}) & (S5g) \\
 \sigma_\pi &\sim Half - Normal(0, .1) & (S5h)
 \end{aligned}$$

Here, V_{EST} is the variance buffering effect for host species h , estimated from the posterior mean (V_{MEAN}) and standard deviation (V_{SD}), propagating uncertainty associated with the effect of symbiosis. The model includes an intercept (α) and slope (β) defining the relationship between variance buffering effect and the life history trait. The residual standard deviation is given by (σ). We used weakly informative priors to aid model convergence. Each prior was centered at zero, except for the residual standard deviation, which we centered at the standard deviation of the estimated variance buffering effect, .05. The phylogenetic random effect (π), modeled as a multivariate normal distribution, has a between-species standard deviation (σ_π) structured by the phylogenetic covariance matrix \mathbf{A} . We ran each MCMC sampling chain for 8000 warmup iterations and 2000 sampling iterations. We assessed model convergence as described above for the vital rate models.

Vital rate mean-variance decomposition

We performed a mean-variance decomposition to quantify the extent that mean and variance effects on stochastic population growth rates arise through different vital rates. Specifically, we repeated the calculation of λ_S as described in the main text for symbiotic populations as well as symbiont-free populations, as well as for four additional “treatments”. These treatments differentiate between mortality and growth related vital rates (adult survival, adult growth, seedling survival, and seedling growth) and reproductive vital rates (probability of flowering, inflorescence production, spikelet production, seed production, and recruitment). Each treatment set vital rate mean and interannual variances according to the symbiont-free parameter values across vital rates while introducing (1) endophyte effects on the vital rate means for survival and growth vital rates only, (2) endophyte effects on the vital rate variances for survival and growth vital rates only, (3) endophyte effects on the vital rate means

1427 for reproductive vital rates only, and (4) endophyte effects on the vital rate variances for
1428 reproductive vital rates only.

1429 The combination of all six λ_S treatments allowed us to quantify to what extent the overall
1430 effect of symbiosis derives from changes in mean and variance of mortality and growth versus
1431 in reproductive vital rates. To explore how these contributions could be expected to change
1431 under increased variability relative to that observed during the study period, we repeated
1432 this decomposition under the scenarios of increased variance described in the main text,
1432 sampling transition matrices associated with the set of either six or two most extreme λ
1433 values experienced by symbiont-free populations.

1434 This analysis revealed that both mean and variance buffering effects are driven primarily
1435 by symbiont effects on survival and growth rather than on reproduction (Fig. S82).

1436

1437

1438

1439

1440

1441

1442

1443

1444

1445

1446

1447

1448

1449

1450

1451

1452

1453

1454

1455

1456

1457

1458

1459

1460

1461

1462

1463

1464

1465

1466

1467

1468

1469

1470

1471

1472

Supplemental Figures S1-S28	1473
Supplemental Figures S1-S89	1474
OS0	1475
	1476
	1477
	1478
	1479
	1480
	1481
	1482
	1483
	1484
	1485
	1486
	1487
	1488
	1489
	1490
	1491
	1492
	1493
	1494
	1495
	1496
	1497
	1498
	1499
	1500
	1501
	1502
	1503
	1504
	1505
	1506
	1507
	1508
	1509
	1510
	1511
	1512
	1513
	1514
	1515
	1516
	1517
	1518

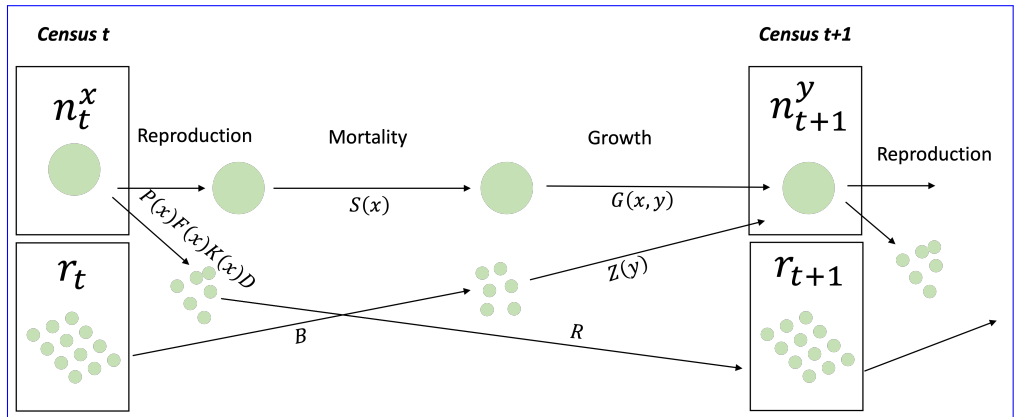
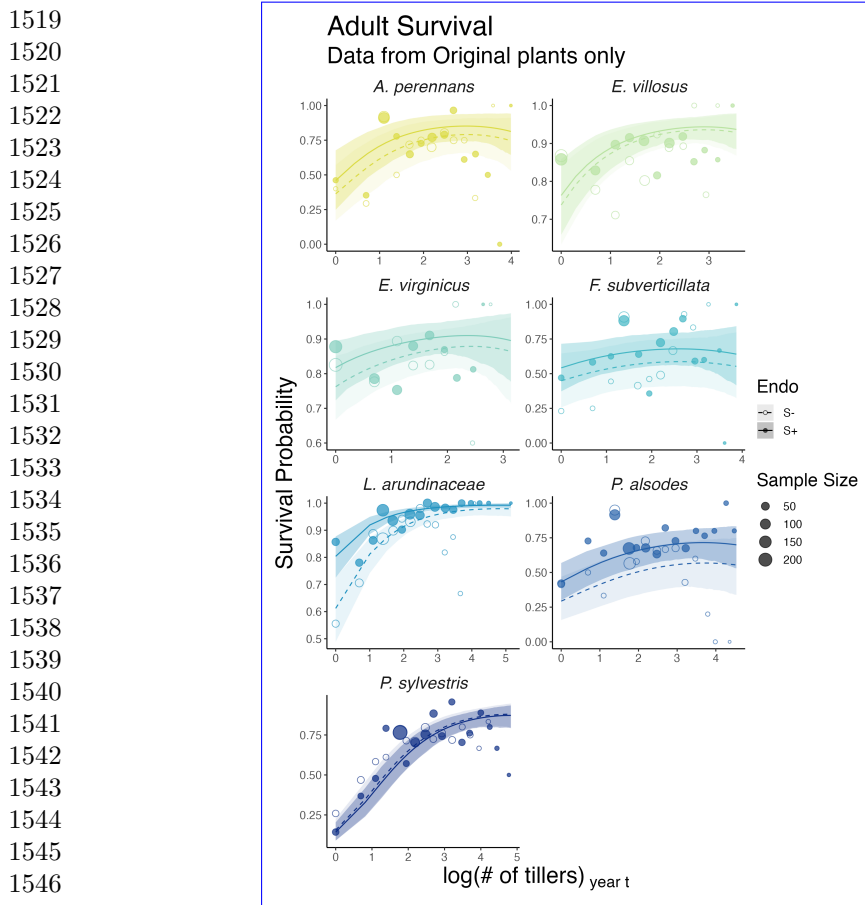


Figure 1: Life cycle diagram depicting the generalized structure of matrix population model. The population consists of different life stages at each census t or census $t+1$. Individuals transition from size x to size y . n is a vector of discrete sizes representing number of tillers, according to their likelihood of survival (S) and growth (G). Reproduction generates new recruits (small circles) through four steps, the probability of flowering (P), the number of flowering tillers produced (F), the number of spikelets per inflorescence produced (K), and the number of seeds per spikelet (D). The probability of successful recruitment (R) determines the success of these offspring, and any new recruits (r) are incorporated into the census. These non-reproductive, typically one-tiller recruits transition into the population of mature individuals with survival (B) and growth (Z) probability. Symbiotic and symbiont-free populations have the same model structure with species-specific and symbiont status-specific transition probabilities used to construct matrices.



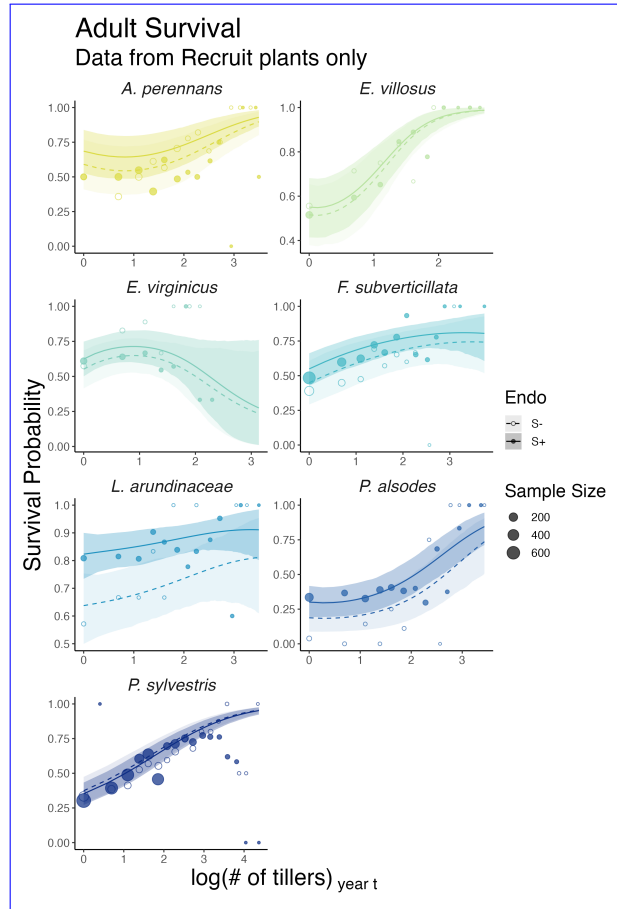
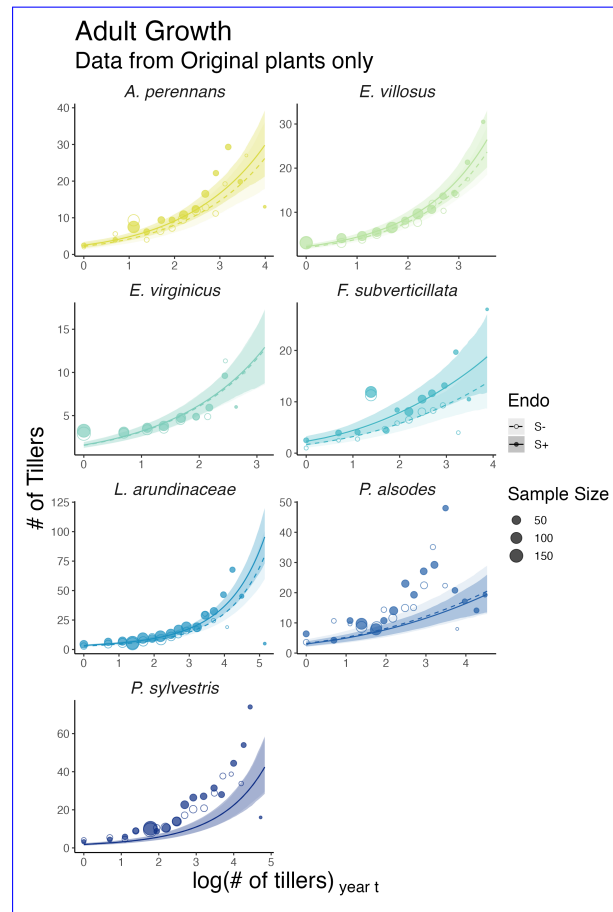


Figure 3: Effect of endophyte symbiosis on mean adult survival. Fitted curves represent the size-specific mean survival probability for recruited plants along with data binned by size and averaged over many individuals, years, and plots shown as open circles with a dashed line for symbiont-free (S-) plants, while the solid line and filled circles represent symbiotic (S+) plants. 80% credible intervals are shown with dark shading for S+, or light shading for S-.

1565
1566
1567
1568
1569
1570
1571
1572
1573
1574
1575
1576
1577
1578
1579
1580
1581
1582
1583
1584
1585
1586
1587
1588
1589
1590
1591
1592
1593
1594
1595
1596
1597
1598
1599
1600
1601
1602
1603
1604
1605
1606
1607
1608
1609
1610

1611
1612
1613
1614
1615
1616
1617
1618
1619
1620
1621
1622
1623
1624
1625
1626
1627
1628
1629
1630
1631
1632
1633
1634
1635
1636
1637
1638



1639 Figure 4: Effect of endophyte symbiosis on mean adult growth. Fitted curves represent
1640 the size-specific mean expected plant size for ~~original~~ originally transplanted plants
1641 along with data binned by size and averaged over many individuals, years, and plots
1642 shown as open circles with a dashed line for symbiont-free (S-) plants, while the solid
1643 line and filled circles represent symbiotic (S+) plants. 80% credible intervals are
1644 shown with dark shading for S+, or light shading for S-.
1645

1646
1647
1648
1649
1650
1651
1652
1653
1654
1655
1656

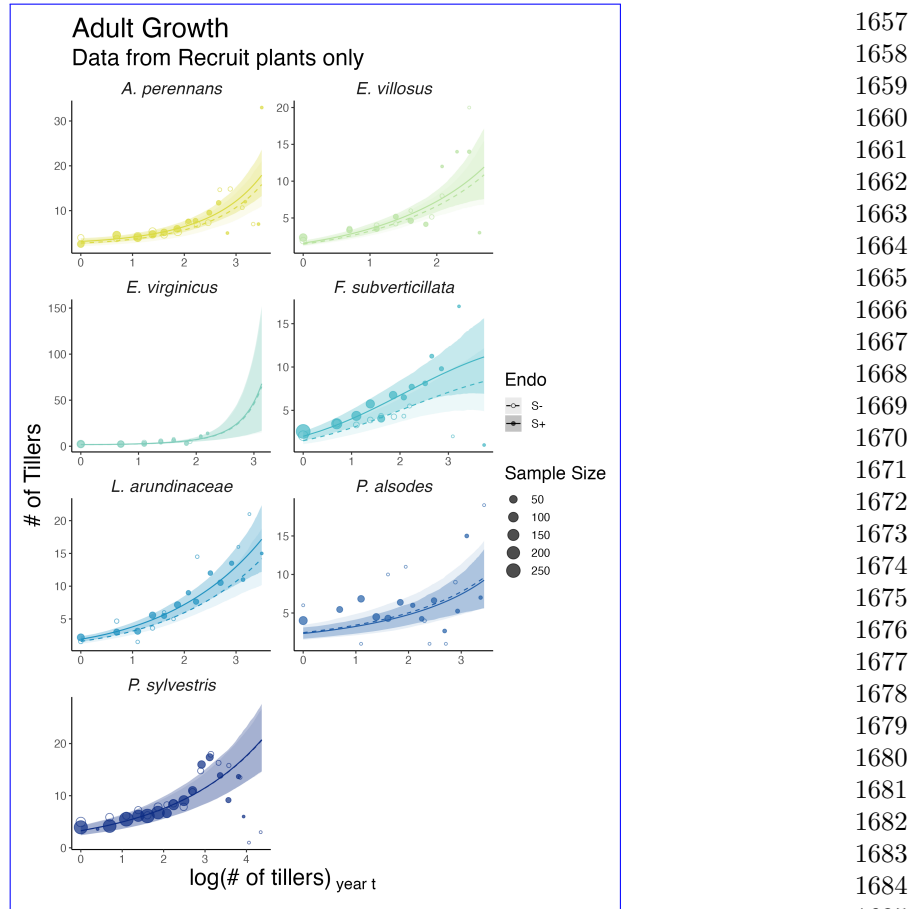
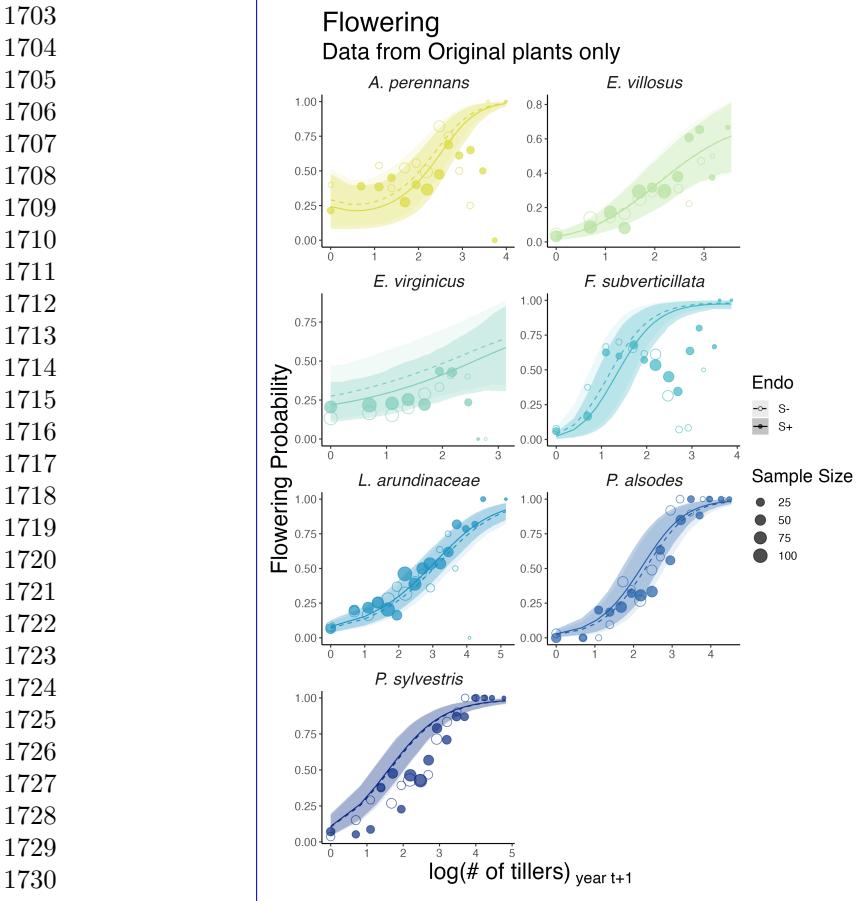


Figure 5: Effect of endophyte symbiosis on mean adult growth. Fitted curves represent the size-specific mean expected plant size for recruited plants along with data binned by size and averaged over many individuals, years, and plots shown as open circles with a dashed line for symbiont-free (S-) plants, while the solid line and filled circles represent symbiotic (S+) plants. 80% credible intervals are shown with dark shading for S+, or light shading for S-.



1731 Figure 6: Effect of endophyte symbiosis on mean flowering. Fitted curves represent the
 1732 size-specific mean flowering probability for ~~original~~ originally transplanted plants along
 1733 with data binned by size and averaged over many individuals, years, and plots shown
 1734 as open circles with a dashed line for symbiont-free (S-) plants, while the solid line
 1735 and filled circles represent symbiotic (S+) plants. 80% credible intervals are shown
 1736 with dark shading for S+, or light shading for S-.
 1737

1738
1739
1740
1741
1742
1743
1744
1745
1746
1747
1748

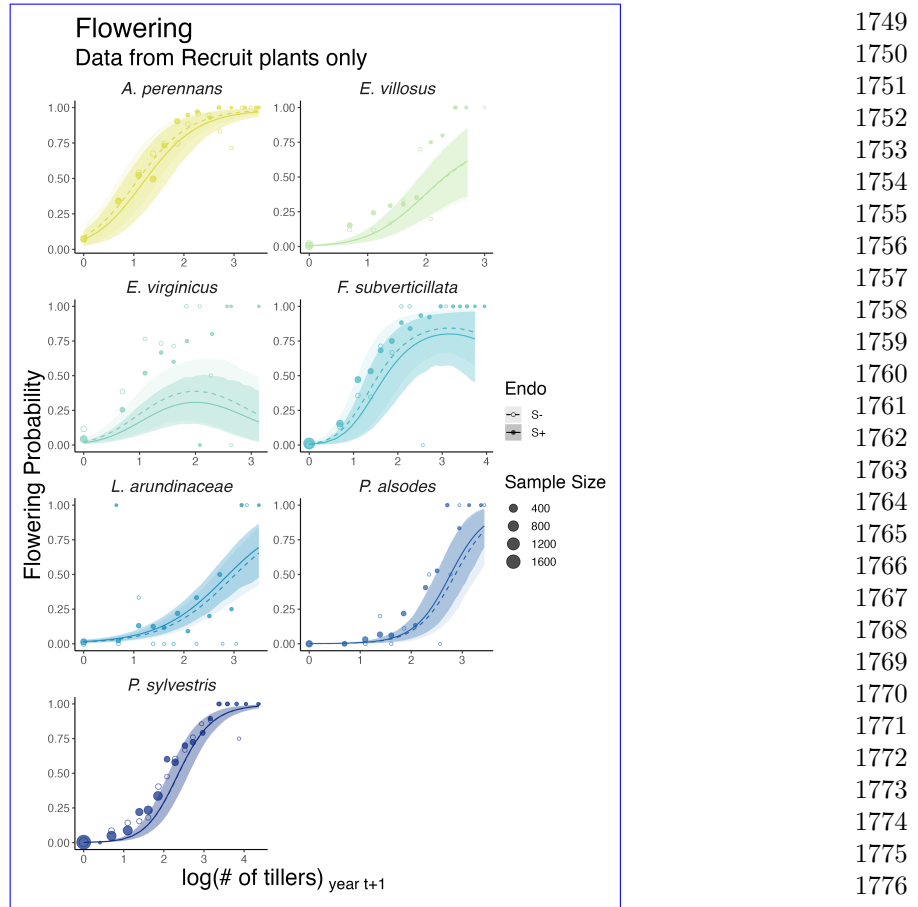


Figure 7: Effect of endophyte symbiosis on mean flowering. Fitted curves represent the size-specific mean flowering probability for recruited plants along with data binned by size and averaged over many individuals, years, and plots shown as open circles with a dashed line for symbiont-free (S-) plants, while the solid line and filled circles represent symbiotic (S+) plants. 80% credible intervals are shown with dark shading for S+, or light shading for S-.

1795

1796

1797

1798

1799

1800

1801

1802

1803

1804

1805

1806

1807

1808

1809

1810

1811

1812

1813

1814

1815

1816

1817

1818

1819

1820

1821

1822

1823

Figure 8: Effect of endophyte symbiosis on mean fertility. Fitted curves represent the size-specific mean expected number of flowering tillers for ~~original~~-originally transplanted plants along with data binned by size and averaged over many individuals, years, and plots shown as open circles with a dashed line for symbiont-free (S-) plants, while the solid line and filled circles represent symbiotic (S+) plants. 80% credible intervals are shown with dark shading for S+, or light shading for S-.

1824

1825

1826

1827

1828

1829

1830

1831

1832

1833

1834

1835

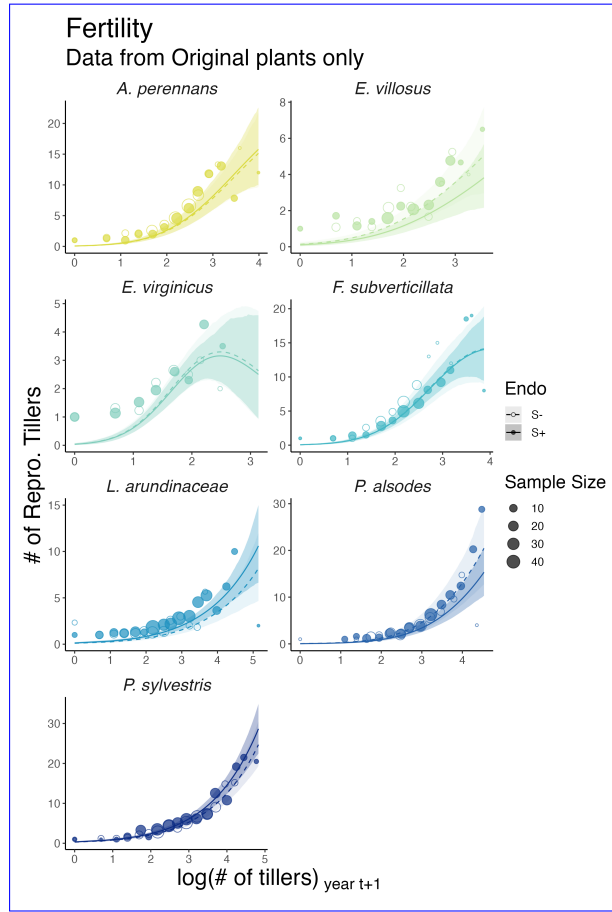
1836

1837

1838

1839

1840



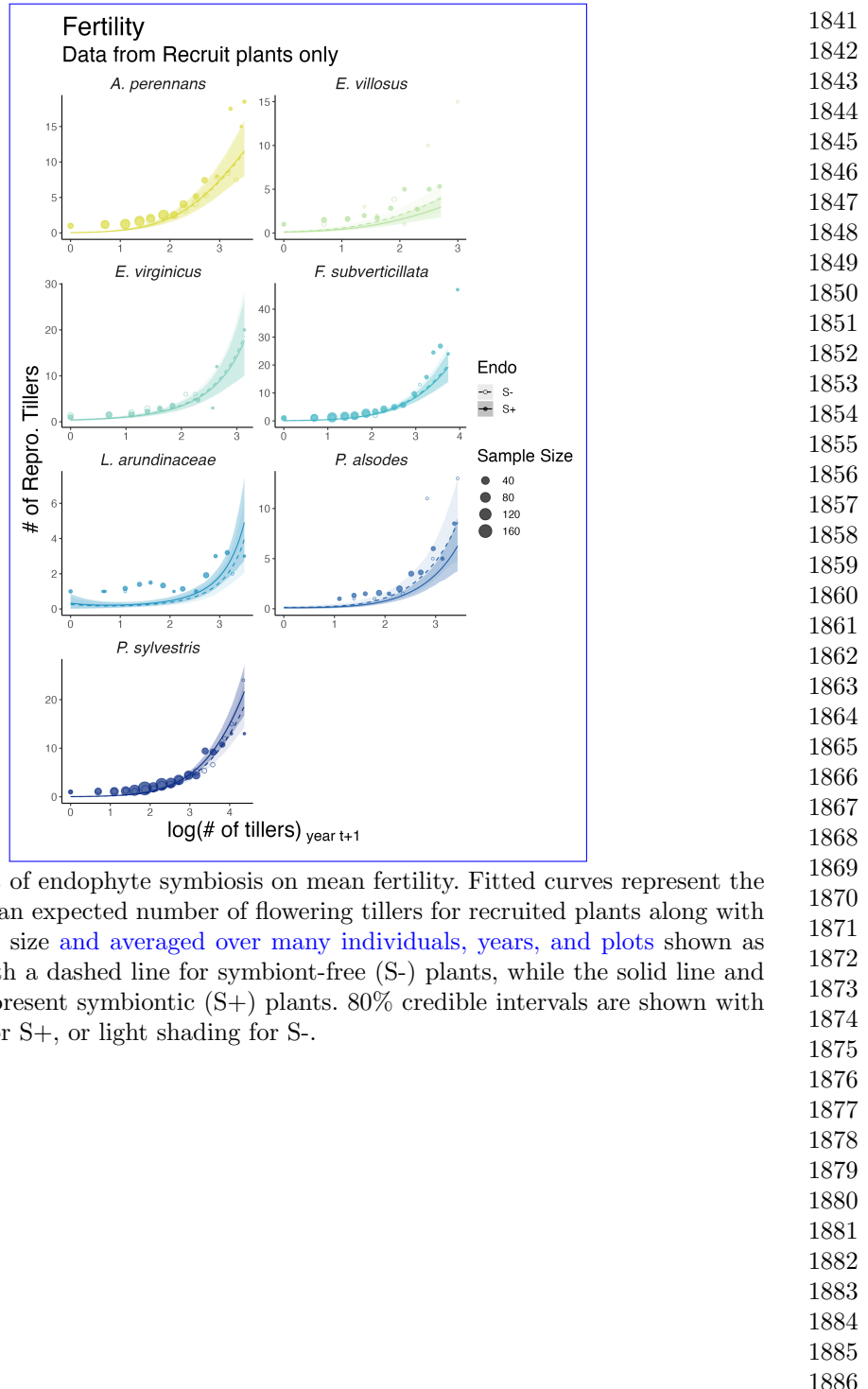


Figure 9: Effect of endophyte symbiosis on mean fertility. Fitted curves represent the size-specific mean expected number of flowering tillers for recruited plants along with data binned by size and averaged over many individuals, years, and plots shown as open circles with a dashed line for symbiont-free (S-) plants, while the solid line and filled circles represent symbiotic (S+) plants. 80% credible intervals are shown with dark shading for S+, or light shading for S-.

1887
 1888
 1889
 1890
 1891
 1892
 1893
 1894
 1895
 1896
 1897
 1898
 1899
 1900
 1901
 1902
 1903
 1904
 1905
 1906
 1907
 1908
 1909
 1910
 1911
 1912
 1913
 1914
 1915
 1916
 1917
 1918
 1919
 1920
 1921
 1922
 1923
 1924
 1925
 1926
 1927
 1928
 1929
 1930
 1931
 1932

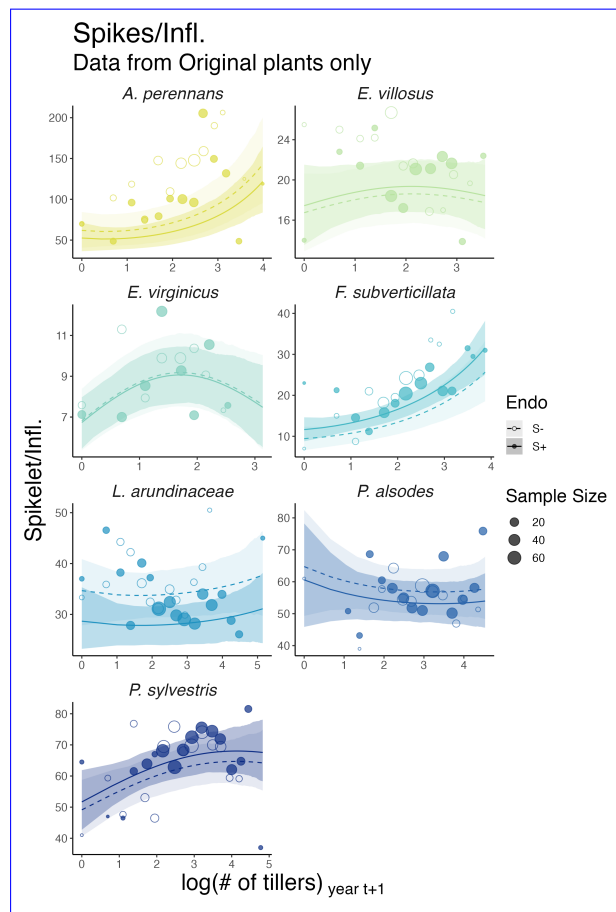


Figure 10: Effect of endophyte symbiosis on mean spikelet production. Fitted curves represent the size-specific mean expected number of spikelets per inflorescence for **original** **originally transplanted** plants along with data binned by size **and averaged** over many individuals, years, and plots shown as open circles with a dashed line for symbiont-free (S-) plants, while the solid line and filled circles represent symbiotic (S+) plants. 80% credible intervals are shown with dark shading for S+, or light shading for S-.

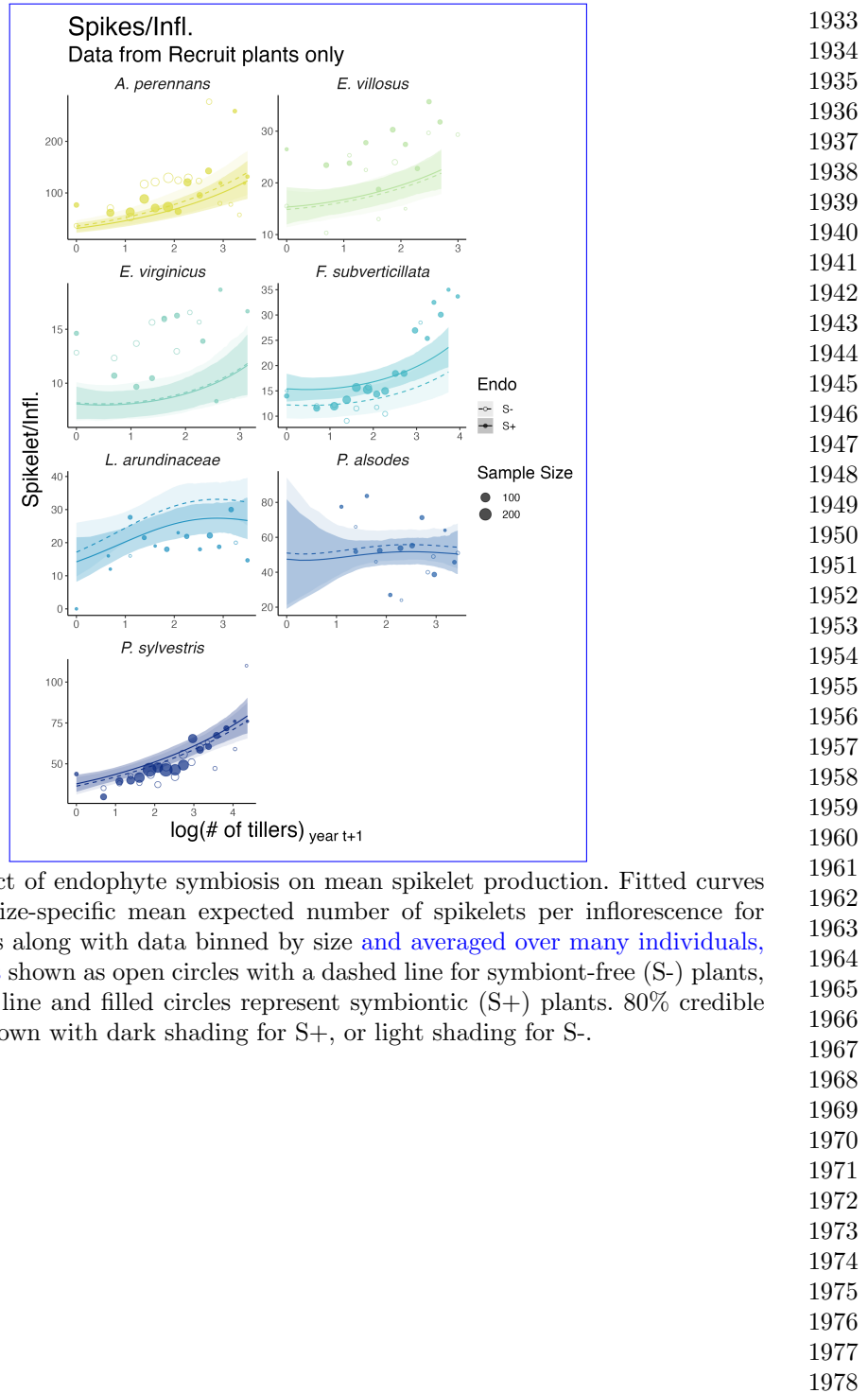


Figure 11: Effect of endophyte symbiosis on mean spikelet production. Fitted curves represent the size-specific mean expected number of spikelets per inflorescence for recruited plants along with data binned by size and averaged over many individuals, years, and plots shown as open circles with a dashed line for symbiont-free (S-) plants, while the solid line and filled circles represent symbiotic (S+) plants. 80% credible intervals are shown with dark shading for S+, or light shading for S-.

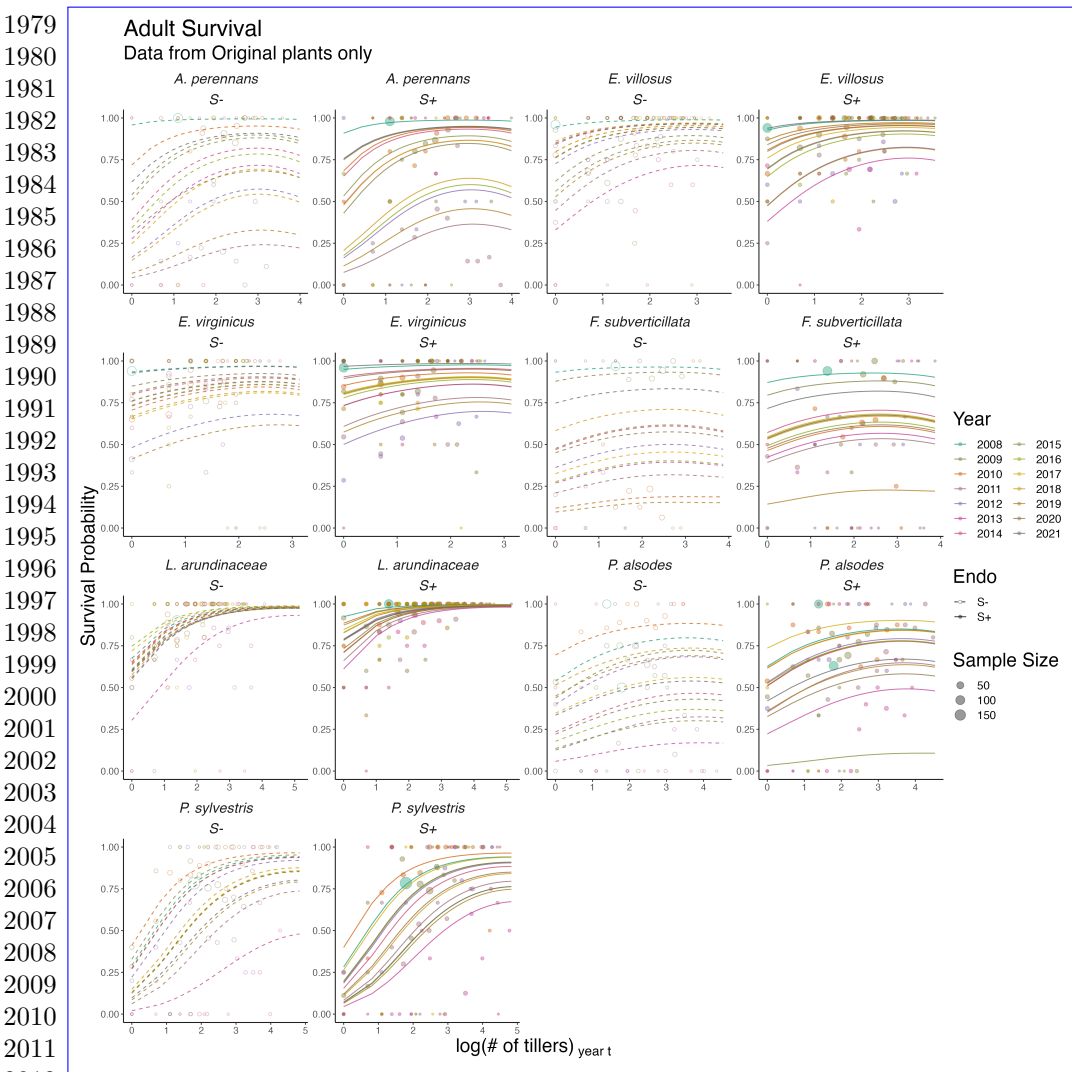


Figure 12: Effect of endophyte symbiosis on yearly adult survival. Fitted curves represent the size-specific annual survival probability for ~~original~~ originally transplanted plants along with data binned by size and census year and averaged over many individuals, and plots shown as open circles with a dashed line for symbiont-free (S-) plants, while the solid line and filled circles represent symbiotic (S+) plants.

2017
2018
2019
2020
2021
2022
2023
2024

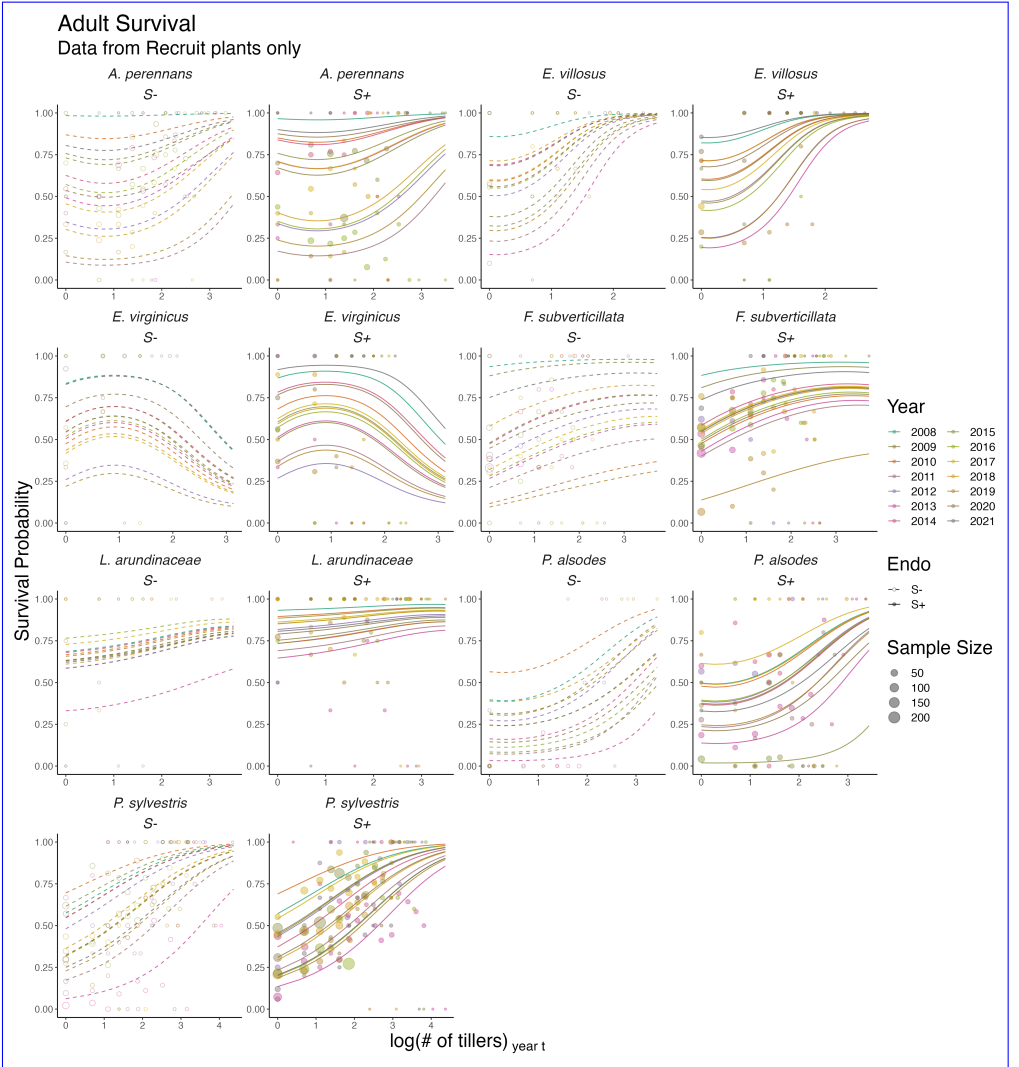
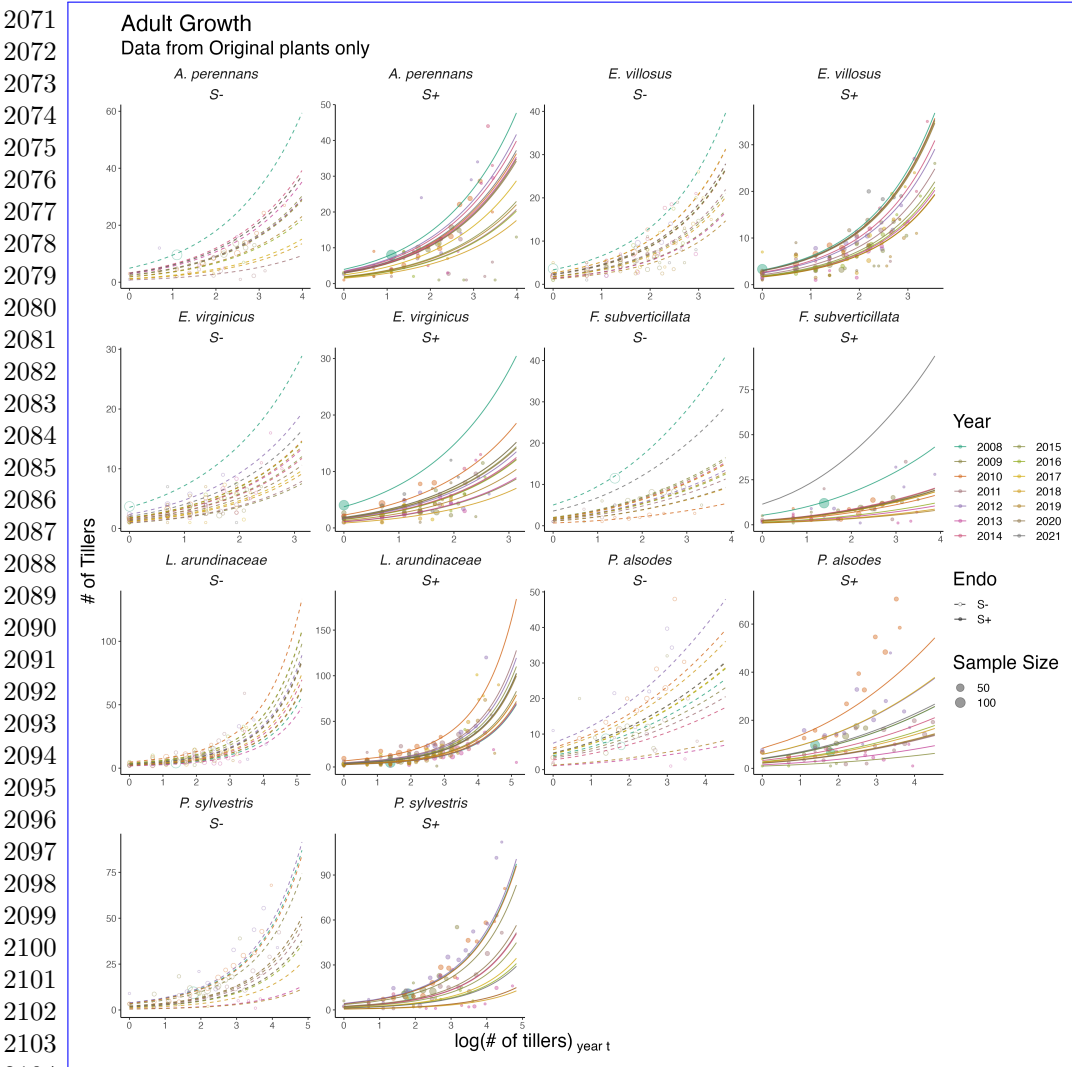


Figure 13: Effect of endophyte symbiosis on yearly adult survival. Fitted curves represent the size-specific annual survival probability for recruited plants along with data binned by size and census year and averaged over many individuals, and plots shown as open circles with a dashed line for symbiont-free (S-) plants, while the solid line and filled circles represent symbiotic (S+) plants.



2104 Figure 14: Effect of endophyte symbiosis on yearly adult growth. Fitted curves rep-
 2105 resent the size-specific annual expected plant size for ~~original~~ originally transplanted
 2106 plants along with data binned by size and census year **and averaged over many individ-**
 2107 **uals, and plots** shown as open circles with a dashed line for symbiont-free (S-) plants,
 2108 while the solid line and filled circles represent symbiotic (S+) plants.
 2109

2110
 2111
 2112
 2113
 2114
 2115
 2116

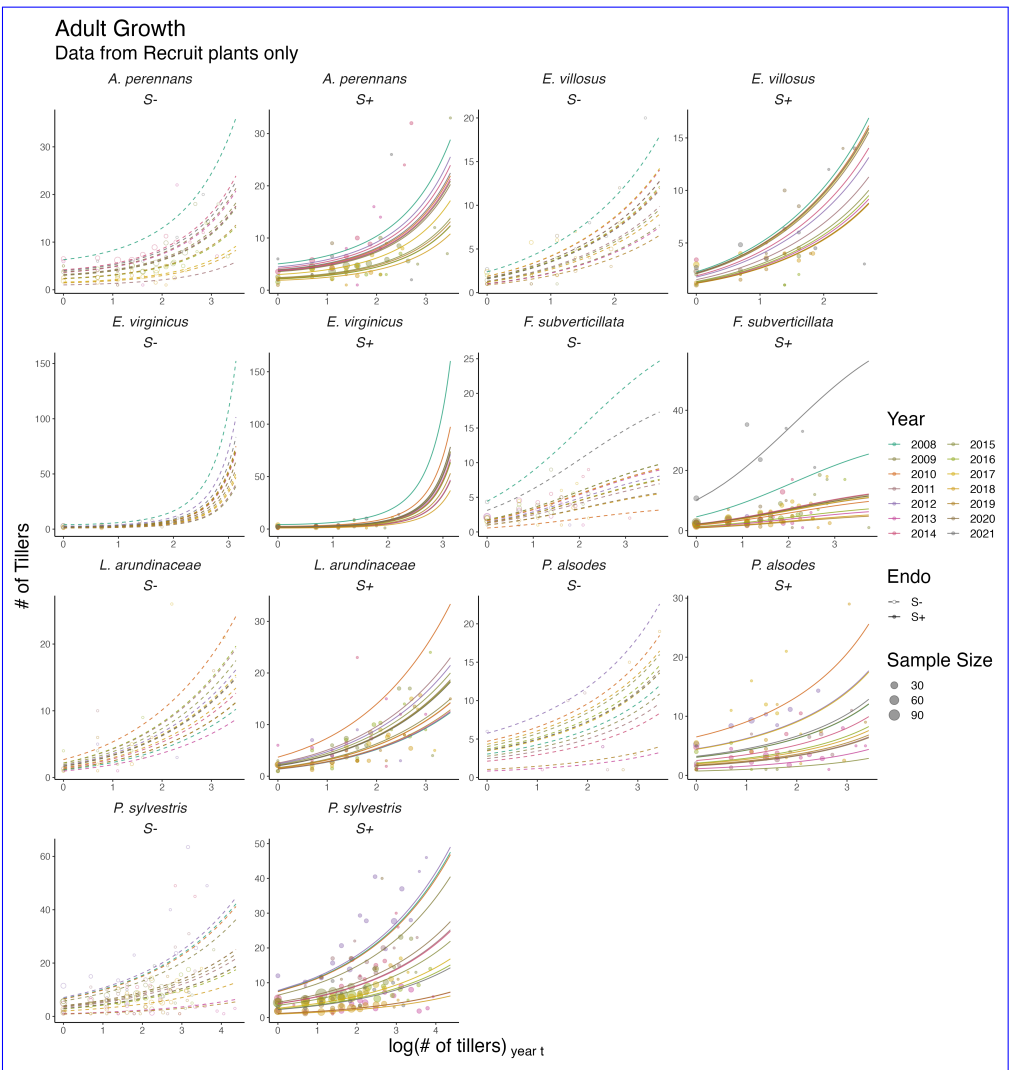
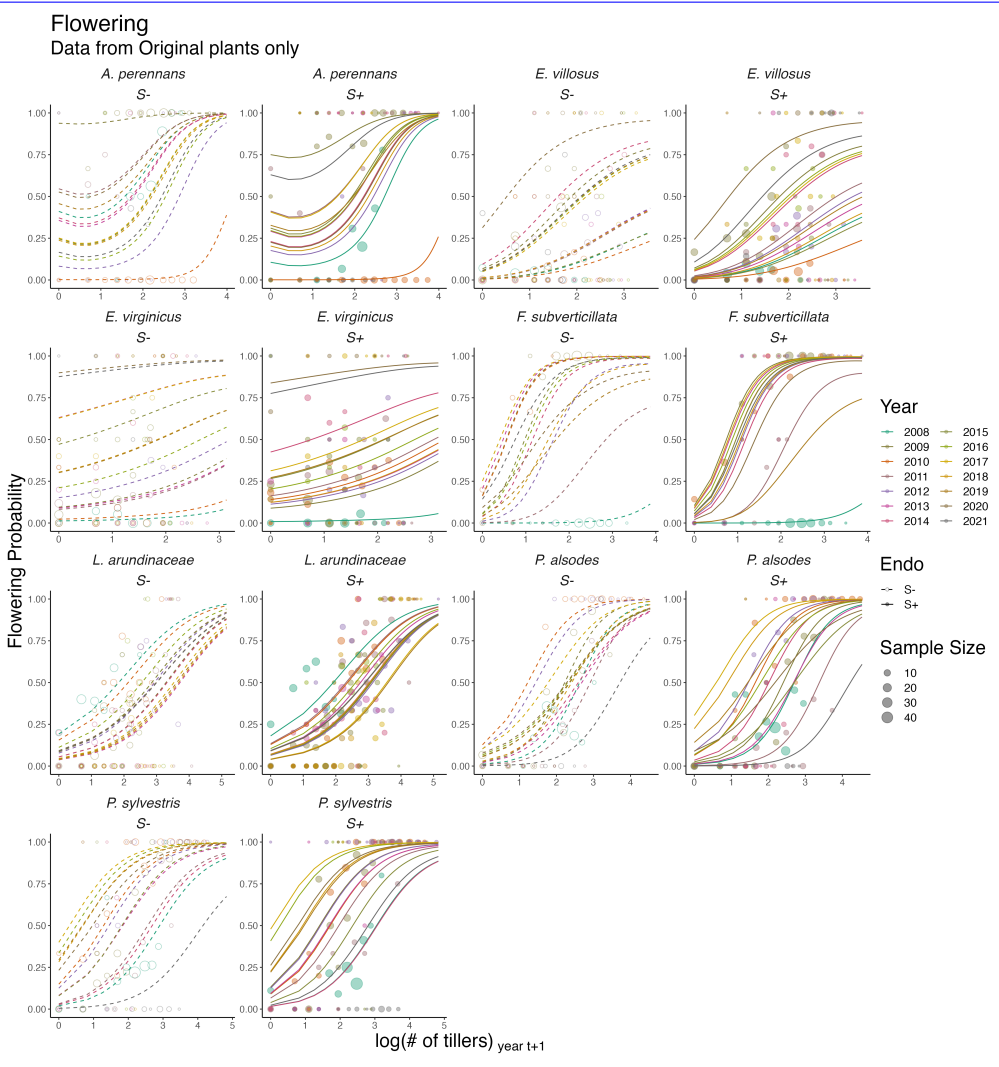


Figure 15: Effect of endophyte symbiosis on yearly adult growth. Fitted curves represent the size-specific annual expected plant size for recruited plants along with data binned by size and census year and averaged over many individuals, and plots shown as open circles with a dashed line for symbiont-free (S-) plants, while the solid line and filled circles represent symbiotic (S+) plants.

2117
 2118
 2119
 2120
 2121
 2122
 2123
 2124
 2125
 2126
 2127
 2128
 2129
 2130
 2131
 2132
 2133
 2134
 2135
 2136
 2137
 2138
 2139
 2140
 2141
 2142
 2143
 2144
 2145
 2146
 2147
 2148
 2149
 2150
 2151
 2152
 2153
 2154
 2155
 2156
 2157
 2158
 2159
 2160
 2161
 2162



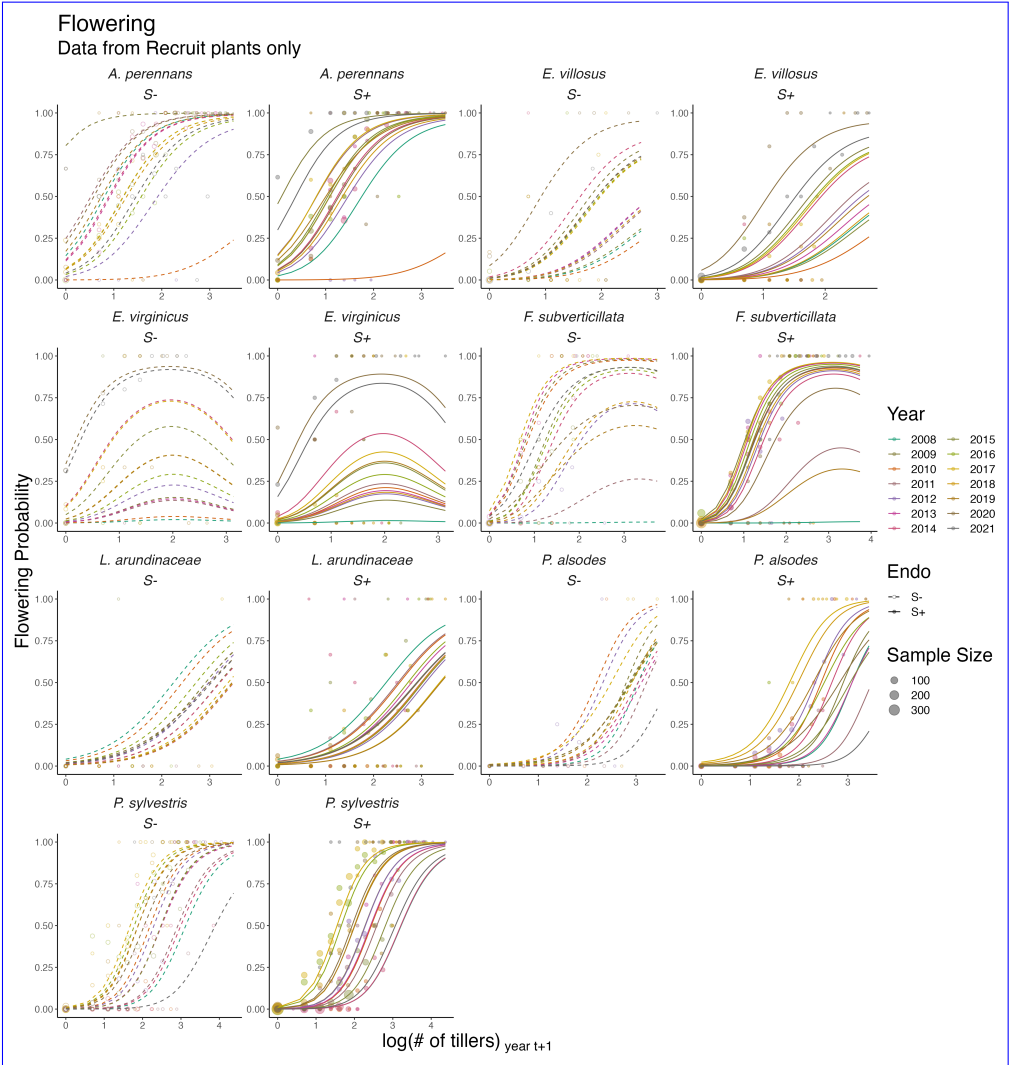
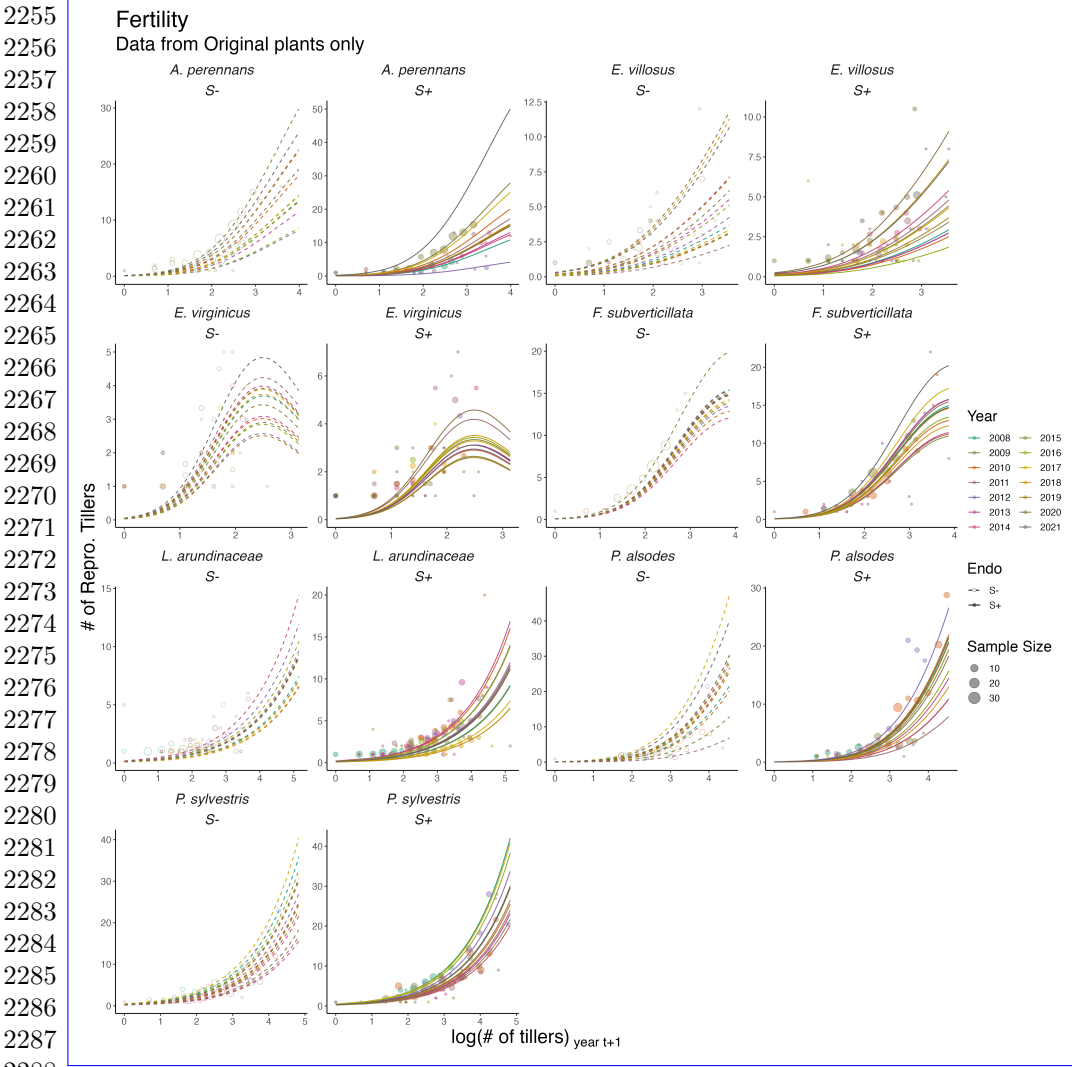


Figure 17: Effect of endophyte symbiosis on yearly flowering. Fitted curves represent the size-specific annual flowering probability for recruited plants along with data binned by size and census year and averaged over many individuals, and plots shown as open circles with a dashed line for symbiont-free (S-) plants, while the solid line and filled circles represent symbiotic (S+) plants.

2209
2210
2211
2212
2213
2214
2215
2216
2217
2218
2219
2220
2221
2222
2223
2224
2225
2226
2227
2228
2229
2230
2231
2232
2233
2234
2235
2236
2237
2238
2239
2240
2241
2242
2243
2244
2245
2246
2247
2248
2249
2250
2251
2252
2253
2254



2289 Figure 18: Effect of endophyte symbiosis on yearly fertility. Fitted curves represent the
2290 size-specific annual expected number of flowering tillers for ~~original~~ originally trans-
2291 planted plants along with data binned by size and census year **and averaged over many**
2292 individuals, **and plots** shown as open circles with a dashed line for symbiont-free (*S-*)
2293 plants, while the solid line and filled circles represent symbiotic (*S+*) plants.
2294
2295
2296
2297
2298
2299
2300

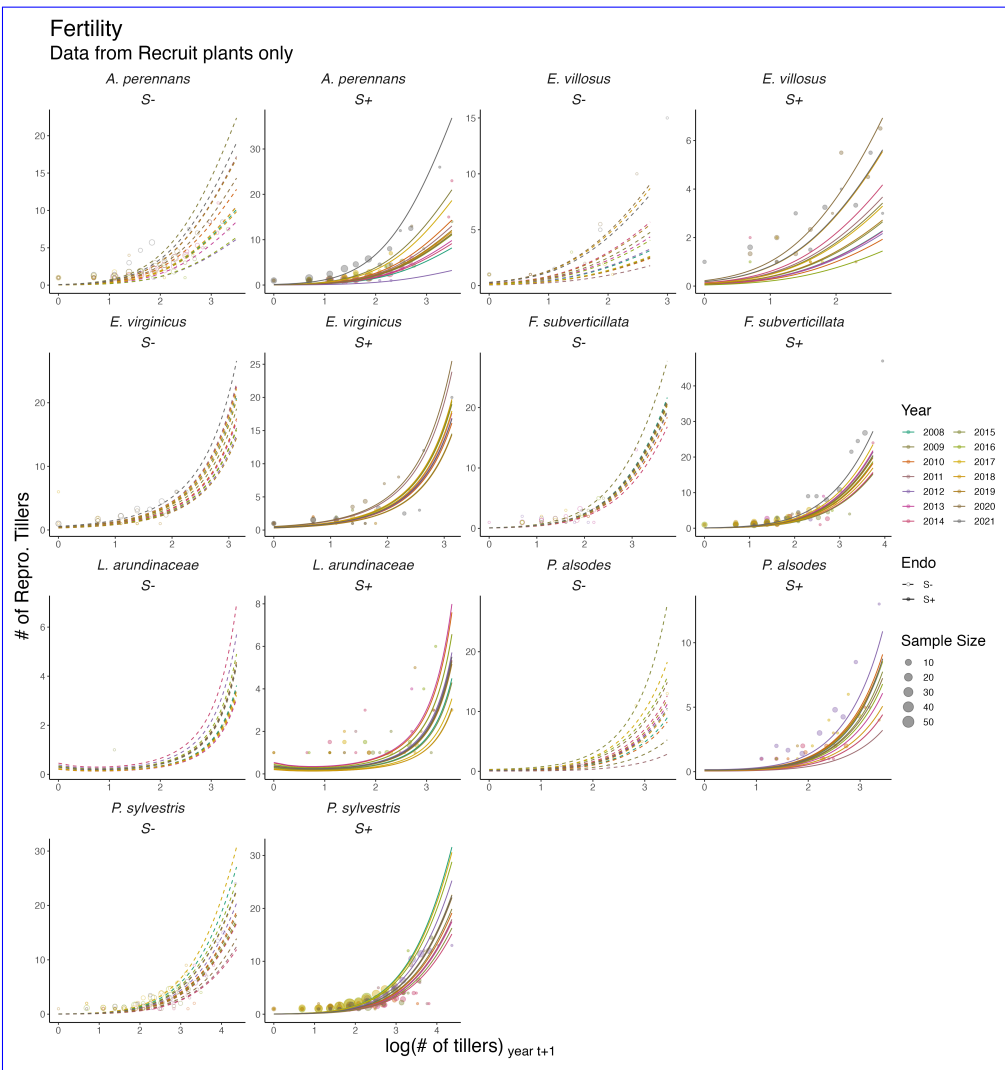
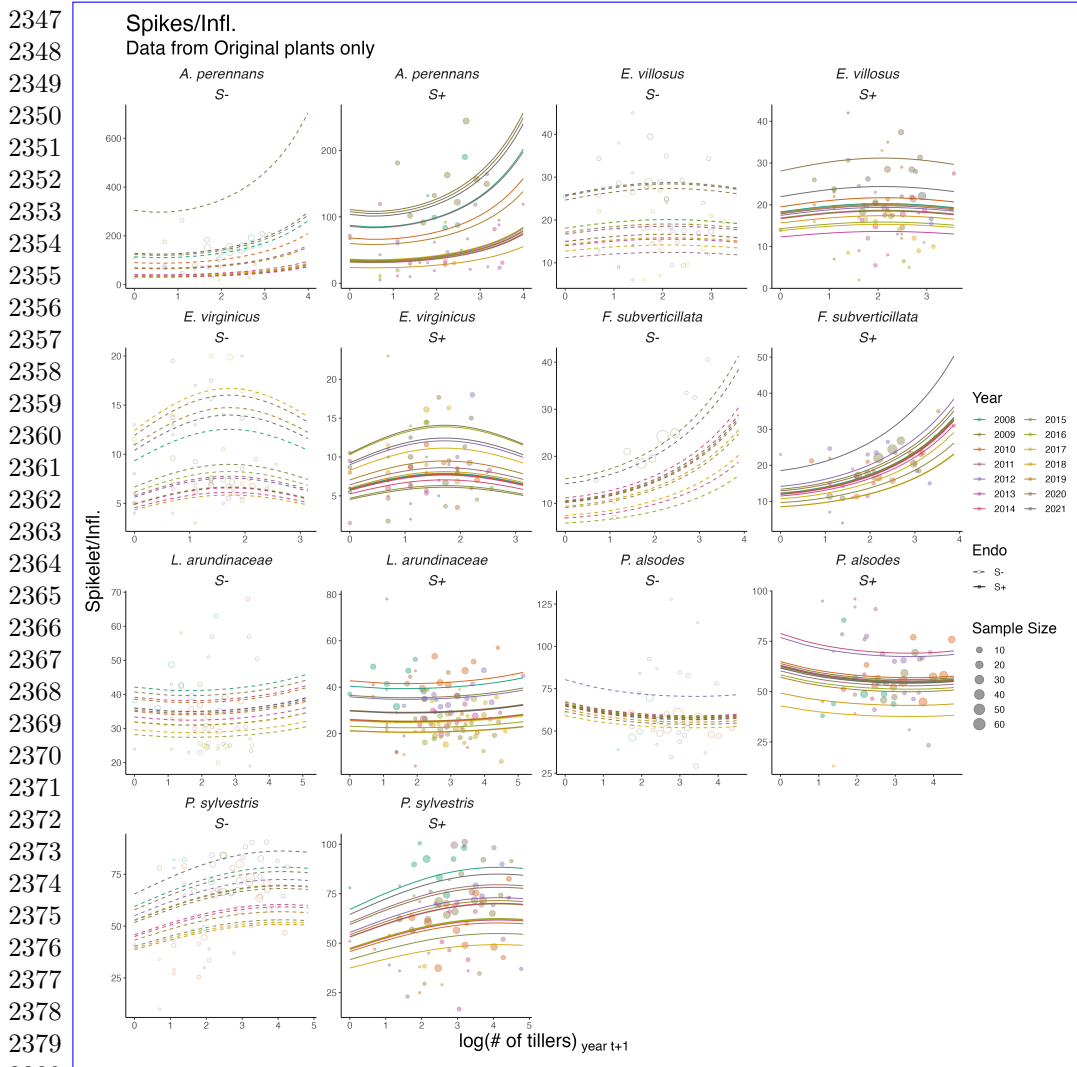


Figure 19: Effect of endophyte symbiosis on yearly fertility. Fitted curves represent the size-specific annual expected number of flowering tillers for recruited plants along with data binned by size and census year and averaged over many individuals, and plots shown as open circles with a dashed line for symbiont-free (S-) plants, while the solid line and filled circles represent symbiotic (S+) plants.

2301
2302
2303
2304
2305
2306
2307
2308
2309
2310
2311
2312
2313
2314
2315
2316
2317
2318
2319
2320
2321
2322
2323
2324
2325
2326
2327
2328
2329
2330
2331
2332
2333
2334
2335
2336
2337
2338
2339
2340
2341
2342
2343
2344
2345
2346



2380 Figure 20: Effect of endophyte symbiosis on yearly spikelet production. Fitted curves
2381 represent the size-specific annual expected number of spikelets per inflorescence for
2382 **original originally transplanted** plants along with data binned by size and census year
2383 and averaged over many individuals, and plots shown as open circles with a dashed line
2384 for symbiont-free (S-) plants, while the solid line and filled circles represent symbiotic
2385 (S+) plants.

2386
2387
2388
2389
2390
2391
2392

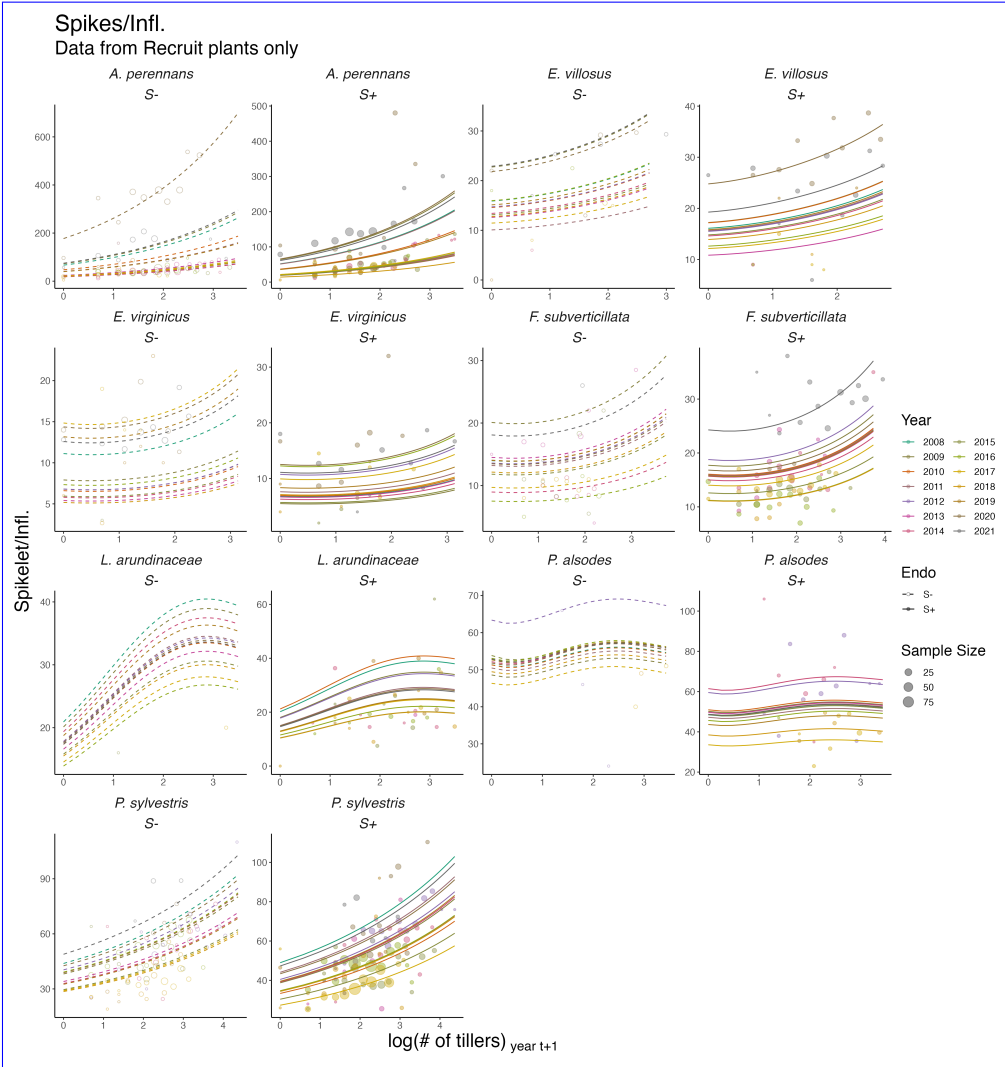
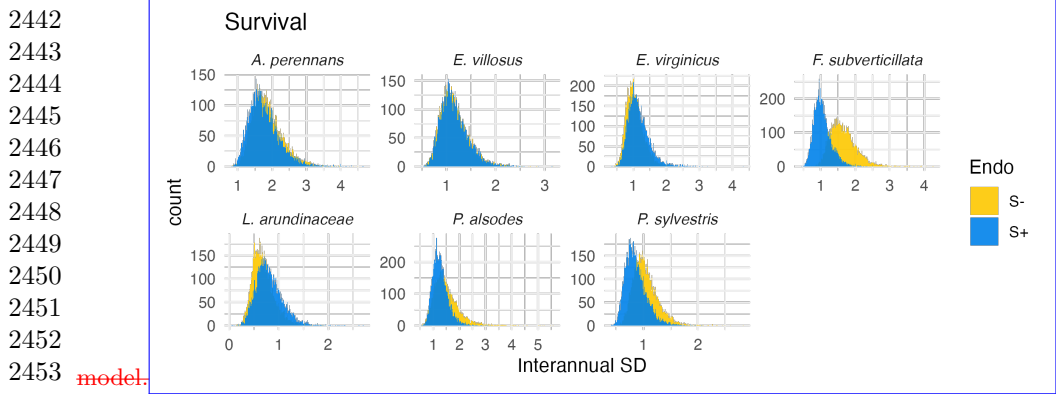


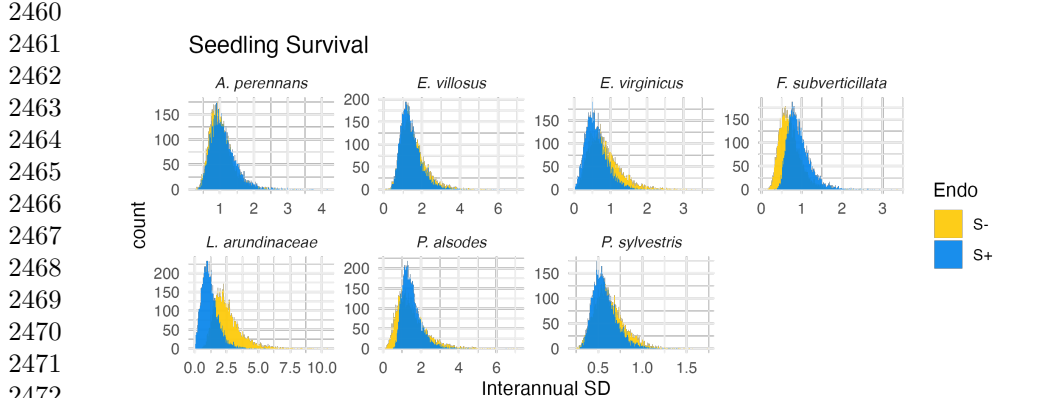
Figure 21: Effect of endophyte symbiosis on yearly spikelet production. Fitted curves represent the size-specific annual expected number of spikelets per inflorescence for recruited plants along with data binned by size and census year **and averaged over many individuals, and plots** shown as open circles with a dashed line for symbiont-free (S-) plants, while the solid line and filled circles represent symbiotic (S+) plants.

2393
2394
2395
2396
2397
2398
2399
2400
2401
2402
2403
2404
2405
2406
2407
2408
2409
2410
2411
2412
2413
2414
2415
2416
2417
2418
2419
2420
2421
2422
2423
2424
2425
2426
2427
2428
2429
2430
2431
2432
2433
2434
2435
2436
2437
2438

2439 Posterior distributions of the standard deviations of inter-annual year effects for survival.
 2440 Histograms include 7500 post-warmup MCMC samples for symbiotic (S+; blue) and
 2441 symbiont-free (S-; tan) plants from fitted vital rate



2454 Figure 22: Posterior distributions of the standard deviations of inter-annual year effects
 2455 for survival. Histograms include 7500 post-warmup MCMC samples for symbiotic (S+;
 2456 blue) and symbiont-free (S-; tan) plants from fitted vital rate model.
 2457



2473 Figure 23: Posterior distributions of the standard deviations of inter-annual year
 2474 effects for seedling survival. Histograms include 7500 post-warmup MCMC samples for
 2475 symbiotic (S+; blue) and symbiont-free (S-; tan) plants from fitted vital rate model.
 2476

2477
 2478
 2479
 2480
 2481
 2482
 2483
 2484

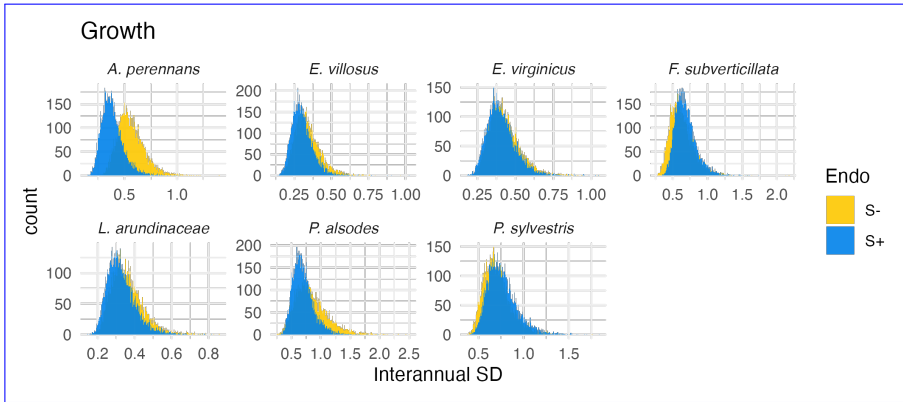


Figure 24: Posterior distributions of the standard deviations of inter-annual year effects for growth. Histograms include 7500 post-warmup MCMC samples for symbiotic (S+; blue) and symbiont-free (S-; tan) plants from fitted vital rate model.

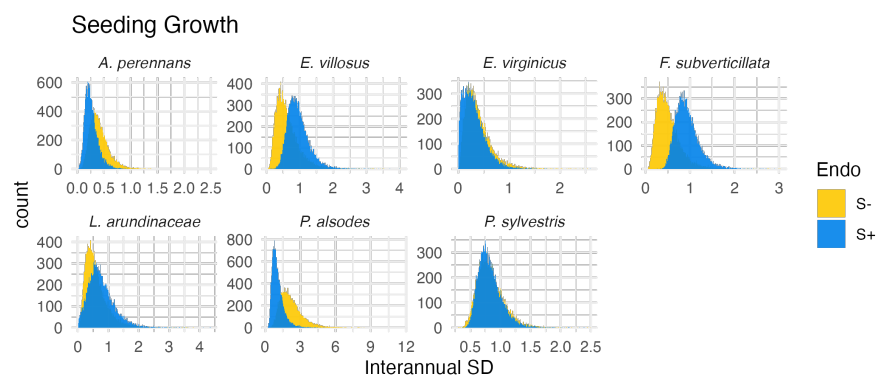
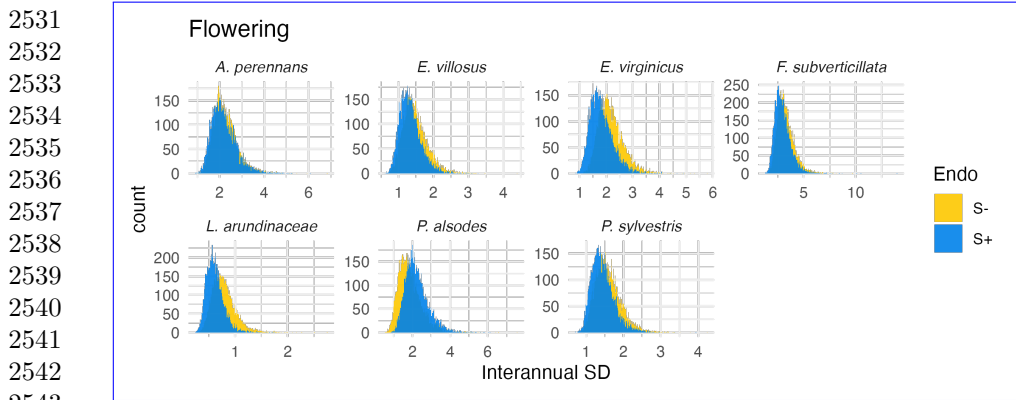
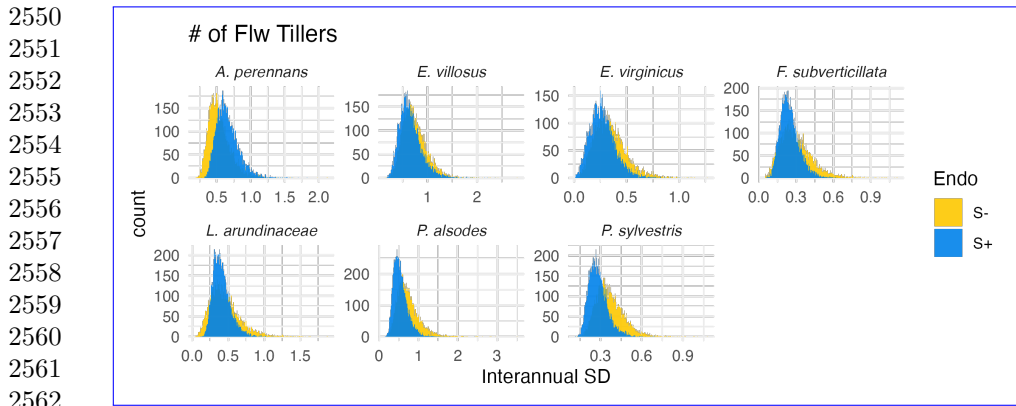


Figure 25: Posterior distributions of the standard deviations of inter-annual year effects for seedling growth. Histograms include 7500 post-warmup MCMC samples for symbiotic (S+; blue) and symbiont-free (S-; tan) plants from fitted vital rate model.

2485
2486
2487
2488
2489
2490
2491
2492
2493
2494
2495
2496
2497
2498
2499
2500
2501
2502
2503
2504
2505
2506
2507
2508
2509
2510
2511
2512
2513
2514
2515
2516
2517
2518
2519
2520
2521
2522
2523
2524
2525
2526
2527
2528
2529
2530



2547
 2548
 2549



2567
 2568
 2569
 2570
 2571
 2572
 2573
 2574
 2575
 2576

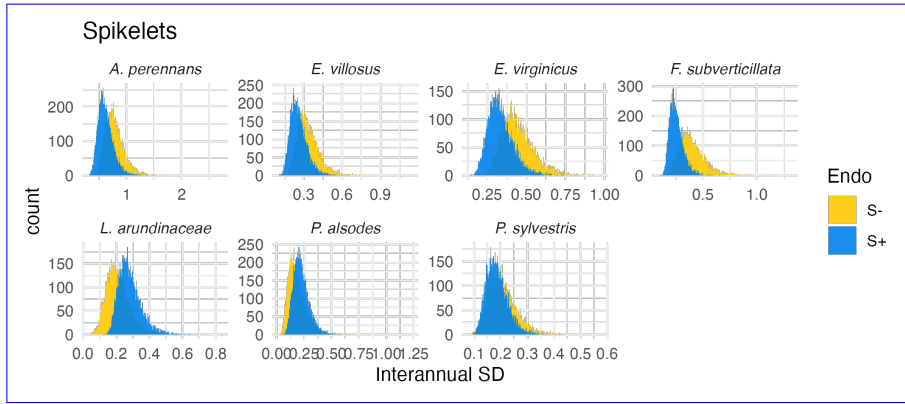


Figure 28: Posterior distributions of the standard deviations of inter-annual year effects for spikelets per inflorescence. Histograms include 7500 post-warmup MCMC samples for symbiotic (S+; blue) and symbiont-free (S-; tan) plants from fitted vital rate model.

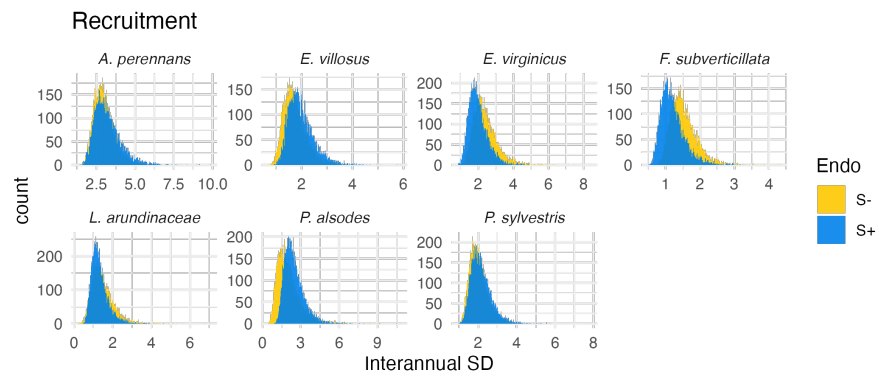
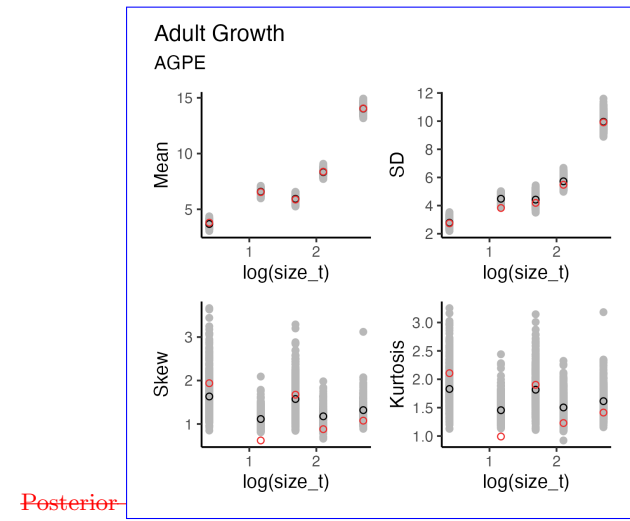


Figure 29: Posterior distributions of the standard deviations of inter-annual year effects for recruitment. Histograms include 7500 post-warmup MCMC samples for symbiotic (S+; blue) and symbiont-free (S-; tan) plants from fitted vital rate model.

2577
2578
2579
2580
2581
2582
2583
2584
2585
2586
2587
2588
2589
2590
2591
2592
2593
2594
2595
2596
2597
2598
2599
2600
2601
2602
2603
2604
2605
2606
2607
2608
2609
2610
2611
2612
2613
2614
2615
2616
2617
2618
2619
2620
2621
2622

2623
2624
2625
2626
2627
2628
2629
2630
2631
2632
2633
2634
2635
2636
2637
2638



2639 Figure 30: Graphical posterior predictive check for ~~statistical model~~-mean and higher
2640 moments of ~~Adult Survival~~*A. perennans* growth model across size. Consistency between
2641 real data and ~~simulated~~ fitted values across sizes indicates that ~~fitted models describe~~ the
2642 ~~data well~~vital rate models are accurately capturing size dependence. ~~Lines Points~~ show
2643 ~~density distributions~~the value of statistical moments binned across size for the observed
2644 data (~~blue lines~~red circles) compared to ~~data~~the simulated ~~from fitted models~~datasets
2645 (~~tan lines~~grey circles) and the median of the simulated values (black circles) generated
2646 from 500 posterior draws from ~~posterior distributions of model parameters along with the~~
2647 ~~distribution's moments~~fitted model.

2648
2649
2650
2651
2652
2653
2654
2655
2656
2657
2658
2659
2660
2661
2662
2663
2664
2665
2666
2667
2668

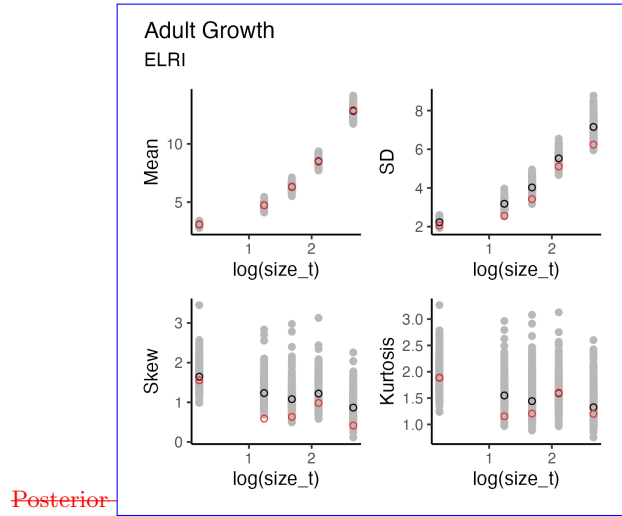
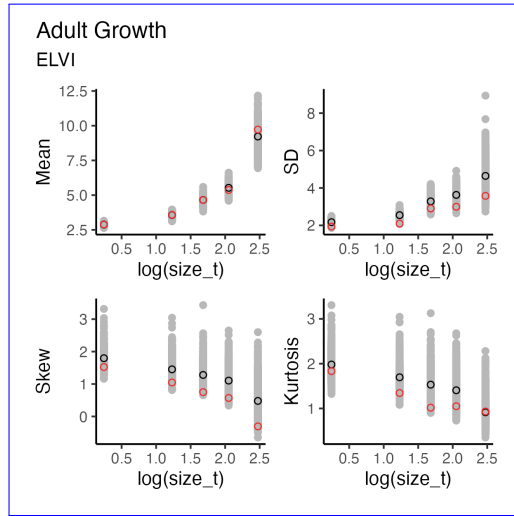


Figure 31: Graphical posterior predictive check for [statistical model mean](#) and higher moments of [Seedling Survival](#) *E. villosus* growth model across size. Consistency between real data and [simulated fitted](#) values across sizes indicates that [fitted models describe](#) the [data well](#) vital rate models are accurately capturing size dependence. [Lines Points](#) show [density distributions](#) the value of statistical moments binned across size for the observed data ([blue lined circles](#)) compared to [data](#) the simulated [from fitted models](#) datasets ([tan lines](#) grey circles) and the median of the simulated values (black circles) generated from 500 posterior draws from [posterior distributions of model parameters along with](#) the [distribution's moments](#) fitted model.

2669
2670
2671
2672
2673
2674
2675
2676
2677
2678
2679
2680
2681
2682
2683
2684
2685
2686
2687
2688
2689
2690
2691
2692
2693
2694
2695
2696
2697
2698
2699
2700
2701
2702
2703
2704
2705
2706
2707
2708
2709
2710
2711
2712
2713
2714

2715
2716
2717
2718
2719
2720
2721
2722
2723
2724
2725
2726
2727
2728
2729
2730



2731 Figure 32: Graphical posterior predictive check for mean and higher moments of *E.*
2732 *virginicus* growth model across size. Consistency between real data and fitted values
2733 across sizes indicates that the vital rate models are accurately capturing size depen-
2734 dence. Points show the value of statistical moments binned across size for the observed
2735 data (red circles) compared to the simulated datasets (grey circles) and the median
2736 of the simulated values (black circles) generated from 500 posterior draws from the
2737 fitted model.

2738
2739
2740
2741
2742
2743
2744
2745
2746
2747
2748
2749
2750
2751
2752
2753
2754
2755
2756
2757
2758
2759
2760

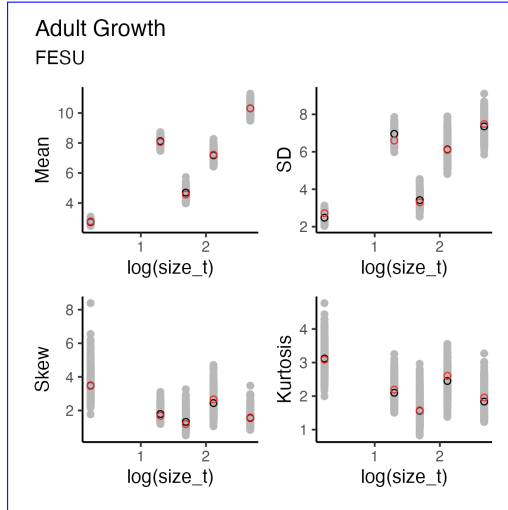


Figure 33: Graphical posterior predictive check for mean and higher moments of *F. subverticillata* growth model across size. Consistency between real data and fitted values across sizes indicates that the vital rate models are accurately capturing size dependence. Points show the value of statistical moments binned across size for the observed data (red circles) compared to the simulated datasets (grey circles) and the median of the simulated values (black circles) generated from 500 posterior draws from the fitted model.

2761
 2762
 2763
 2764
 2765
 2766
 2767
 2768
 2769
 2770
 2771
 2772
 2773
 2774
 2775
 2776
 2777
 2778
 2779
 2780
 2781
 2782
 2783
 2784
 2785
 2786
 2787
 2788
 2789
 2790
 2791
 2792
 2793
 2794
 2795
 2796
 2797
 2798
 2799
 2800
 2801
 2802
 2803
 2804
 2805
 2806

2807

2808

2809

2810

2811

2812

2813

2814

2815

2816

2817

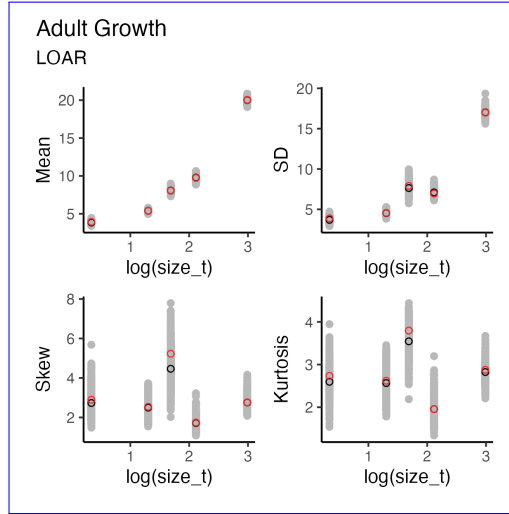
2818

2819

2820

2821

2822



2823 Figure 34: Graphical posterior predictive check for mean and higher moments of *L.*
 2824 *arundinacea* growth model across size. Consistency between real data and fitted values
 2825 across sizes indicates that the vital rate models are accurately capturing size depen-
 2826 dence. Points show the value of statistical moments binned across size for the observed
 2827 data (red circles) compared to the simulated datasets (grey circles) and the median
 2828 of the simulated values (black circles) generated from 500 posterior draws from the
 2829 fitted model.

2830

2831

2832

2833

2834

2835

2836

2837

2838

2839

2840

2841

2842

2843

2844

2845

2846

2847

2848

2849

2850

2851

2852

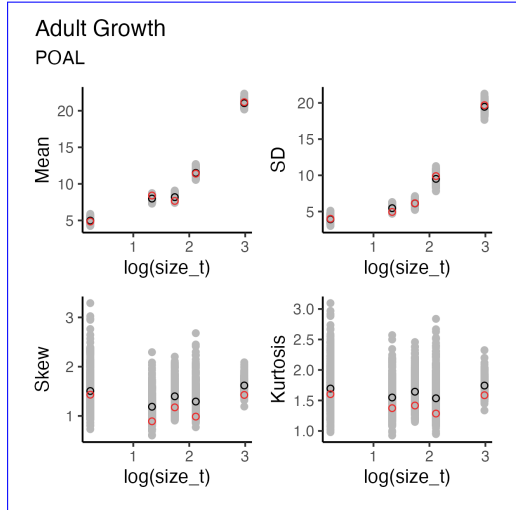


Figure 35: Graphical posterior predictive check for mean and higher moments of *P. alsodes* growth model across size. Consistency between real data and fitted values across sizes indicates that the vital rate models are accurately capturing size dependence. Points show the value of statistical moments binned across size for the observed data (red circles) compared to the simulated datasets (grey circles) and the median of the simulated values (black circles) generated from 500 posterior draws from the fitted model.

```

2853
2854
2855
2856
2857
2858
2859
2860
2861
2862
2863
2864
2865
2866
2867
2868
2869
2870
2871
2872
2873
2874
2875
2876
2877
2878
2879
2880
2881
2882
2883
2884
2885
2886
2887
2888
2889
2890
2891
2892
2893
2894
2895
2896
2897
2898

```

2899

2900

2901

2902

2903

2904

2905

2906

2907

2908

2909

2910

2911

2912

2913

2914

2915

Figure 36: Graphical posterior predictive check for mean and higher moments of *P. sylvestris* growth model across size. Consistency between real data and fitted values across sizes indicates that the vital rate models are accurately capturing size dependence. Points show the value of statistical moments binned across size for the observed data (red circles) compared to the simulated datasets (grey circles) and the median of the simulated values (black circles) generated from 500 posterior draws from the fitted model.

2916

2917

2918

2919

2920

2921

2922

2923

2924

2925

2926

2927

2928

2929

2930

2931

2932

2933

2934

2935

2936

2937

2938

2939

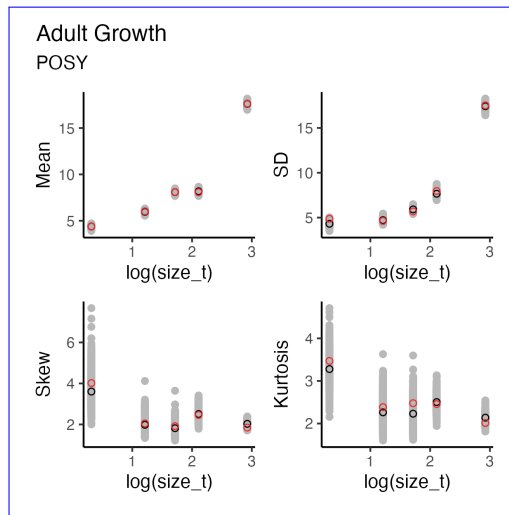
2940

2941

2942

2943

2944



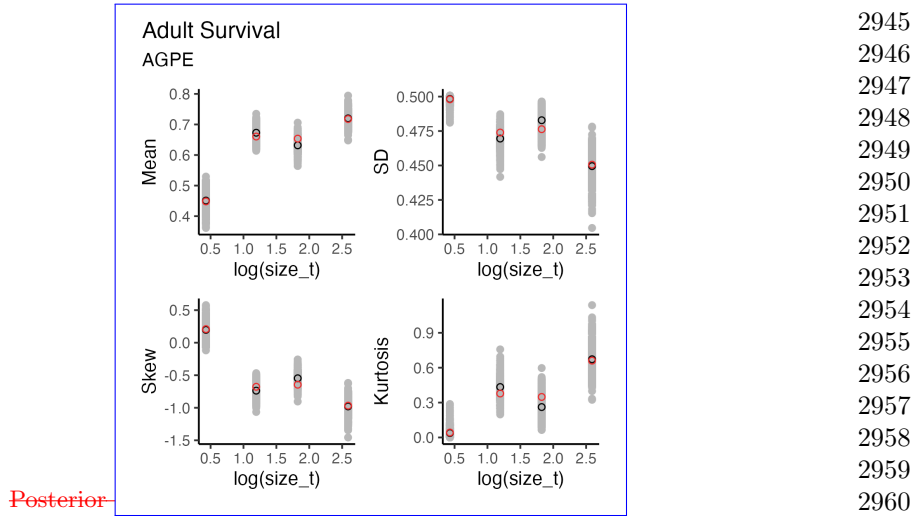
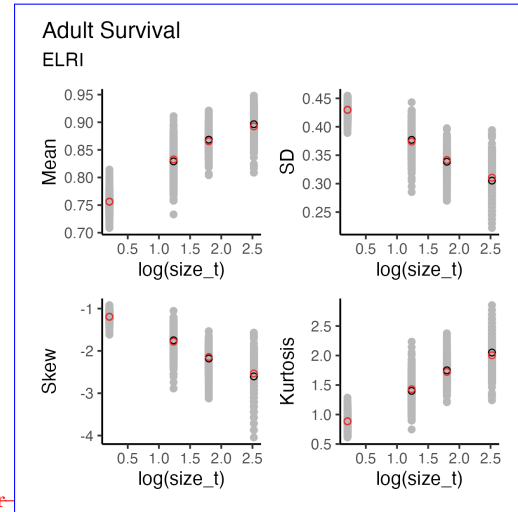


Figure 37: Graphical posterior predictive check for [statistical model mean](#) and higher moments of [Adult Growth](#). *A. perennans* survival model across size. Consistency between real data and [simulated fitted](#) values across sizes indicates that [fitted models describe](#) the [data well](#) vital rate models are accurately capturing size dependence. [Lines Points](#) show [density distributions](#) the value of statistical moments binned across size for the observed data ([blue lined circles](#)) compared to [data](#) the simulated [from fitted models](#) datasets ([tan lines](#) grey circles) and the median of the simulated values (black circles) generated from 500 posterior draws from [posterior distributions of model parameters along with](#) the [distribution's moments](#) fitted model.

2945
2946
2947
2948
2949
2950
2951
2952
2953
2954
2955
2956
2957
2958
2959
2960
2961
2962
2963
2964
2965
2966
2967
2968
2969
2970
2971
2972
2973
2974
2975
2976
2977
2978
2979
2980
2981
2982
2983
2984
2985
2986
2987
2988
2989
2990

2991
 2992
 2993
 2994
 2995
 2996
 2997
 2998
 2999
 3000
 3001
 3002
 3003
 3004
 3005
 3006
 3016
 3017
 3018
 3019
 3020
 3021
 3022
 3023
 3024
 3025
 3026
 3027
 3028
 3029
 3030
 3031
 3032
 3033
 3034
 3035
 3036



3007 Figure 38: Graphical posterior predictive check for ~~statistical model~~-mean and higher
 3008 moments of ~~Seedling Growth~~*E. villosus* survival model across size. Consistency between
 3009 real data and ~~simulated~~ fitted values across sizes indicates that ~~fitted models describe~~ the
 3010 ~~data well~~vital rate models are accurately capturing size dependence. ~~Lines Points~~ show
 3011 ~~density distributions~~the value of statistical moments binned across size for the observed
 3012 data (~~blue line~~red circles) compared to ~~data~~the simulated ~~from fitted models~~datasets
 3013 (~~tan lines~~grey circles) and the median of the simulated values (black circles) generated
 3014 from 500 posterior draws from ~~posterior distributions of model parameters along with the~~
 3015 ~~distribution's moments~~fitted model.

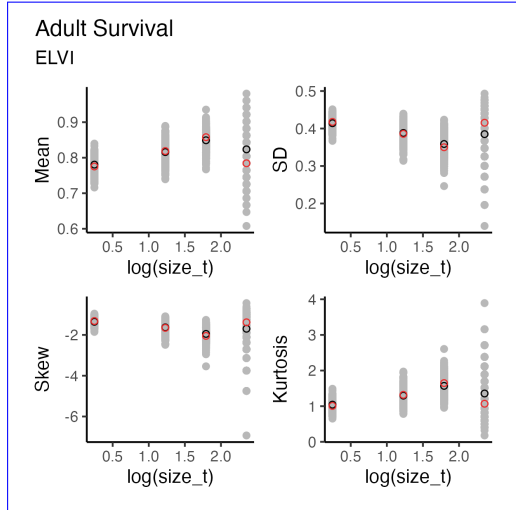
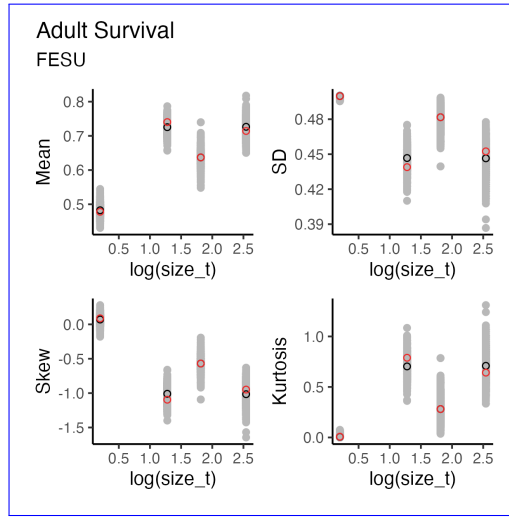


Figure 39: Graphical posterior predictive check for mean and higher moments of *E. virginicus* survival model across size. Consistency between real data and fitted values across sizes indicates that the vital rate models are accurately capturing size dependence. Points show the value of statistical moments binned across size for the observed data (red circles) compared to the simulated datasets (grey circles) and the median of the simulated values (black circles) generated from 500 posterior draws from the fitted model.

3037
3038
3039
3040
3041
3042
3043
3044
3045
3046
3047
3048
3049
3050
3051
3052
3053
3054
3055
3056
3057
3058
3059
3060
3061
3062
3063
3064
3065
3066
3067
3068
3069
3070
3071
3072
3073
3074
3075
3076
3077
3078
3079
3080
3081
3082

3083
3084
3085
3086
3087
3088
3089
3090
3091
3092
3093
3094
3095
3096
3097
3098



3099 Figure 40: Graphical posterior predictive check for mean and higher moments of *F.*
3100 *subverticillata* survival model across size. Consistency between real data and fitted
3101 values across sizes indicates that the vital rate models are accurately capturing size
3102 dependence. Points show the value of statistical moments binned across size for the
3103 observed data (red circles) compared to the simulated datasets (grey circles) and the
3104 median of the simulated values (black circles) generated from 500 posterior draws from
3105 the fitted model.

3106
3107
3108
3109
3110
3111
3112
3113
3114
3115
3116
3117
3118
3119
3120
3121
3122
3123
3124
3125
3126
3127
3128

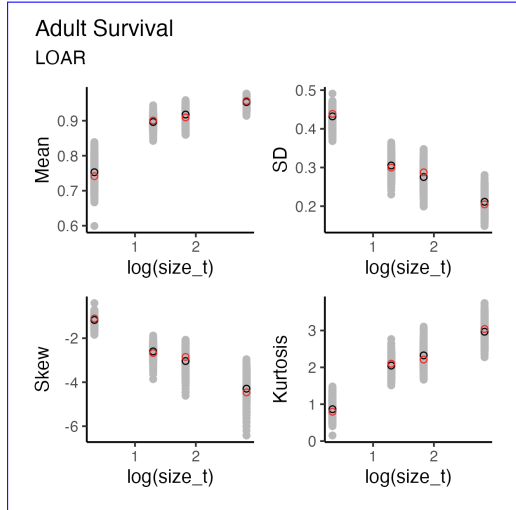
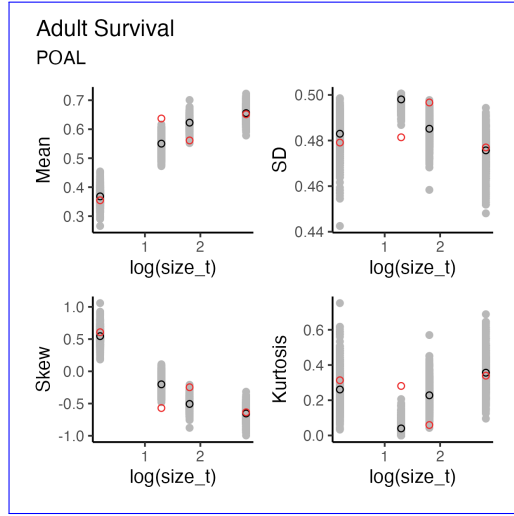


Figure 41: Graphical posterior predictive check for mean and higher moments of *L. arundinacea* survival model across size. Consistency between real data and fitted values across sizes indicates that the vital rate models are accurately capturing size dependence. Points show the value of statistical moments binned across size for the observed data (red circles) compared to the simulated datasets (grey circles) and the median of the simulated values (black circles) generated from 500 posterior draws from the fitted model.

3129
3130
3131
3132
3133
3134
3135
3136
3137
3138
3139
3140
3141
3142
3143
3144
3145
3146
3147
3148
3149
3150
3151
3152
3153
3154
3155
3156
3157
3158
3159
3160
3161
3162
3163
3164
3165
3166
3167
3168
3169
3170
3171
3172
3173
3174

3175
3176
3177
3178
3179
3180
3181
3182
3183
3184
3185
3186
3187
3188
3189
3190



3191 Figure 42: Graphical posterior predictive check for mean and higher moments of P .
3192 *alsodes* survival model across size. Consistency between real data and fitted values
3193 across sizes indicates that the vital rate models are accurately capturing size depen-
3194 dence. Points show the value of statistical moments binned across size for the observed
3195 data (red circles) compared to the simulated datasets (grey circles) and the median
3196 of the simulated values (black circles) generated from 500 posterior draws from the
3197 fitted model.

3198
3199
3200
3201
3202
3203
3204
3205
3206
3207
3208
3209
3210
3211
3212
3213
3214
3215
3216
3217
3218
3219
3220

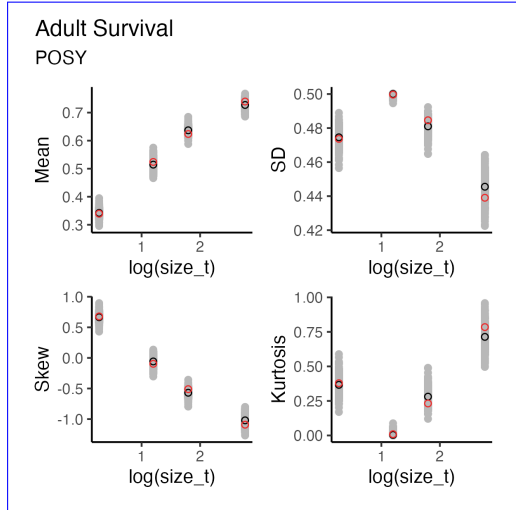
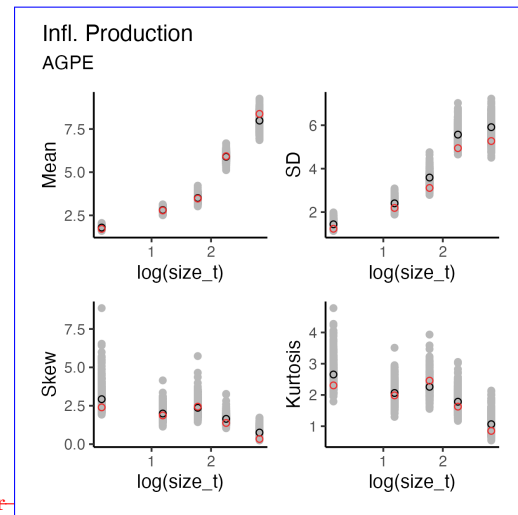


Figure 43: Graphical posterior predictive check for mean and higher moments of *P. sylvestris* survival model across size. Consistency between real data and fitted values across sizes indicates that the vital rate models are accurately capturing size dependence. Points show the value of statistical moments binned across size for the observed data (red circles) compared to the simulated datasets (grey circles) and the median of the simulated values (black circles) generated from 500 posterior draws from the fitted model.

3221
3222
3223
3224
3225
3226
3227
3228
3229
3230
3231
3232
3233
3234
3235
3236
3237
3238
3239
3240
3241
3242
3243
3244
3245
3246
3247
3248
3249
3250
3251
3252
3253
3254
3255
3256
3257
3258
3259
3260
3261
3262
3263
3264
3265
3266

3267
 3268
 3269
 3270
 3271
 3272
 3273
 3274
 3275
 3276
 3277
 3278
 3279
 3280
 3281
 3282
 3283
 3284
 3285
 3286
 3287
 3288
 3289
 3290
 3291
 3292
 3293
 3294
 3295
 3296
 3297
 3298
 3299
 3300
 3301
 3302
 3303
 3304
 3305
 3306
 3307
 3308
 3309
 3310
 3311
 3312



3283 Figure 44: Graphical posterior predictive check for ~~statistical model~~-mean and higher
 3284 moments of ~~Flowering Probability~~*A. perennans* inflorescence production model across
 3285 size. Consistency between real data and ~~simulated~~-fitted values ~~across~~ sizes indicates
 3286 that ~~fitted models describe~~ the ~~data~~-well vital rate models are accurately capturing size
 3287 dependence. ~~Lines Points~~ show ~~density distributions~~ the value of statistical moments
 3288 binned across size for the observed data (~~blue lined~~ circles) compared to ~~data~~-the
 3289 simulated ~~from fitted models~~-datasets (~~tan lines~~grey circles) and the median of the
 3290 simulated values (black circles) generated from 500 posterior draws from ~~posterior~~
 3291 ~~distributions of model parameters along with the distribution's moments~~fitted model.
 3292
 3293
 3294
 3295
 3296
 3297
 3298
 3299
 3300
 3301
 3302
 3303
 3304
 3305
 3306
 3307
 3308
 3309
 3310
 3311
 3312

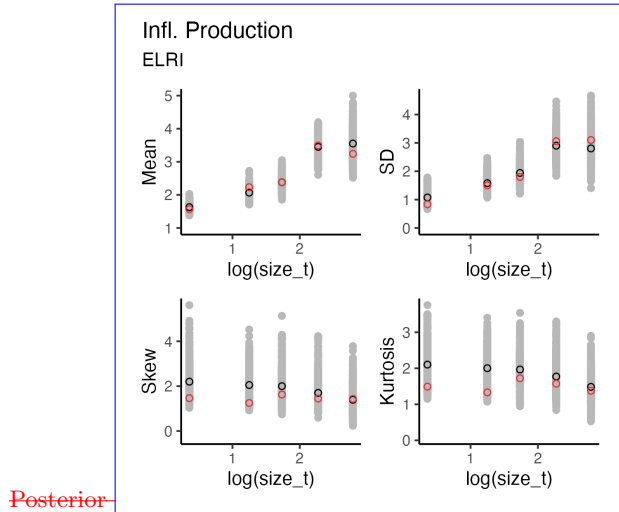


Figure 45: Graphical posterior predictive check for ~~statistical model~~ mean and higher moments of ~~Flowering Tiller~~ *E. villosus* inflorescence production model across size. Consistency between real data and ~~simulated~~ fitted values across sizes indicates that ~~fitted models describe the data well~~ vital rate models are accurately capturing size dependence. Lines-Points show ~~density distributions~~ the value of statistical moments binned across size for the observed data (~~blue-lined circles~~) compared to ~~data~~ the simulated ~~from fitted models datasets~~ (~~tan lines~~grey circles) and the median of the simulated values (black circles) generated from ~~posterior distributions of model parameters along with the distribution's moments~~ fitted model.

3313
3314
3315
3316
3317
3318
3319
3320
3321
3322
3323
3324
3325
3326
3327
3328
3329
3330
3331
3332
3333
3334
3335
3336
3337
3338
3339
3340
3341
3342
3343
3344
3345
3346
3347
3348
3349
3350
3351
3352
3353
3354
3355
3356
3357
3358

3359

3360

3361

3362

3363

3364

3365

3366

3367

3368

3369

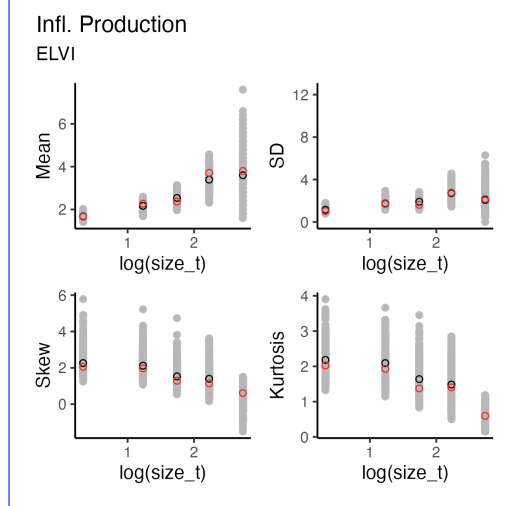
3370

3371

3372

3373

3374



3375 Figure 46: Graphical posterior predictive check for mean and higher moments of *E.*
 3376 *virginicus* inflorescence production model across size. Consistency between real data
 3377 and fitted values across sizes indicates that the vital rate models are accurately cap-
 3378 turing size dependence. Points show the value of statistical moments binned across size
 3379 for the observed data (red circles) compared to the simulated datasets (grey circles)
 3380 and the median of the simulated values (black circles) generated from 500 posterior
 3381 draws from the fitted model.

3382

3383

3384

3385

3386

3387

3388

3389

3390

3391

3392

3393

3394

3395

3396

3397

3398

3399

3400

3401

3402

3403

3404

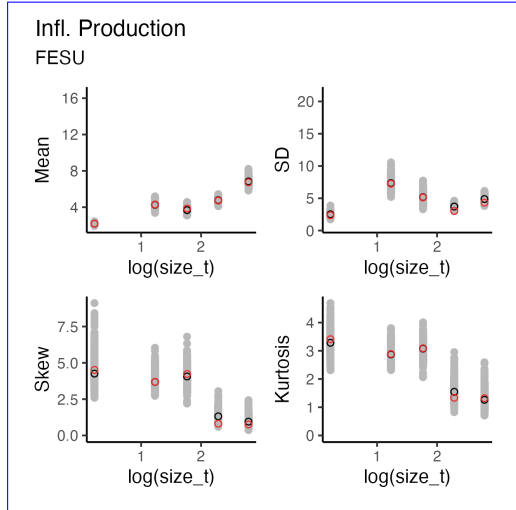


Figure 47: Graphical posterior predictive check for mean and higher moments of *F. subverticillata* inflorescence production model across size. Consistency between real data and fitted values across sizes indicates that the vital rate models are accurately capturing size dependence. Points show the value of statistical moments binned across size for the observed data (red circles) compared to the simulated datasets (grey circles) and the median of the simulated values (black circles) generated from 500 posterior draws from the fitted model.

3405
 3406
 3407
 3408
 3409
 3410
 3411
 3412
 3413
 3414
 3415
 3416
 3417
 3418
 3419
 3420
 3421
 3422
 3423
 3424
 3425
 3426
 3427
 3428
 3429
 3430
 3431
 3432
 3433
 3434
 3435
 3436
 3437
 3438
 3439
 3440
 3441
 3442
 3443
 3444
 3445
 3446
 3447
 3448
 3449
 3450

3451

3452

3453

3454

3455

3456

3457

3458

3459

3460

3461

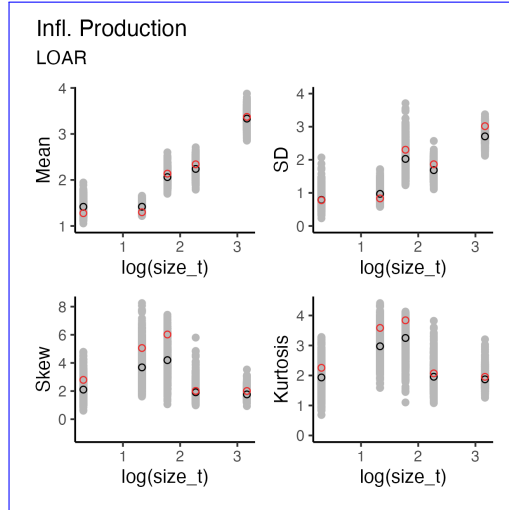
3462

3463

3464

3465

3466



3467 Figure 48: Graphical posterior predictive check for mean and higher moments of *L.*
 3468 *arundinacea* inflorescence production model across size. Consistency between real data
 3469 and fitted values across sizes indicates that the vital rate models are accurately cap-
 3470 turing size dependence. Points show the value of statistical moments binned across size
 3471 for the observed data (red circles) compared to the simulated datasets (grey circles)
 3472 and the median of the simulated values (black circles) generated from 500 posterior
 3473 draws from the fitted model.

3474

3475

3476

3477

3478

3479

3480

3481

3482

3483

3484

3485

3486

3487

3488

3489

3490

3491

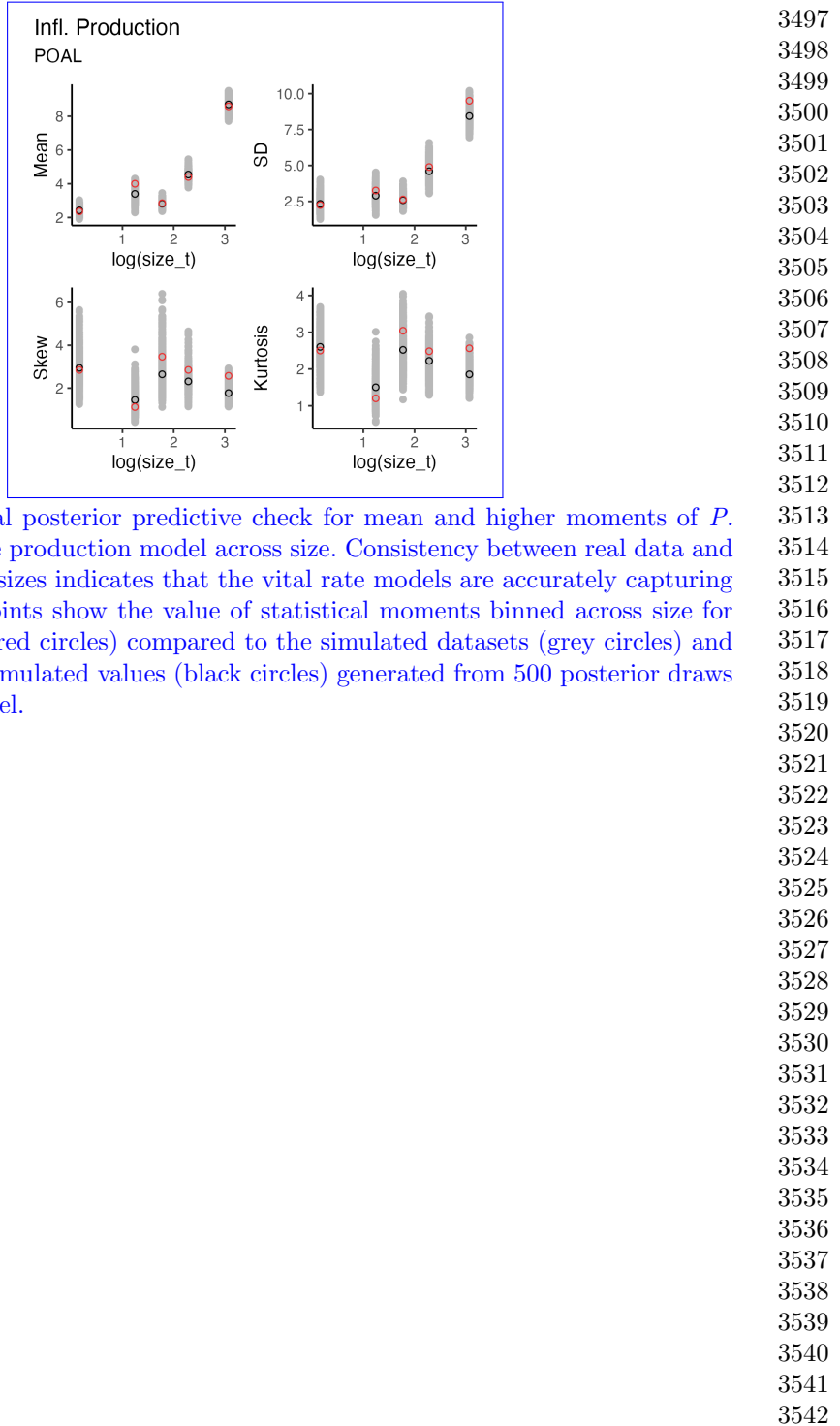
3492

3493

3494

3495

3496



3543

3544

3545

3546

3547

3548

3549

3550

3551

3552

3553

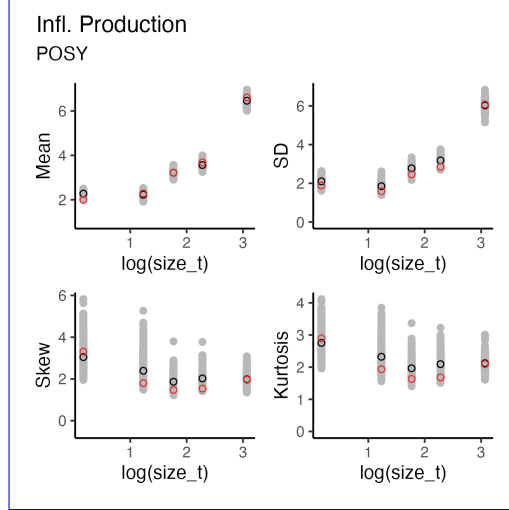
3554

3555

3556

3557

3558



3559 Figure 50: Graphical posterior predictive check for mean and higher moments of *P.*
3560 *sylvestris* inflorescence production model across size. Consistency between real data
3561 and fitted values across sizes indicates that the vital rate models are accurately cap-
3562 turing size dependence. Points show the value of statistical moments binned across size
3563 for the observed data (red circles) compared to the simulated datasets (grey circles)
3564 and the median of the simulated values (black circles) generated from 500 posterior
3565 draws from the fitted model.

3566

3567

3568

3569

3570

3571

3572

3573

3574

3575

3576

3577

3578

3579

3580

3581

3582

3583

3584

3585

3586

3587

3588

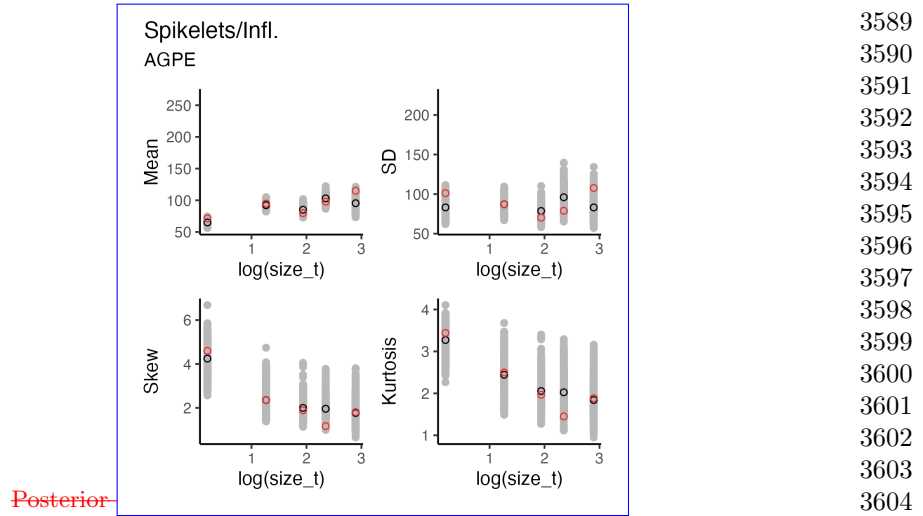
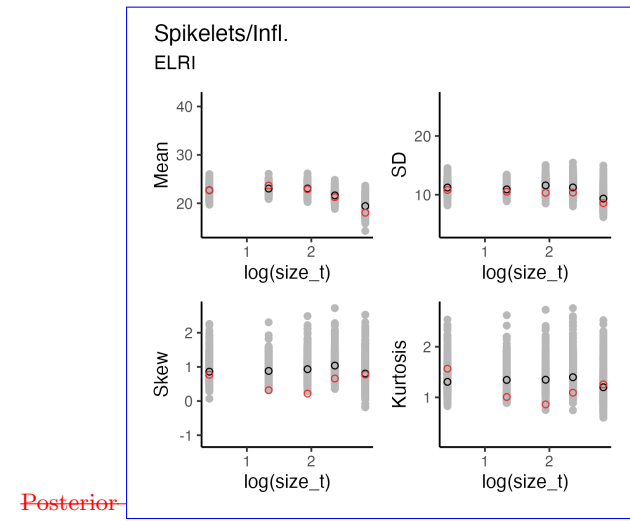


Figure 51: Graphical posterior predictive check for ~~statistical model~~ mean and higher moments of *Spikelets/Inflorescence A. perennans* spikelet model across size. Consistency between real data and ~~simulated~~ fitted values across sizes indicates that ~~fitted models describe~~ the ~~data well~~ vital rate models are accurately capturing size dependence. Lines Points show ~~density distributions~~ the value of statistical moments binned across size for the observed data (~~blue lined circles~~) compared to ~~data~~ the simulated ~~from fitted models~~ datasets (~~tan lines~~grey circles) and the median of the simulated values (black circles) generated from 500 posterior draws from ~~posterior distributions of model parameters along with the distribution's moments~~ fitted model.

3589
3590
3591
3592
3593
3594
3595
3596
3597
3598
3599
3600
3601
3602
3603
3604
3605
3606
3607
3608
3609
3610
3611
3612
3613
3614
3615
3616
3617
3618
3619
3620
3621
3622
3623
3624
3625
3626
3627
3628
3629
3630
3631
3632
3633
3634

3635
3636
3637
3638
3639
3640
3641
3642
3643
3644
3645
3646
3647
3648
3649
3650



3651 Figure 52: Graphical posterior predictive check for ~~statistical model~~-mean and higher
3652 moments of ~~Mean~~-Seeds/~~Spikelet~~*E. villosus* spikelet model across size. Consistency
3653 between real data and ~~simulated~~-fitted values across sizes indicates that ~~fitted~~-models
3654 ~~describe~~the ~~data-well~~vital rate models are accurately capturing size dependence. Lines
3655 Points show ~~density distributions~~the value of statistical moments binned across size
3656 for the observed data (~~blue~~-lined red circles) compared to ~~data~~-the simulated ~~from fitted~~
3657 ~~models~~-datasets (~~tan~~-lines grey circles) and the median of the simulated values (black cir-
3658 cles) generated from 500 posterior draws from ~~posterior distributions of model parameters~~
3659 ~~along with the distribution's moments~~-fitted model.

3660
3661
3662
3663
3664
3665
3666
3667
3668
3669
3670
3671
3672
3673
3674
3675
3676
3677
3678
3679
3680

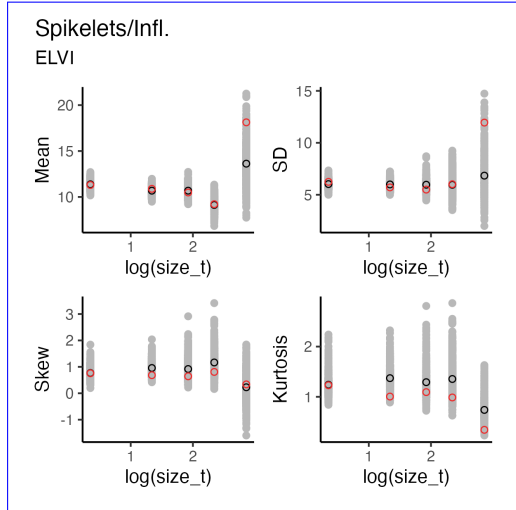


Figure 53: Graphical posterior predictive check for mean and higher moments of *E. virginicus* spikelet model across size. Consistency between real data and fitted values across sizes indicates that the vital rate models are accurately capturing size dependence. Points show the value of statistical moments binned across size for the observed data (red circles) compared to the simulated datasets (grey circles) and the median of the simulated values (black circles) generated from 500 posterior draws from the fitted model.

```

3681
3682
3683
3684
3685
3686
3687
3688
3689
3690
3691
3692
3693
3694
3695
3696
3697
3698
3699
3700
3701
3702
3703
3704
3705
3706
3707
3708
3709
3710
3711
3712
3713
3714
3715
3716
3717
3718
3719
3720
3721
3722
3723
3724
3725
3726

```

3727

3728

3729

3730

3731

3732

3733

3734

3735

3736

3737

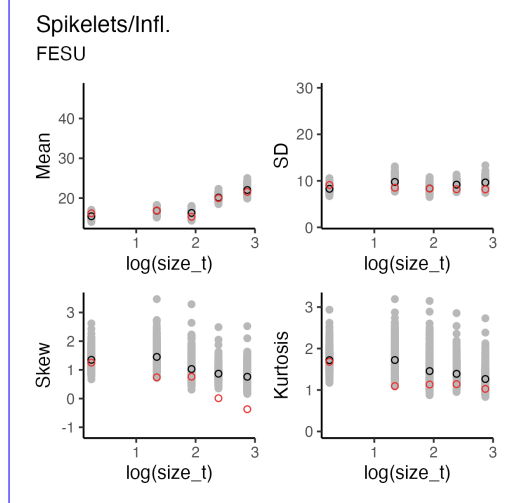
3738

3739

3740

3741

3742



3743 Figure 54: Graphical posterior predictive check for mean and higher moments of *F.*
 3744 *subverticillata* spikelet model across size. Consistency between real data and fitted
 3745 values across sizes indicates that the vital rate models are accurately capturing size
 3746 dependence. Points show the value of statistical moments binned across size for the
 3747 observed data (red circles) compared to the simulated datasets (grey circles) and the
 3748 median of the simulated values (black circles) generated from 500 posterior draws from
 3749 the fitted model.

3750

3751

3752

3753

3754

3755

3756

3757

3758

3759

3760

3761

3762

3763

3764

3765

3766

3767

3768

3769

3770

3771

3772

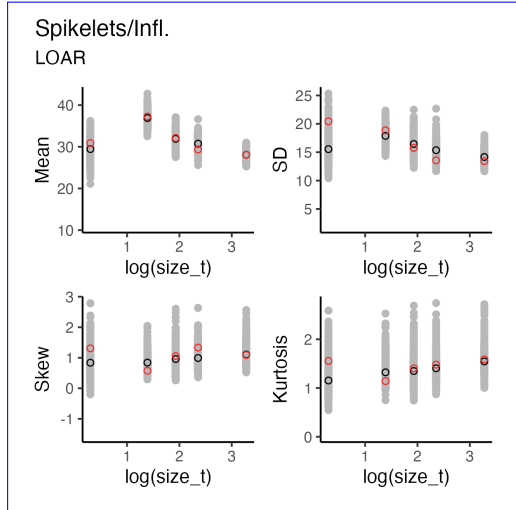


Figure 55: Graphical posterior predictive check for mean and higher moments of *L. arundinacea* spikelet model across size. Consistency between real data and fitted values across sizes indicates that the vital rate models are accurately capturing size dependence. Points show the value of statistical moments binned across size for the observed data (red circles) compared to the simulated datasets (grey circles) and the median of the simulated values (black circles) generated from 500 posterior draws from the fitted model.

3773
3774
3775
3776
3777
3778
3779
3780
3781
3782
3783
3784
3785
3786
3787
3788
3789
3790
3791
3792
3793
3794
3795
3796
3797
3798
3799
3800
3801
3802
3803
3804
3805
3806
3807
3808
3809
3810
3811
3812
3813
3814
3815
3816
3817
3818

3819

3820

3821

3822

3823

3824

3825

3826

3827

3828

3829

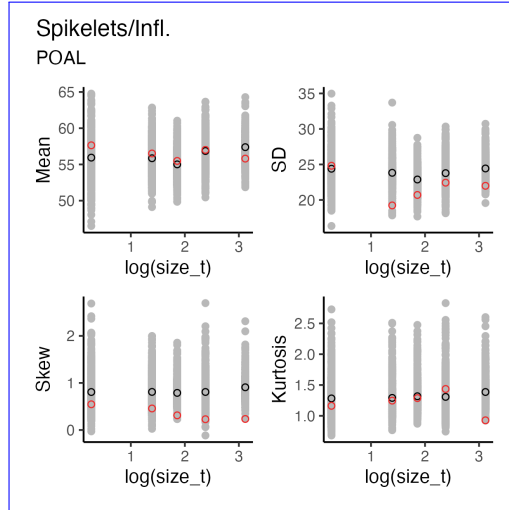
3830

3831

3832

3833

3834



3835 Figure 56: Graphical posterior predictive check for mean and higher moments of $P.$
 3836 *alsodes* spikelet model across size. Consistency between real data and fitted values
 3837 across sizes indicates that the vital rate models are accurately capturing size depen-
 3838 dence. Points show the value of statistical moments binned across size for the observed
 3839 data (red circles) compared to the simulated datasets (grey circles) and the median
 3840 of the simulated values (black circles) generated from 500 posterior draws from the
 3841 fitted model.

3842

3843

3844

3845

3846

3847

3848

3849

3850

3851

3852

3853

3854

3855

3856

3857

3858

3859

3860

3861

3862

3863

3864

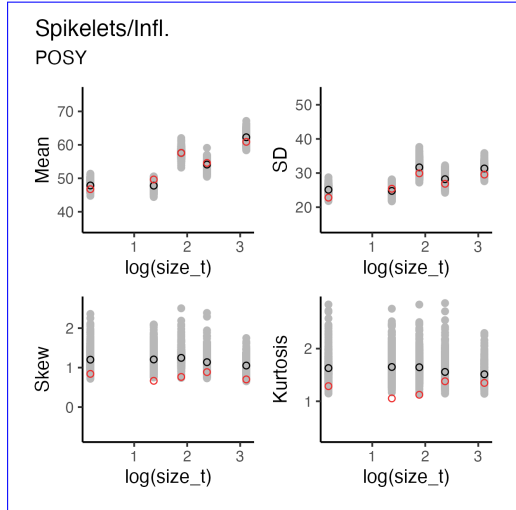


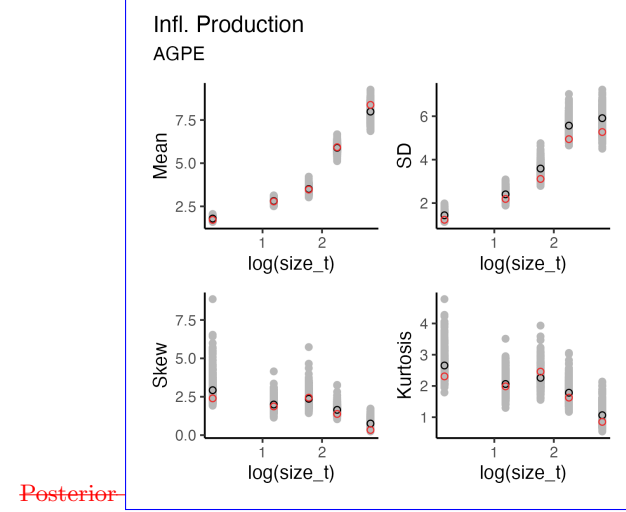
Figure 57: Graphical posterior predictive check for mean and higher moments of *P. sylvestris* spikelet model across size. Consistency between real data and fitted values across sizes indicates that the vital rate models are accurately capturing size dependence. Points show the value of statistical moments binned across size for the observed data (red circles) compared to the simulated datasets (grey circles) and the median of the simulated values (black circles) generated from 500 posterior draws from the fitted model.

```

3865
3866
3867
3868
3869
3870
3871
3872
3873
3874
3875
3876
3877
3878
3879
3880
3881
3882
3883
3884
3885
3886
3887
3888
3889
3890
3891
3892
3893
3894
3895
3896
3897
3898
3899
3900
3901
3902
3903
3904
3905
3906
3907
3908
3909
3910

```

3911
3912
3913
3914
3915
3916
3917
3918
3919
3920
3921
3922
3923
3924
3925
3926



3927 Figure 58: Graphical posterior predictive check for ~~statistical model~~-mean and higher
3928 moments of ~~Recruitment~~*A. perennans* flowering model across size. Consistency between
3929 real data and ~~simulated~~ fitted values across sizes indicates that ~~fitted models describe~~ the
3930 ~~data well~~vital rate models are accurately capturing size dependence. ~~Lines Points~~ Points show
3931 ~~density distributions~~the value of statistical moments binned across size for the observed
3932 data (~~blue lined~~red circles) compared to ~~data~~the simulated ~~from fitted models~~datasets
3933 (~~tan lines~~grey circles) and the median of the simulated values (black circles) generated
3934 from 500 posterior draws from ~~posterior distributions of model parameters along with the~~ the
3935 ~~distribution's moments~~fitted model.

3936
3937
3938
3939
3940
3941
3942
3943
3944
3945
3946
3947
3948
3949
3950
3951
3952
3953
3954
3955
3956

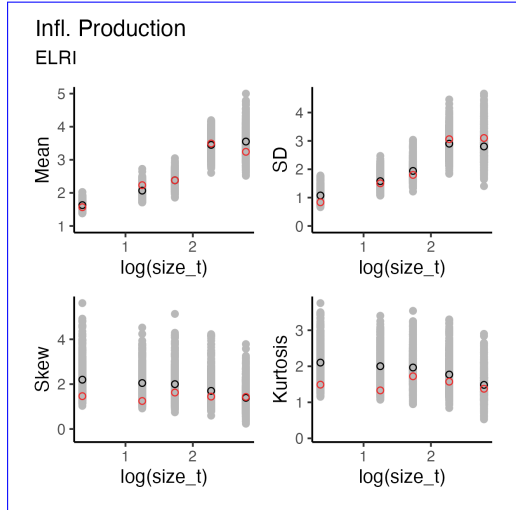
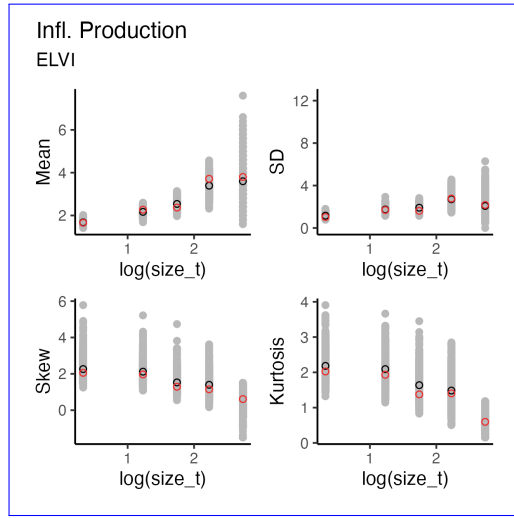


Figure 59: [Graphical posterior predictive check for mean and higher moments of *E. villosus* flowering model across size](#). Consistency between real data and fitted values across sizes indicates that the vital rate models are accurately capturing size dependence. [Graphs of posterior predictive check for mean and higher moments of the vital rate models across size](#). Points show the value of statistical moments binned across size for the observed data (red circles) compared to the simulated datasets (grey circles) and the median of the simulated values (black circles) generated from 500 posterior draws from the fitted model.

3957
3958
3959
3960
3961
3962
3963
3964
3965
3966
3967
3968
3969
3970
3971
3972
3973
3974
3975
3976
3977
3978
3979
3980
3981
3982
3983
3984
3985
3986
3987
3988
3989
3990
3991
3992
3993
3994
3995
3996
3997
3998
3999
4000
4001
4002

4003
4004
4005
4006
4007
4008
4009
4010
4011
4012
4013
4014
4015
4016
4017
4018



4019 Figure 60: Graphical posterior predictive check for mean and higher moments of *E.*
4020 *virginicus* flowering model across size. Consistency between real data and fitted values
4021 across sizes indicates that the vital rate models are accurately capturing size depen-
4022 dence. Points show the value of statistical moments binned across size for the observed
4023 data (red circles) compared to the simulated datasets (grey circles) and the median
4024 of the simulated values (black circles) generated from 500 posterior draws from the
4025 fitted model.

4026
4027
4028
4029
4030
4031
4032
4033
4034
4035
4036
4037
4038
4039
4040
4041
4042
4043
4044
4045
4046
4047
4048

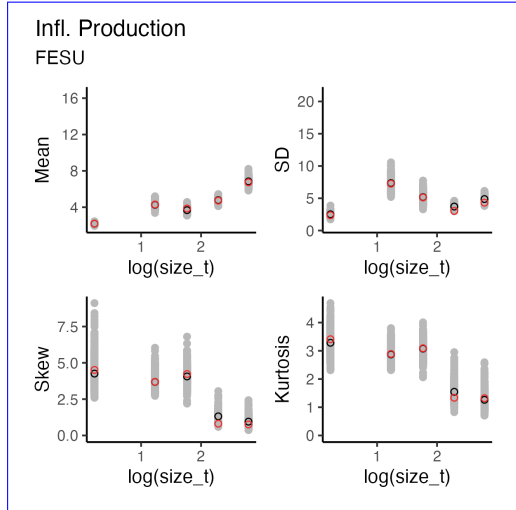


Figure 61: Graphical posterior predictive check for mean and higher moments of *F. subverticillata* flowering model across size. Consistency between real data and fitted values across sizes indicates that the vital rate models are accurately capturing size dependence. Points show the value of statistical moments binned across size for the observed data (red circles) compared to the simulated datasets (grey circles) and the median of the simulated values (black circles) generated from 500 posterior draws from the fitted model.

4049
4050
4051
4052
4053
4054
4055
4056
4057
4058
4059
4060
4061
4062
4063
4064
4065
4066
4067
4068
4069
4070
4071
4072
4073
4074
4075
4076
4077
4078
4079
4080
4081
4082
4083
4084
4085
4086
4087
4088
4089
4090
4091
4092
4093
4094

4095

4096

4097

4098

4099

4100

4101

4102

4103

4104

4105

4106

4107

4108

4109

4110

4111

4112

4113

4114

4115

4116

4117

4118 Figure 62: Graphical posterior predictive check for mean and higher moments of *L.*4119 *arundinacea* flowering model across size. Consistency between real data and fitted

4120 values across sizes indicates that the vital rate models are accurately capturing size

4121 dependence. Points show the value of statistical moments binned across size for the

4122 observed data (red circles) compared to the simulated datasets (grey circles) and the

4123 median of the simulated values (black circles) generated from 500 posterior draws from

4124 the fitted model.

4125

4126

4127

4128

4129

4130

4131

4132

4133

4134

4135

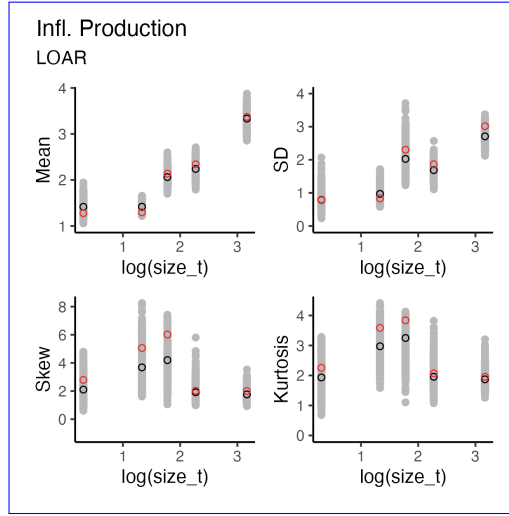
4136

4137

4138

4139

4140



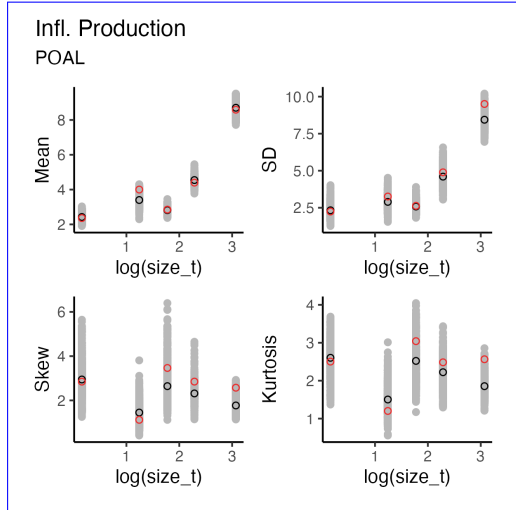


Figure 63: Graphical posterior predictive check for mean and higher moments of *P. alsodes* flowering model across size. Consistency between real data and fitted values across sizes indicates that the vital rate models are accurately capturing size dependence. Points show the value of statistical moments binned across size for the observed data (red circles) compared to the simulated datasets (grey circles) and the median of the simulated values (black circles) generated from 500 posterior draws from the fitted model.

```

4141
4142
4143
4144
4145
4146
4147
4148
4149
4150
4151
4152
4153
4154
4155
4156
4157
4158
4159
4160
4161
4162
4163
4164
4165
4166
4167
4168
4169
4170
4171
4172
4173
4174
4175
4176
4177
4178
4179
4180
4181
4182
4183
4184
4185
4186

```

4187

4188

4189

4190

4191

4192

4193

4194

4195

4196

4197

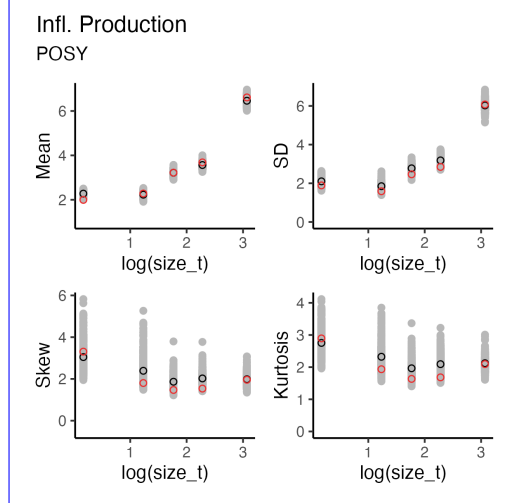
4198

4199

4200

4201

4202



4203 Figure 64: Graphical posterior predictive check for mean and higher moments of $P.$
4204 *sylvestris* flowering model across size. Consistency between real data and fitted values
4205 across sizes indicates that the vital rate models are accurately capturing size depen-
4206 dence. Points show the value of statistical moments binned across size for the observed
4207 data (red circles) compared to the simulated datasets (grey circles) and the median
4208 of the simulated values (black circles) generated from 500 posterior draws from the
4209 fitted model.

4210

4211

4212

4213

4214

4215

4216

4217

4218

4219

4220

4221

4222

4223

4224

4225

4226

4227

4228

4229

4230

4231

4232

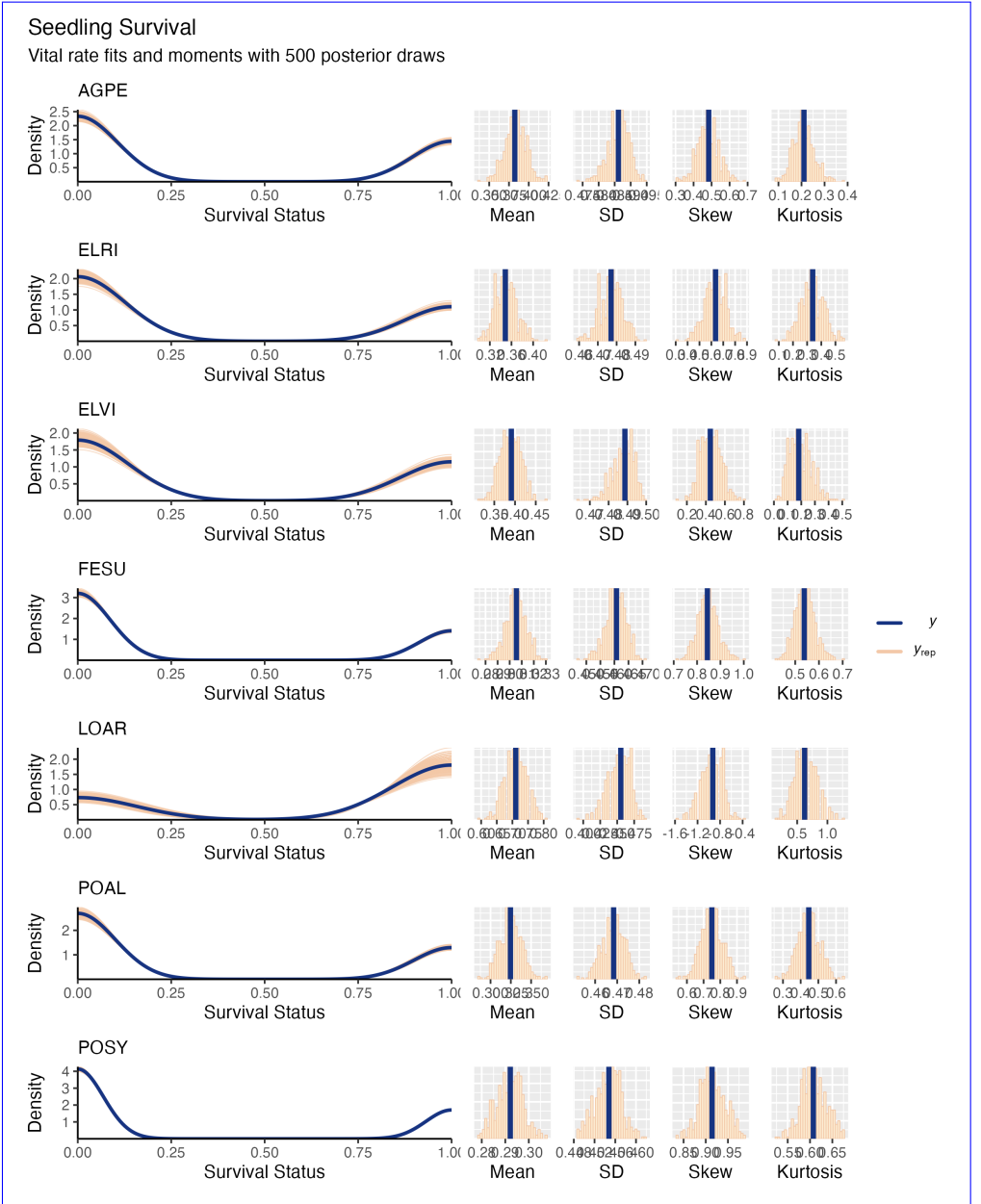
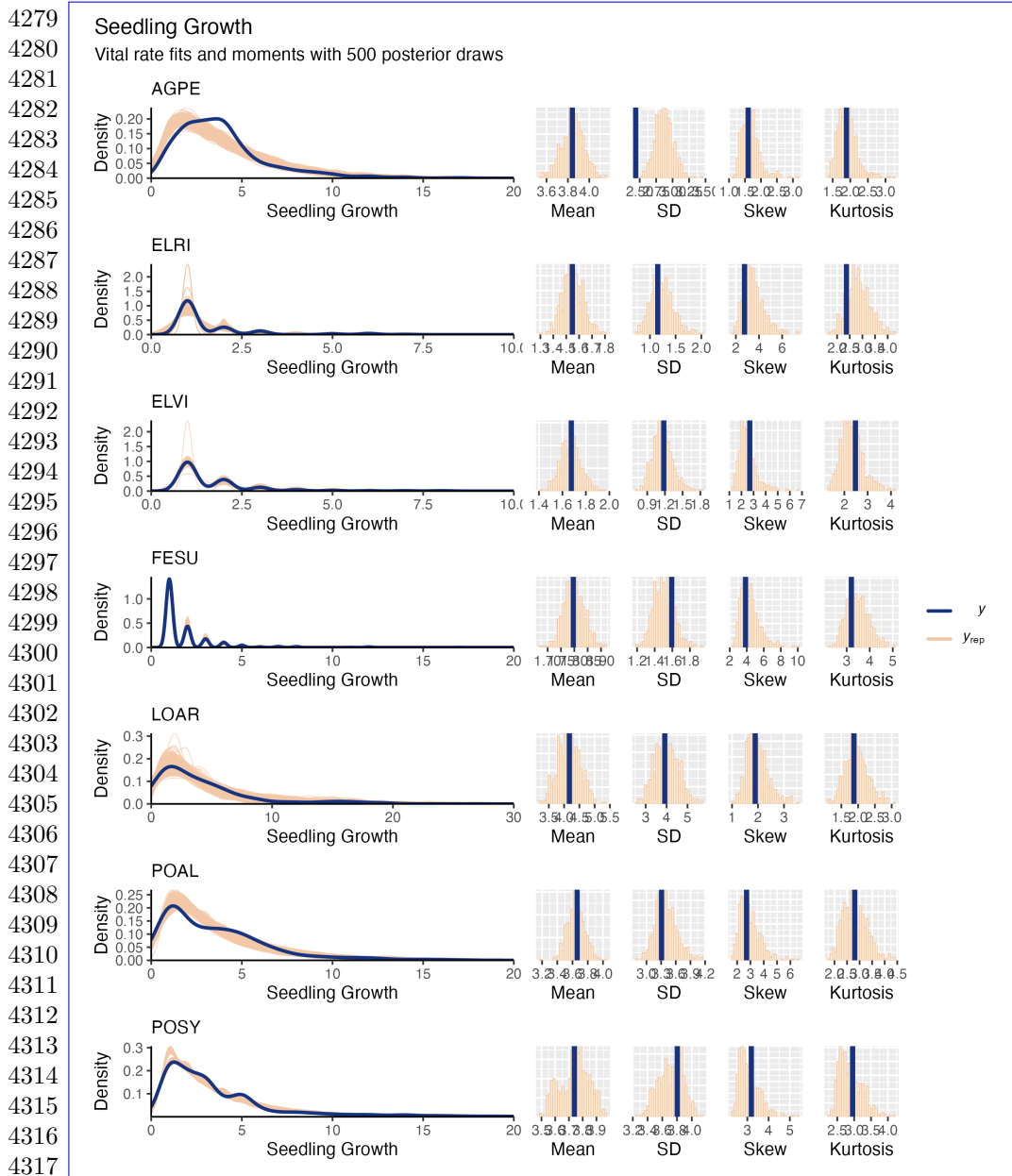


Figure 65: Graphical posterior predictive check for statistical model of Seedling Survival. Consistency between real data and simulated values indicates that fitted models describe the data well. Lines show density distributions of observed data (blue line) compared to data simulated from fitted models (tan lines) generated from 500 draws from posterior distributions of model parameters along with the distribution's moments.



4318 Figure 66: Graphical posterior predictive check for statistical model of Seedling
4319 Growth. Consistency between real data and simulated values indicates that fitted
4320 models describe the data well. Lines show density distributions of observed data (blue
4321 line) compared to data simulated from fitted models (tan lines) generated from 500
4322 draws from posterior distributions of model parameters along with the distribution's
4323 moments.
4324

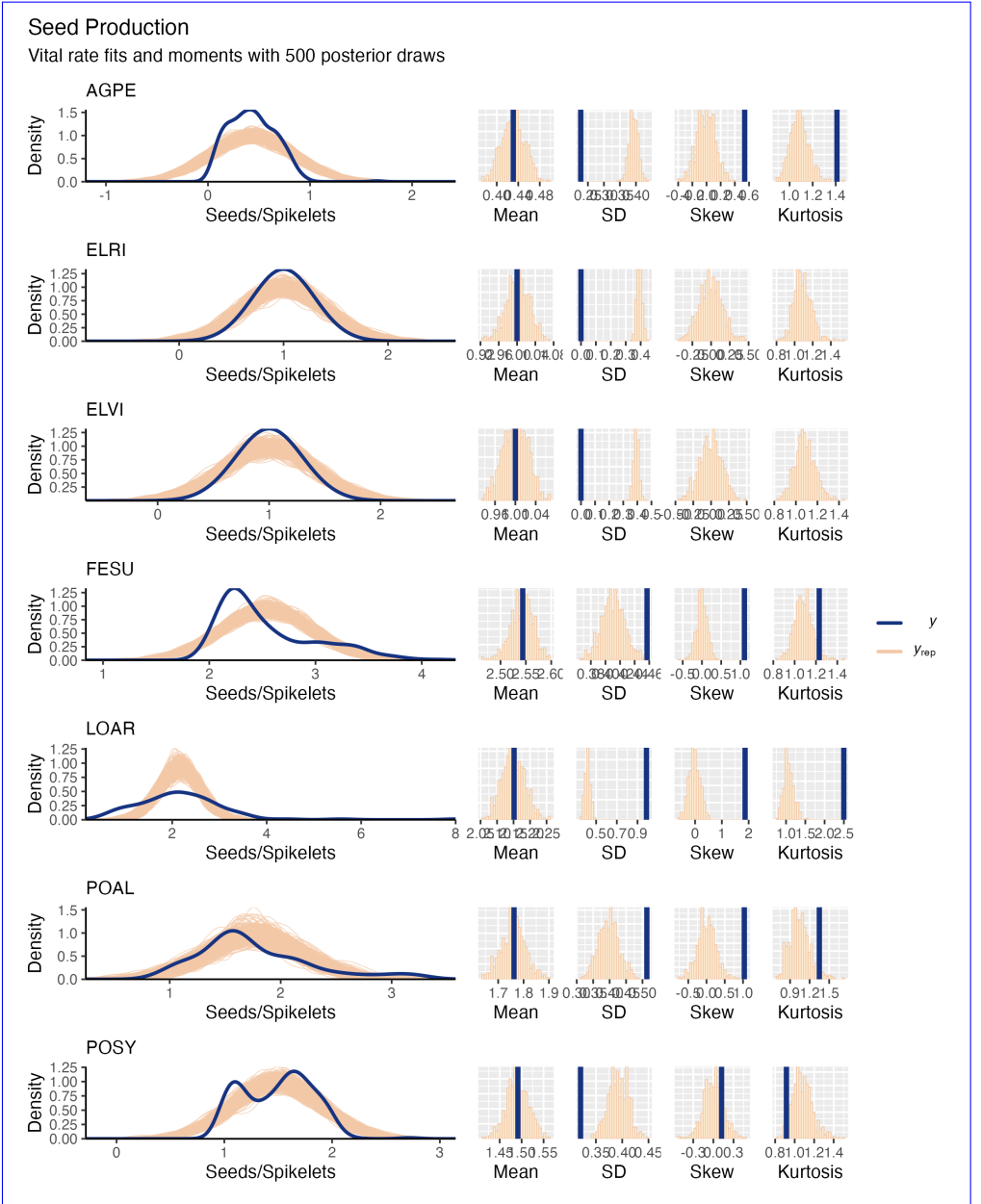
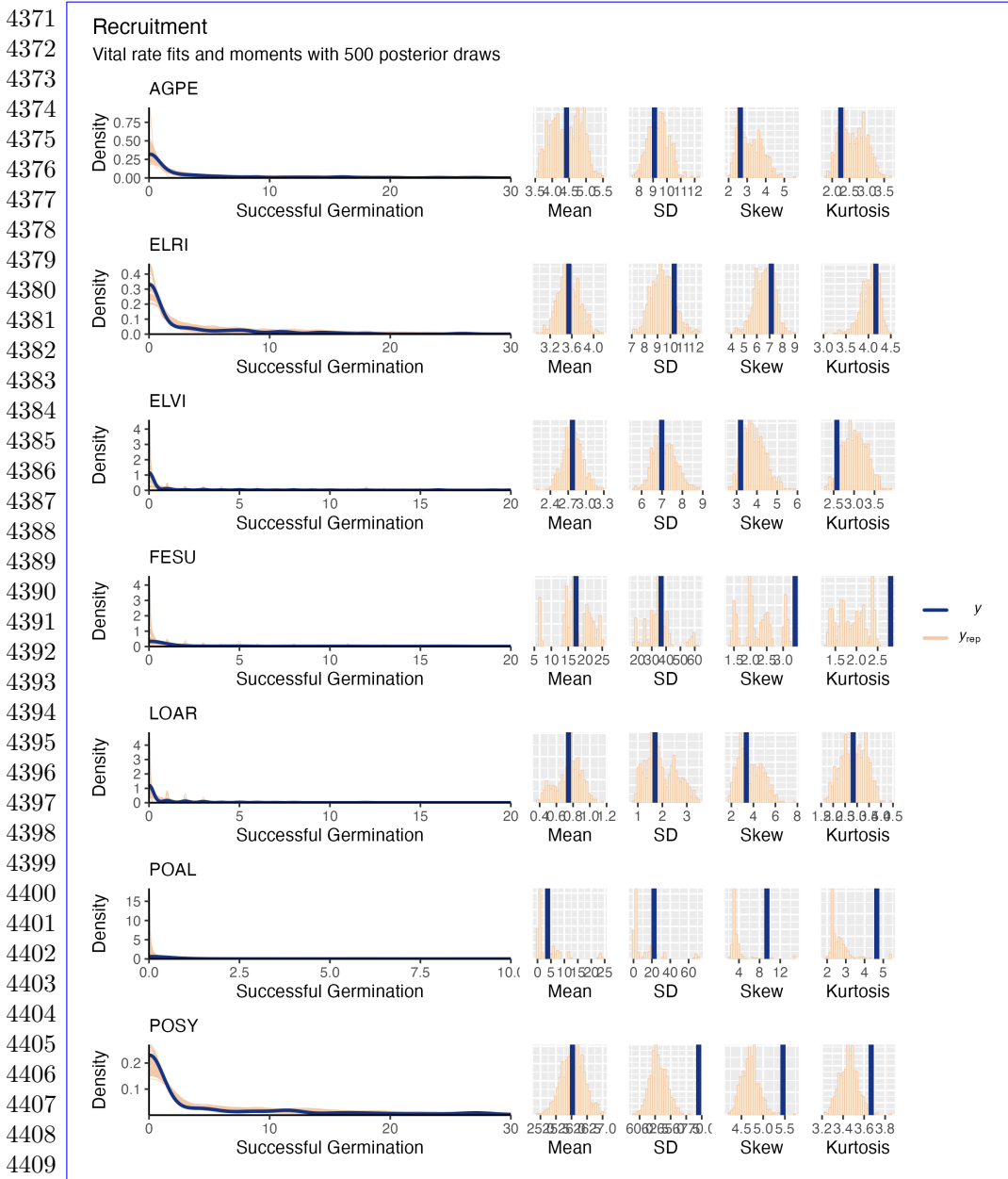


Figure 67: Graphical posterior predictive check for statistical model of Mean Seeds/Spikelet. Consistency between real data and simulated values indicates that fitted models describe the data well. Lines show density distributions of observed data (blue line) compared to data simulated from fitted models (tan lines) generated from 500 draws from posterior distributions of model parameters along with the distribution's moments.

4325
4326
4327
4328
4329
4330
4331
4332
4333
4334
4335
4336
4337
4338
4339
4340
4341
4342
4343
4344
4345
4346
4347
4348
4349
4350
4351
4352
4353
4354
4355
4356
4357
4358
4359
4360
4361
4362
4363
4364
4365
4366
4367
4368
4369
4370



4410 Figure 68: Graphical posterior predictive check for statistical model of Recruitment.

4411 Consistency between real data and simulated values indicates that fitted models

4412 describe the data well. Lines show density distributions of observed data (blue

4413 line) compared to data simulated from fitted models (tan lines) generated from 500

4414 draws from posterior distributions of model parameters along with the distribution's

4415 moments.

4416

Adult Survival
 Posterior mean with 80% credible intervals

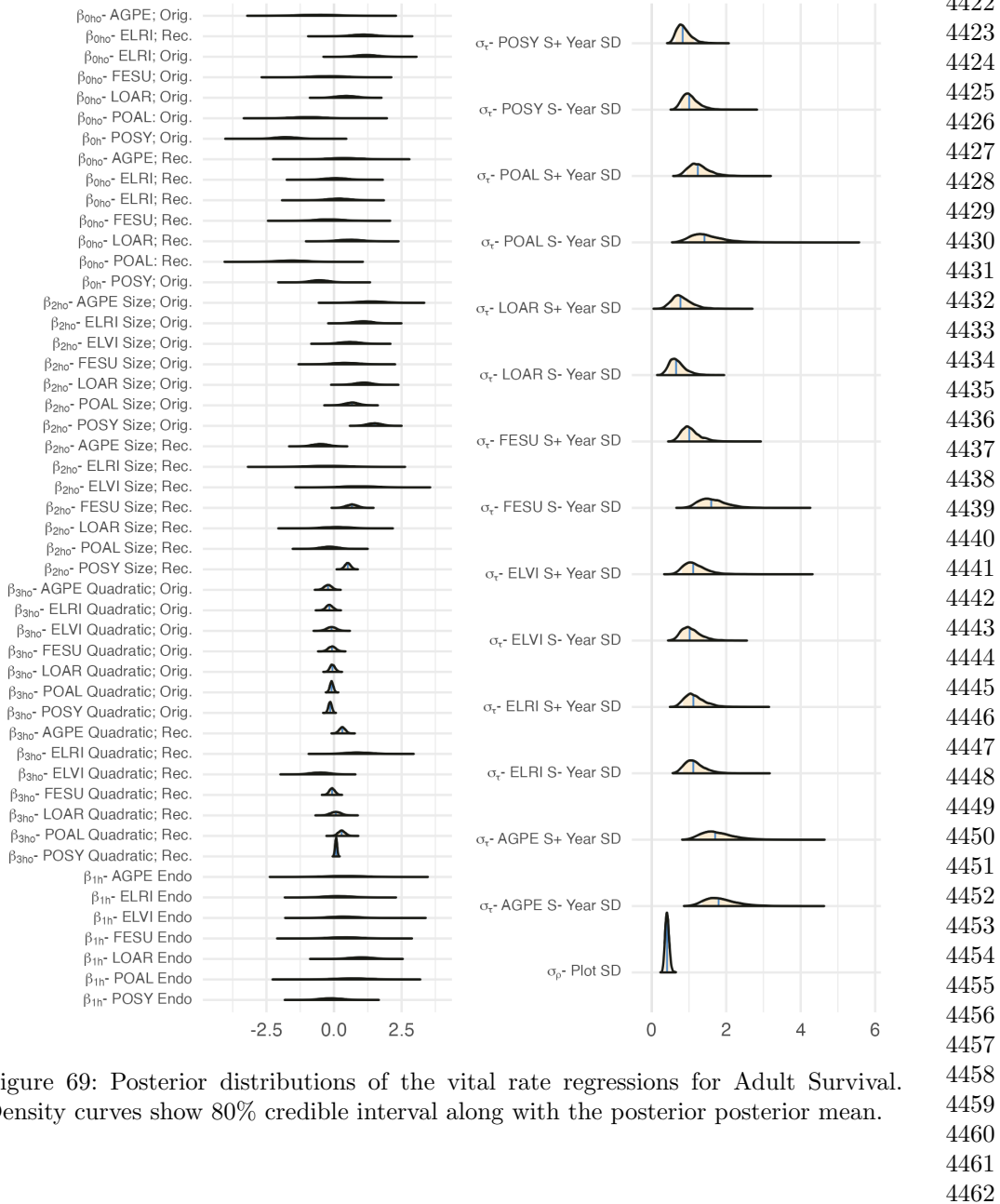
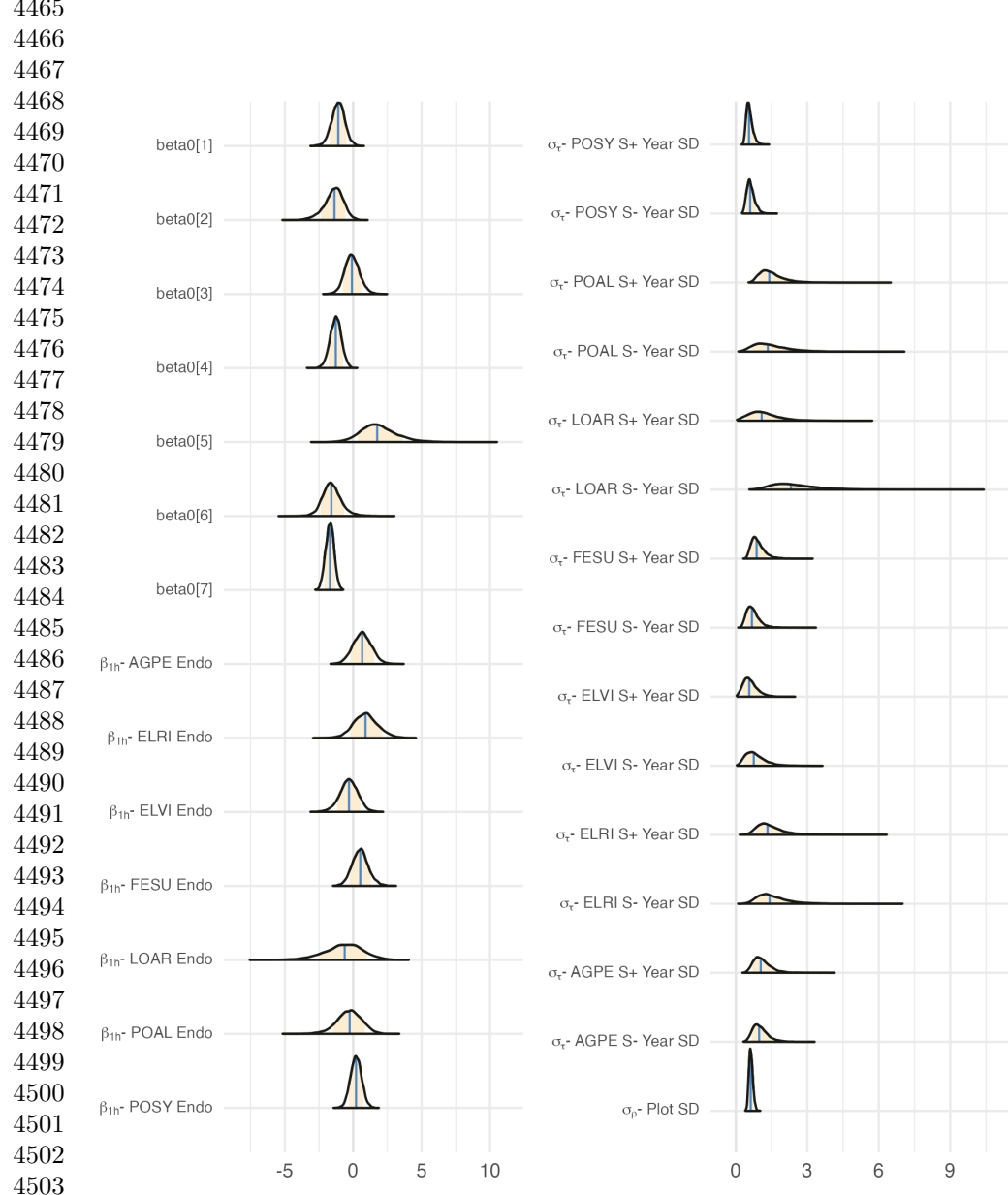


Figure 69: Posterior distributions of the vital rate regressions for Adult Survival. Density curves show 80% credible interval along with the posterior posterior mean.

4463 Seedling Survival
4464 Posterior mean with 80% credible intervals



4504 Figure 70: Posterior distributions of the vital rate regressions for Seedling Survival.
4505 Density curves show 80% credible interval along with the posterior posterior mean.
4506
4507
4508

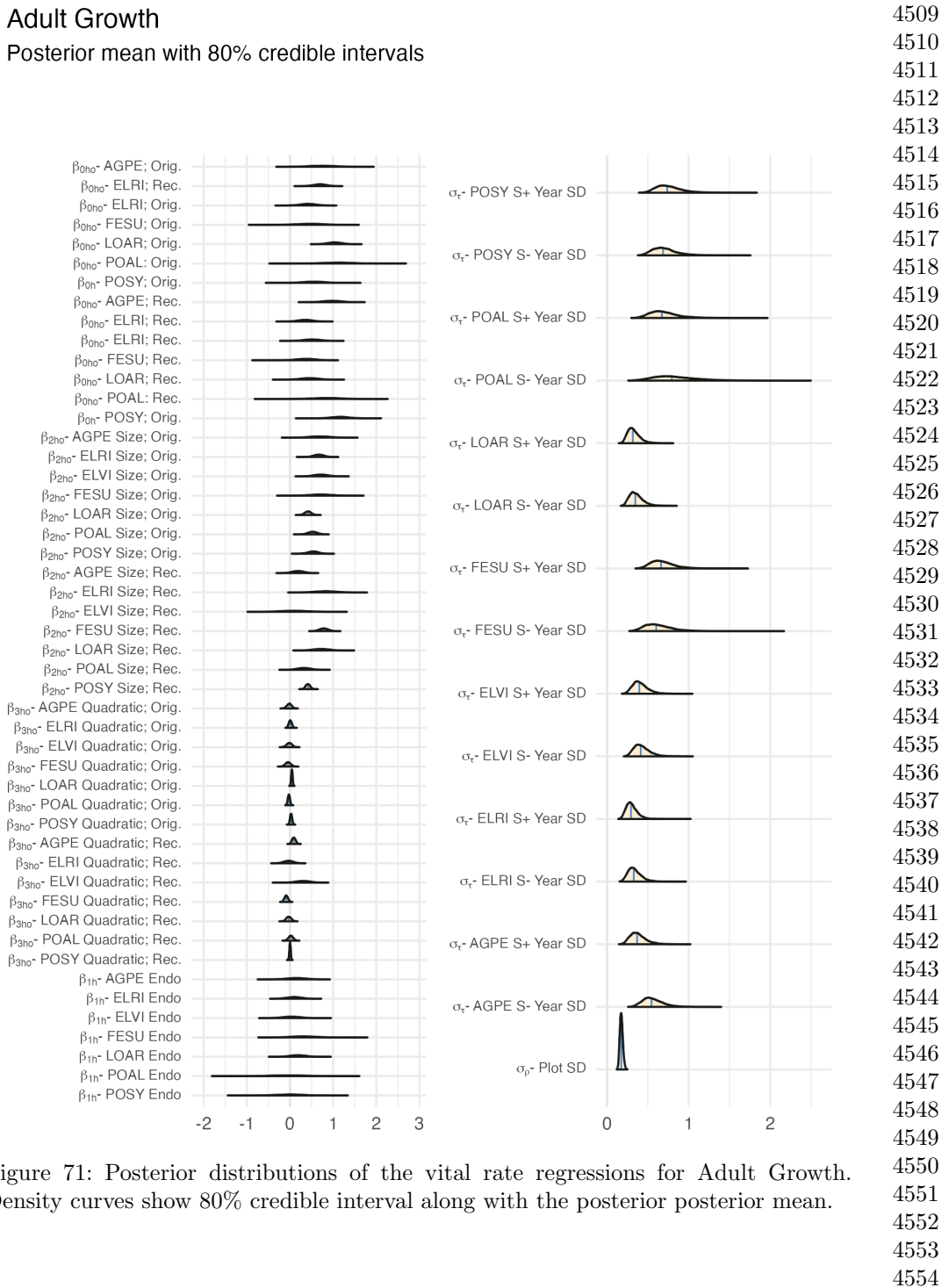
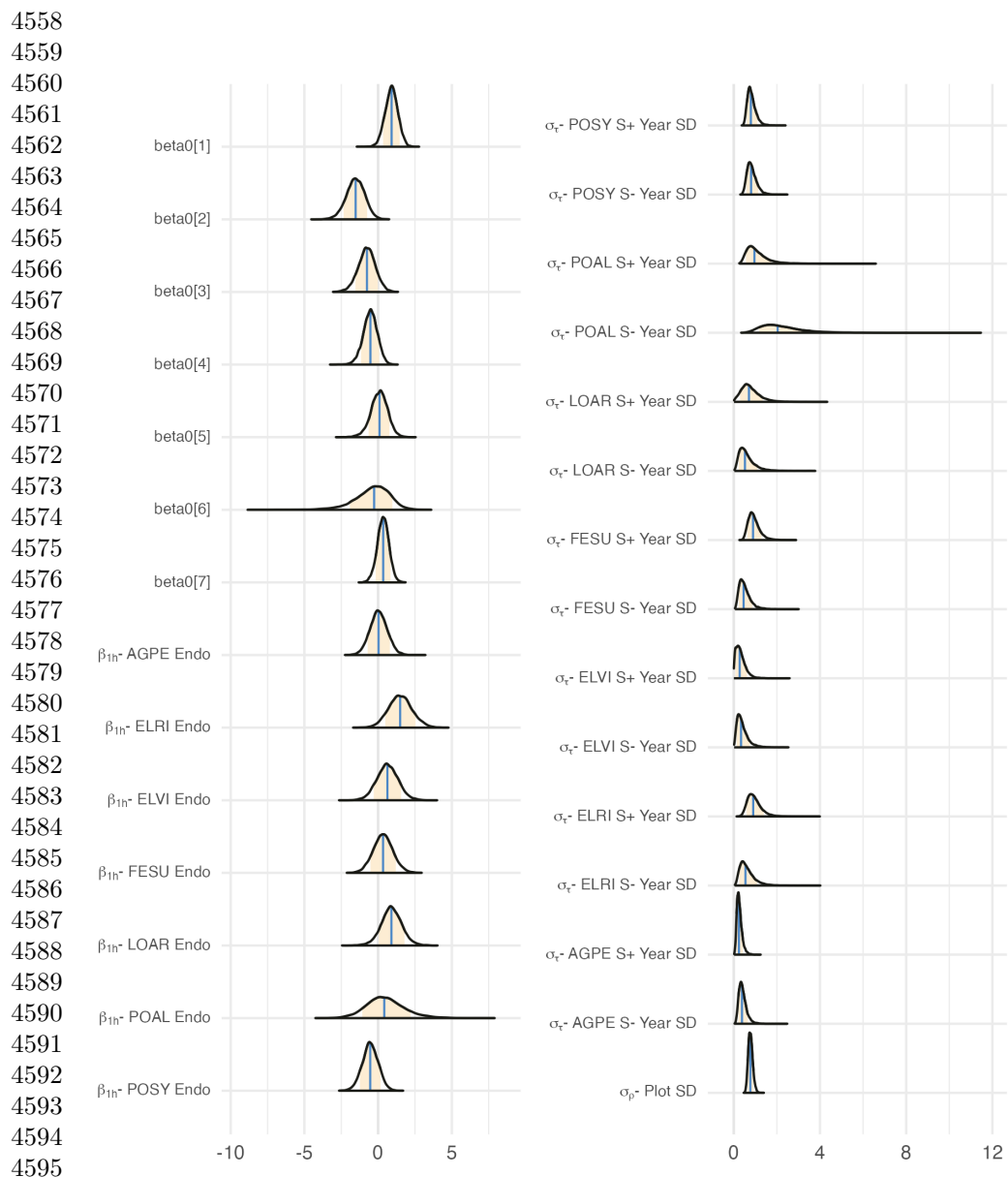


Figure 71: Posterior distributions of the vital rate regressions for Adult Growth. Density curves show 80% credible interval along with the posterior posterior mean.

4555 Seedling Growth
 4556 Posterior mean with 80% credible intervals
 4557



4596 Figure 72: Posterior distributions of the vital rate regressions for Seedling Growth.
 4597 Density curves show 80% credible interval along with the posterior posterior mean.
 4598
 4599
 4600

Flowering Probability

Posterior mean with 80% credible intervals

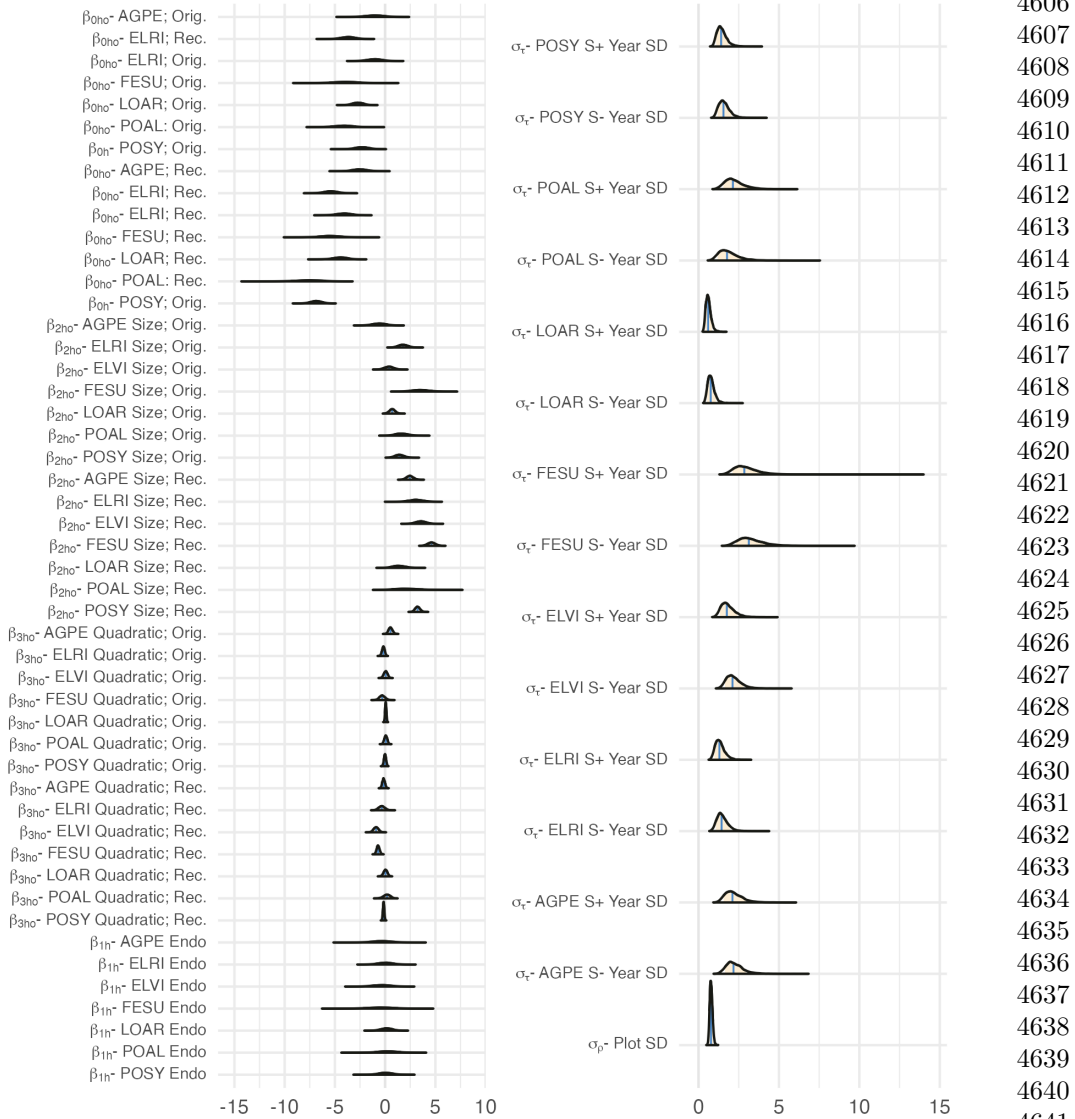


Figure 73: Posterior distributions of the vital rate regressions for Flowering Probability. Density curves show 80% credible interval along with the posterior posterior mean.

4647 Infl. Production

4648 Posterior mean with 80% credible intervals

4649

4650

4651

4652

β_{0h} - AGPE; Orig.

4653 β_{0h} - ELRI; Rec.

4654 β_{0h} - ELRI; Orig.

4655 β_{0h} - FESU; Orig.

4656 β_{0h} - LOAR; Orig.

4657 β_{0h} - POAL; Orig.

4658 β_{0h} - POSY; Orig.

4659 β_{0h} - AGPE; Rec.

4660 β_{0h} - ELRI; Rec.

4661 β_{0h} - ELRI; Orig.

4662 β_{0h} - FESU; Rec.

4663 β_{0h} - LOAR; Rec.

4664 β_{0h} - POAL; Rec.

4665 β_{0h} - POSY; Orig.

4666 β_{2h} - AGPE Size; Orig.

4667 β_{2h} - ELRI Size; Orig.

4668 β_{2h} - ELVI Size; Orig.

4669 β_{2h} - FESU Size; Orig.

4670 β_{2h} - LOAR Size; Orig.

4671 β_{2h} - POAL Size; Orig.

4672 β_{2h} - POSY Size; Orig.

4673 β_{2h} - AGPE Quadratic; Orig.

4674 β_{2h} - ELRI Quadratic; Orig.

4675 β_{2h} - ELVI Quadratic; Orig.

4676 β_{2h} - FESU Quadratic; Orig.

4677 β_{2h} - LOAR Quadratic; Orig.

4678 β_{2h} - POAL Quadratic; Orig.

4679 β_{2h} - POSY Quadratic; Orig.

4680 β_{2h} - AGPE Quadratic; Rec.

4681 β_{2h} - ELRI Quadratic; Rec.

4682 β_{2h} - ELVI Quadratic; Rec.

4683 β_{2h} - FESU Quadratic; Rec.

4684 β_{2h} - LOAR Quadratic; Rec.

4685 β_{2h} - POAL Quadratic; Rec.

4686 β_{2h} - POSY Quadratic; Rec.

4687 β_{1h} - AGPE Endo

4688 β_{1h} - ELRI Endo

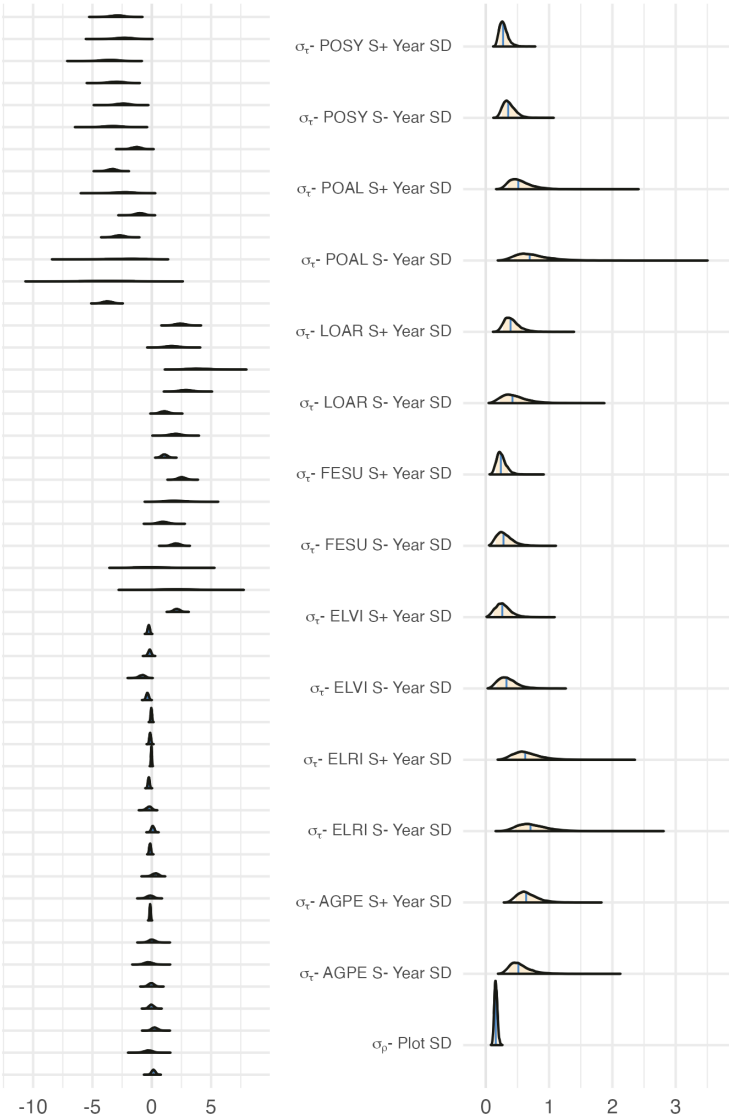
4689 β_{1h} - ELVI Endo

4690 β_{1h} - FESU Endo

4691 β_{1h} - LOAR Endo

4692 β_{1h} - POAL Endo

4693 β_{1h} - POSY Endo



4688 Figure 74: Posterior distributions of the vital rate regressions for Inflorescence Production. Density curves show 80% credible interval along with the posterior posterior mean.

4691

4692

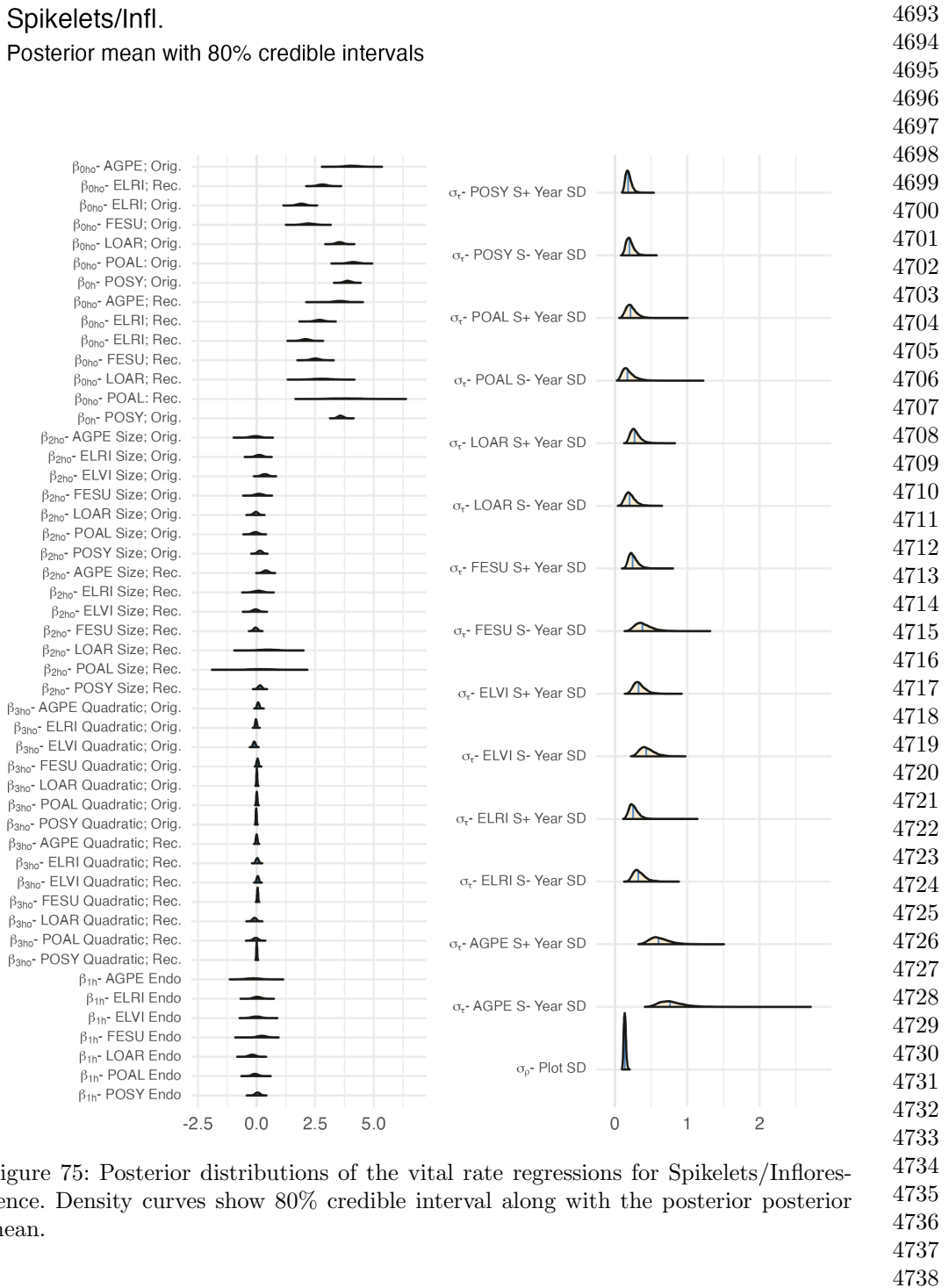
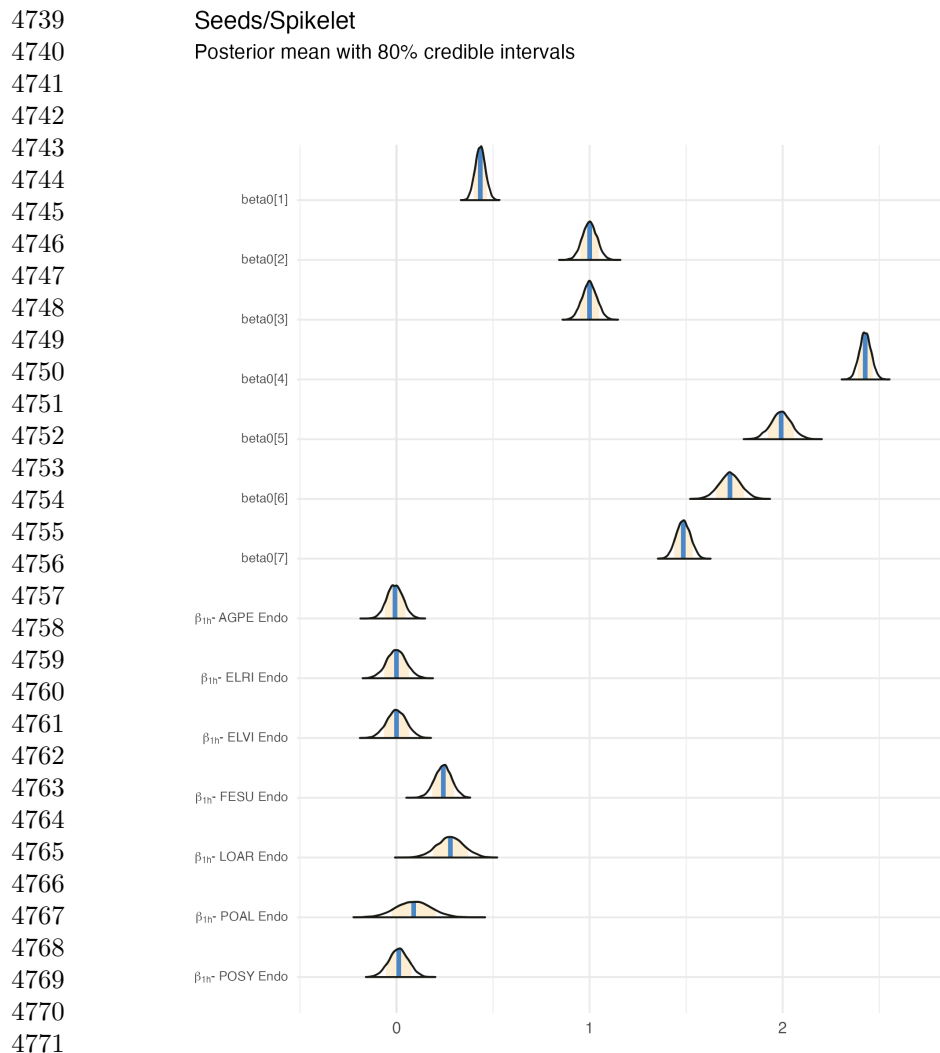


Figure 75: Posterior distributions of the vital rate regressions for Spikelets/Inflorescence. Density curves show 80% credible interval along with the posterior posterior mean.



4772 Figure 76: Posterior distributions of the vital rate regressions for Seeds/Spikelet.
 4773 Density curves show 80% credible interval along with the posterior posterior mean.

4774
 4775
 4776
 4777
 4778
 4779
 4780
 4781
 4782
 4783
 4784

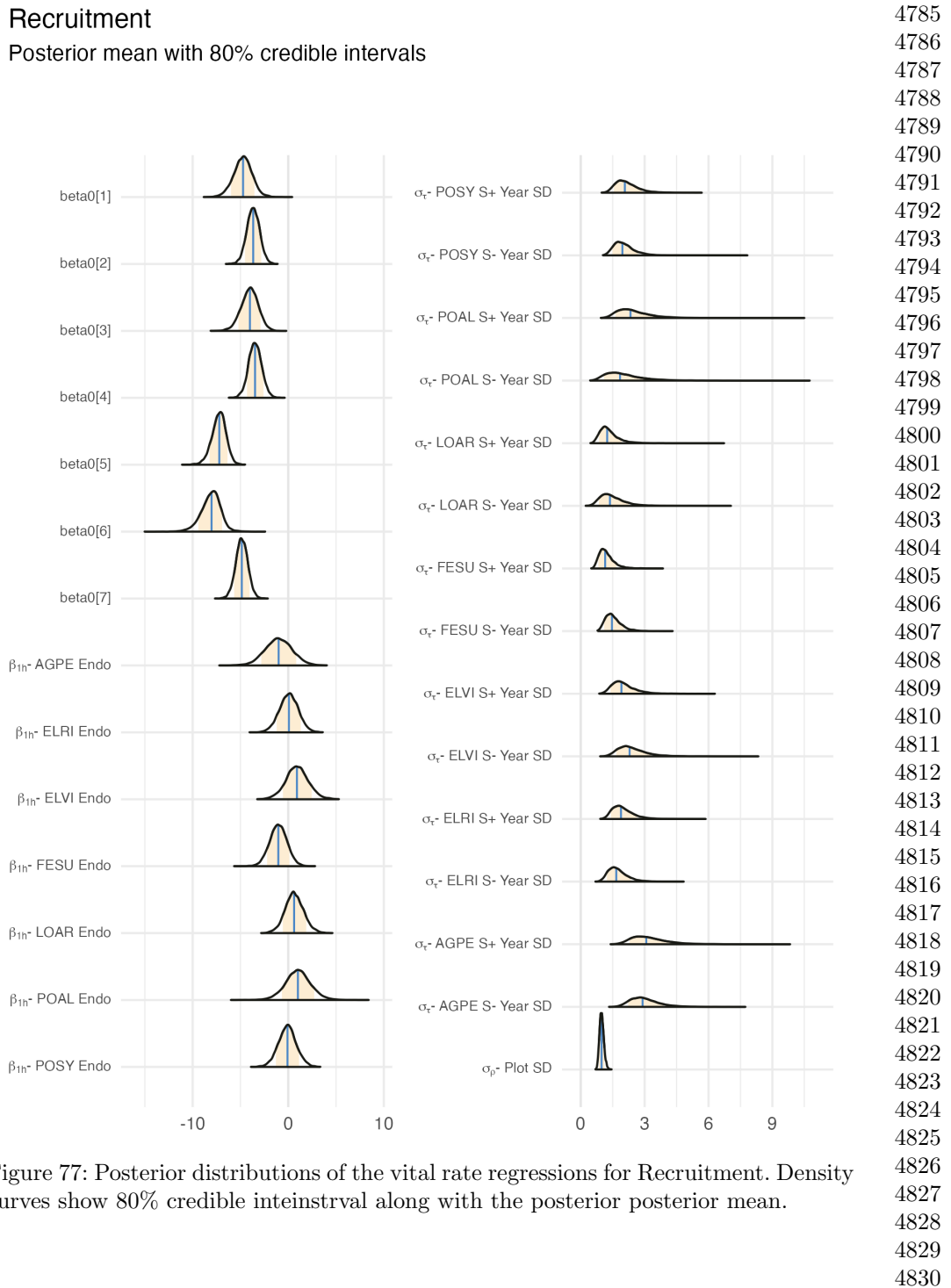
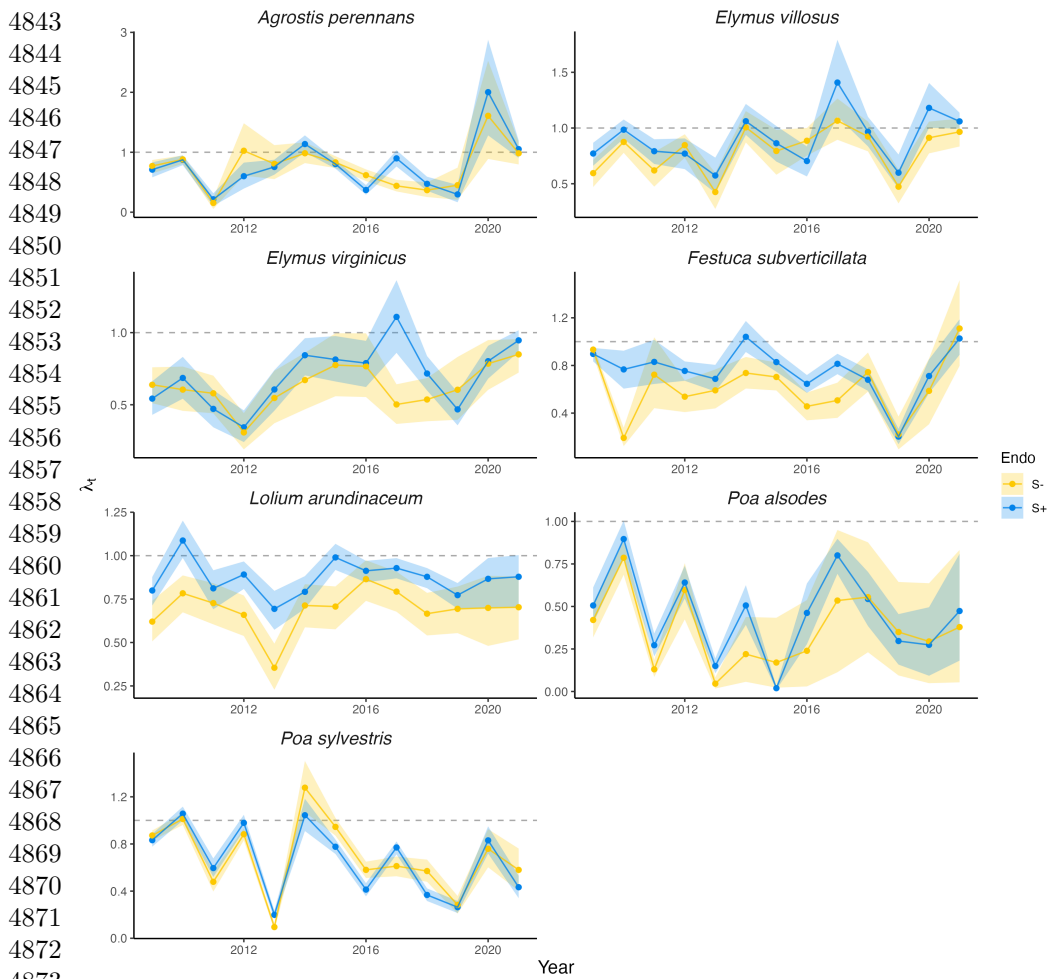


Figure 77: Posterior distributions of the vital rate regressions for Recruitment. Density curves show 80% credible interval along with the posterior mean.

4831 Life cycle diagram depicting the generalized structure of matrix population model. The
 4832 population consists of different life stages at each census t or census $t+1$. Individuals
 4833 transition from size x to size y . n is a vector of discrete sizes representing number of tillers,
 4834 according to their likelihood of survival (S) and growth (G). Reproduction generates new
 4835 recruits (small circles) through four steps, the probability of flowering (P), the number of
 4836 flowering tillers produced (F), the number of spikelets per inflorescence produced (K), and
 4837 the number of seeds per spikelet (D). The probability of successful recruitment (R)
 4838 determines the success of these offspring, and any new recruits (r) are incorporated into the
 4839 census. These non-reproductive, typically one-tiller recruits transition into the population of
 4840 mature individuals with survival (B) and growth (Z) probability. Symbiotic and
 4841 symbiont-free populations have the same model structure with species-specific and
 4842 symbiont status-specific transition probabilities used to construct matrices.



4873 Figure 78: Annual growth rate values (λ_t) over thirteen years. Mean values for symbiotic
 4874 (blue) and symbiont-free (yellow) population growth rates are shown along
 4875 with 80% credible intervals. Dashed line at ($\lambda_t = 1$) indicates stable population growth
 4876 rate. All values are calculated from matrix models representing recruit plants.

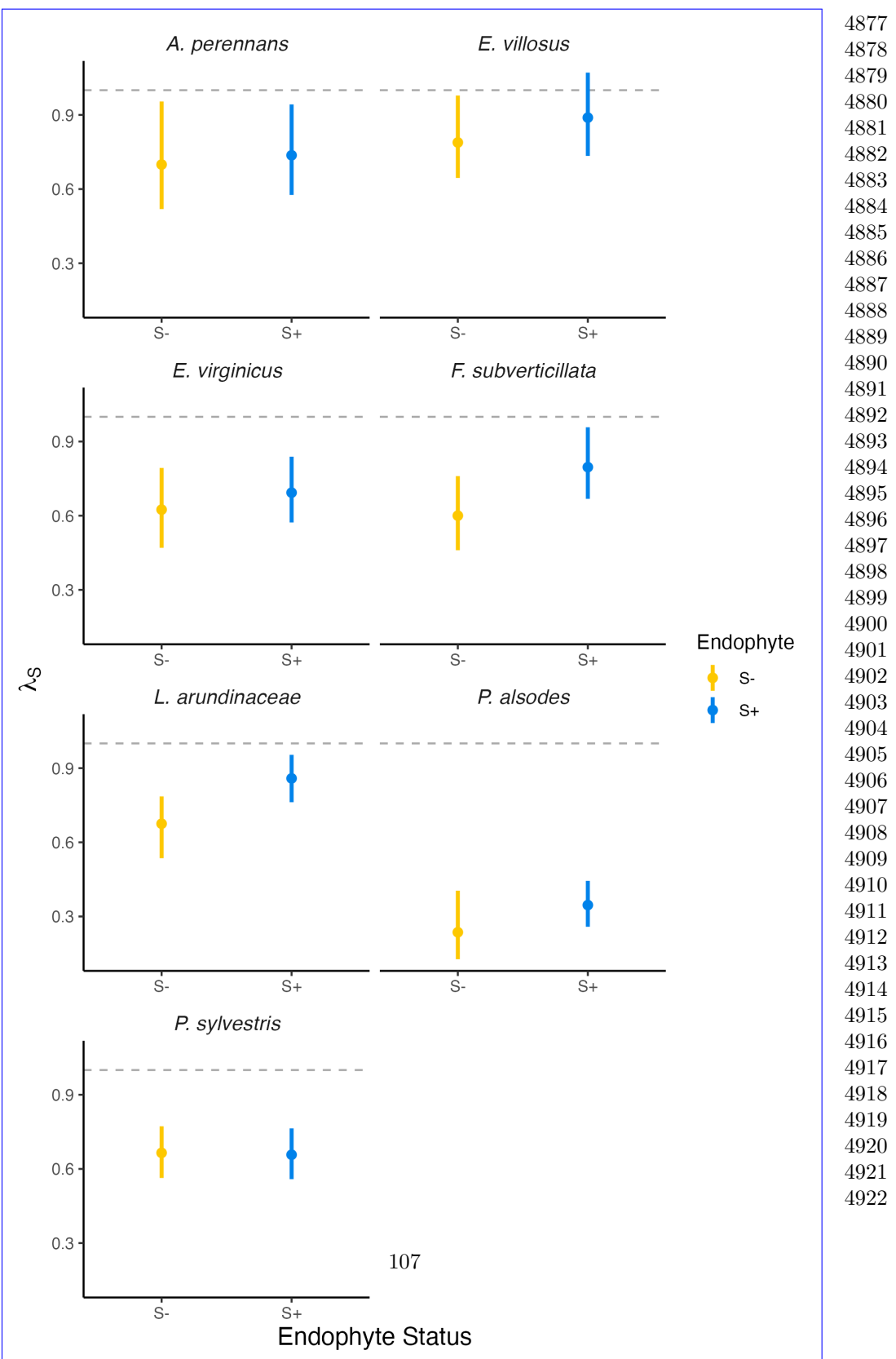
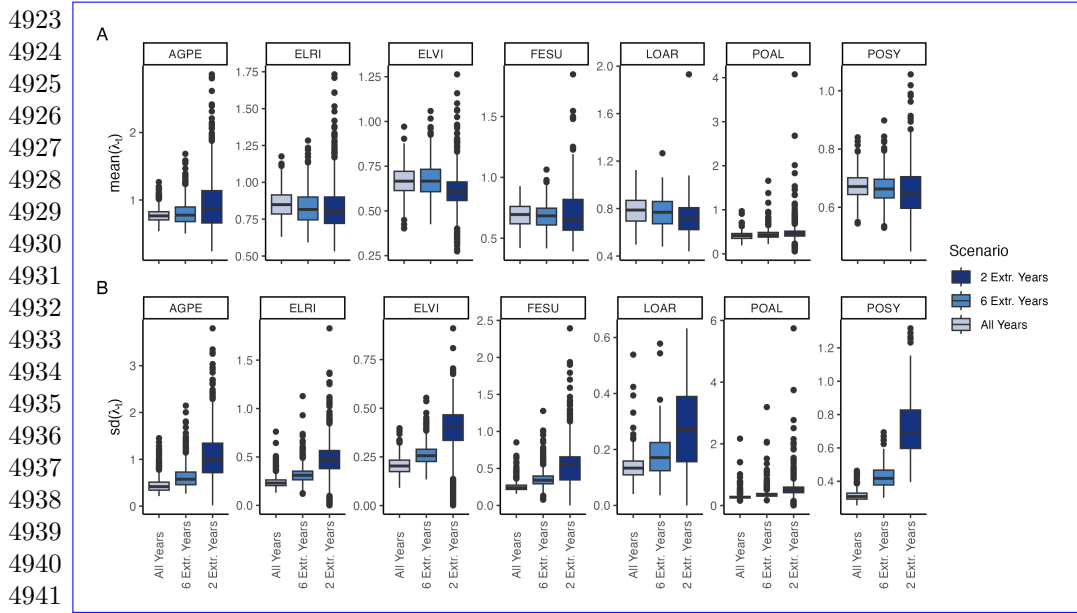


Figure 79: Stochastic population growth rates (λ_S) for symbiotic (blue) and symbiont-free (yellow) populations. Points show posterior medians along with the 95% credible interval and posterior medians. All values are calculated from matrix models representing recruit plants.



4942 Figure 80: (A) Mean and (B) standard deviation of annual growth rate values during
 4943 simulation scenarios. Each scenario selects from observed transition matrixes, increas-
 4944 ing the variance by selecting either all observed years, or a set (6 or 2 years) that have
 4945 the highest and lowest growth rates for symbiont-free populations.

4946

4947

4948

4949

4950

4951

4952

4953

4954

4955

4956

4957

4958

4959

4960

4961

4962

4963

4964

4965

4966

4967

4968

Stochastic population growth rates (λ_s) for symbiotic (blue) and symbiont-free (yellow) populations. Points show posterior medians along with the 95% credible interval 50% and posterior medians. All values are calculated from matrix models representing recruit plants.

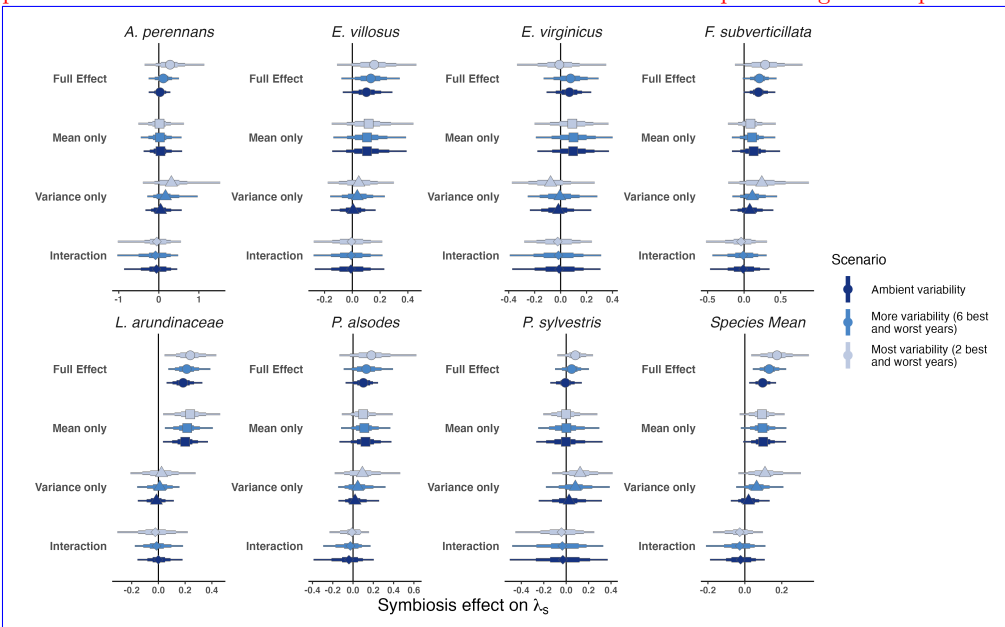
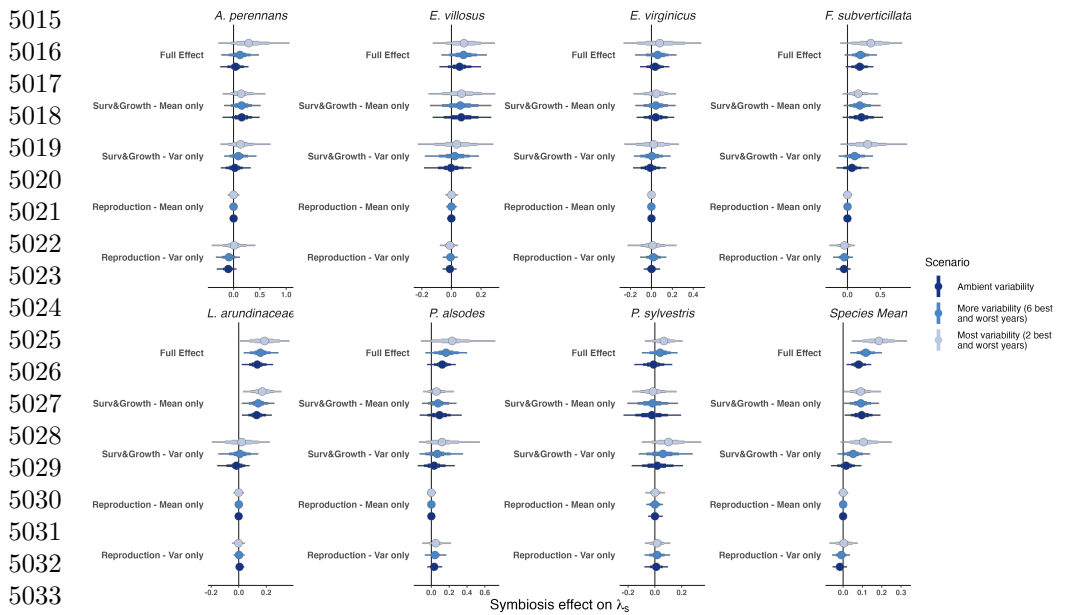


Figure 81: Endophyte contributions to stochastic growth rates under observed and elevated variance across species. The total effect of endophytes (circle) comes from mean benefits (square) and variance buffering (triangle) as well as the interaction between mean and variance effects (diamond). Shapes indicate the posterior mean of each contribution, along with bars for the 50, 75 and 95 % credible intervals. Under scenarios of increasing variance, represented by increasing color intensity, effects of variance buffering increase leading to a more mutualistic symbiosis.

4969
4970
4971
4972
4973
4974
4975
4976
4977
4978
4979
4980
4981
4982
4983
4984
4985
4986
4987
4988
4989
4990
4991
4992
4993
4994
4995
4996
4997
4998
4999
5000
5001
5002
5003
5004
5005
5006
5007
5008
5009
5010
5011
5012
5013
5014



5034 Figure 82: Vital rate decomposition of endophyte contributions to stochastic growth
 5035 rates under observed and elevated variance across species. The total effect of endo-
 5036 phytes comes from mean and variance effects across vital rates, but are primarily
 5037 driver by effect on survival and growth, rather than vital rates associated with repro-
 5038 duction. Circles indicate the posterior mean of each contribution, along with bars for
 5039 the 50, 75 and 95 % credible intervals. Under scenarios of increasing variance, repre-
 5040 sented by increasing color intensity, effects of variance buffering increase leading to a
 5041 more mutualistic symbiosis.

5042

5043

5044

5045

5046

5047

5048

5049

5050

5051

5052

5053

5054

5055

5056

5057

5058

5059

5060

Faithfulness of experimental plots to assigned endophyte status. Counts of plants scored with leaf peels or seed squashes to check the faithfulness of recruits to the assigned plot-level endophyte status. (A) Endophytic plants may be gained in initially S- plots, or (B) lost in initially S+ plots.

Weather station time series for Bloomington, IN. The Seasonal Precipitation-Evapotranspiration Index (SPEI) calculated for the (A) three month growing season and (B) annually from daily weather station observations of (C) average temperatures and (D) cumulative precipitation. Climatic data shown are determined by the census year centered on the month of July.

Predicted population growth rates across drought indices. Symbiotic (S+; blue) and symbiont free (S-; tan) populations respond differently to climate as measured by the (A) 3-month SPEI and (B) 12-month SPEI. Thick lines represent the predicted mean growth rate and thin lines show 500 posterior draws.

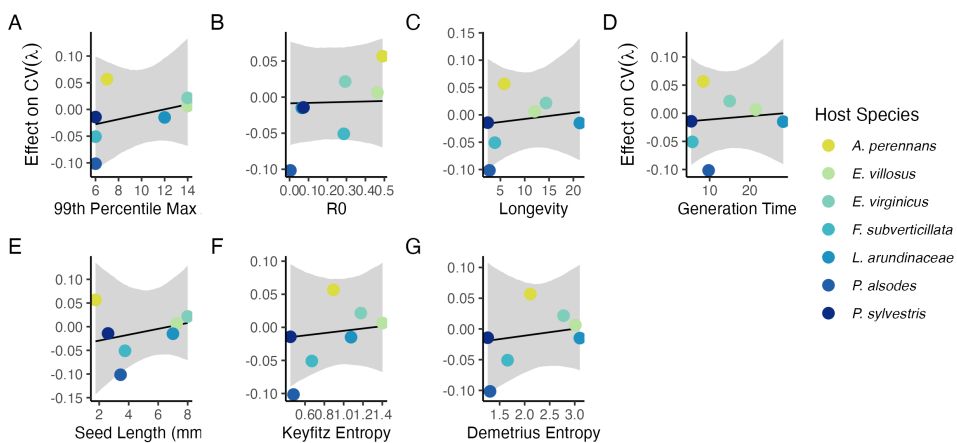
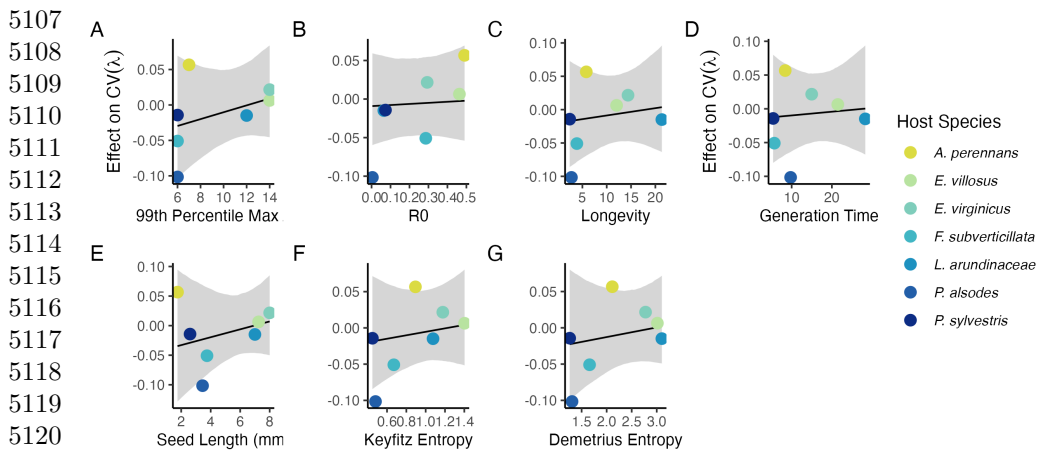


Figure 83: Relationship between variance buffering and life history traits describing the fast-slow life history continuum accounting for phylogenetic covariance between grass host species. Regressions between life history traits describing the fast-slow life history continuum ((A) 99th percentile maximum age observed during long term censuses in years; (B) Net reproductive rate; (C) Longevity; (D) Generation time in years; (G) Seed size) and the effect of endophyte symbiosis on the coefficient of variation in population growth rate (λ). Each panel shows the fitted mean relationship (line) along with the 95% credible interval.

5061
5062
5063
5064
5065
5066
5067
5068
5069
5070
5071
5072
5073
5074
5075
5076
5077
5078
5079
5080
5081
5082
5083
5084
5085
5086
5087
5088
5089
5090
5091
5092
5093
5094
5095
5096
5097
5098
5099
5100
5101
5102
5103
5104
5105
5106



5107
 5108
 5109
 5110
 5111
 5112
 5113
 5114
 5115
 5116
 5117
 5118
 5119
 5120
 5121
 5122
 5123 Figure 84: Relationship between variance buffering and life history traits describing
 5124 the fast-slow life history continuum accounting for phylogenetic covariance between
 5125 *Epichloë* symbionts. Regressions between life history traits describing the fast-slow
 5126 life history continuum ((A) 99th percentile maximum age observed during long term
 5127 censuses in years; (B) Net reproductive rate; (C) Longevity; (D) Generation time in
 5128 years; (G) Seed size) and the effect of endophyte symbiosis on the coefficient of variation
 5129 in population growth rate (λ). Results are similar to regressions accounting for host
 5130 plant phylogeny (Fig. S25S83), however symbionts are all within a single genus. Each
 5131 panel shows the fitted mean relationship (line) along with the 95% credible interval.
 5132
 5133
 5134
 5135
 5136
 5137
 5138
 5139
 5140
 5141
 5142
 5143
 5144
 5145
 5146
 5147
 5148
 5149
 5150
 5151
 5152

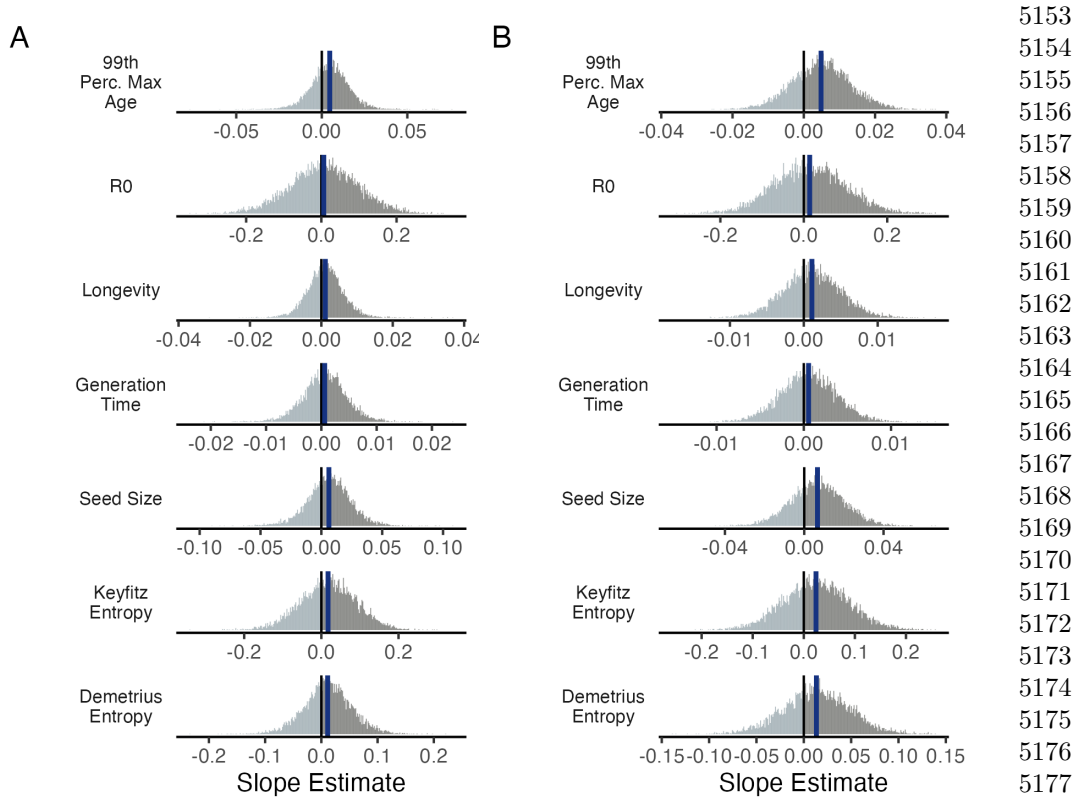
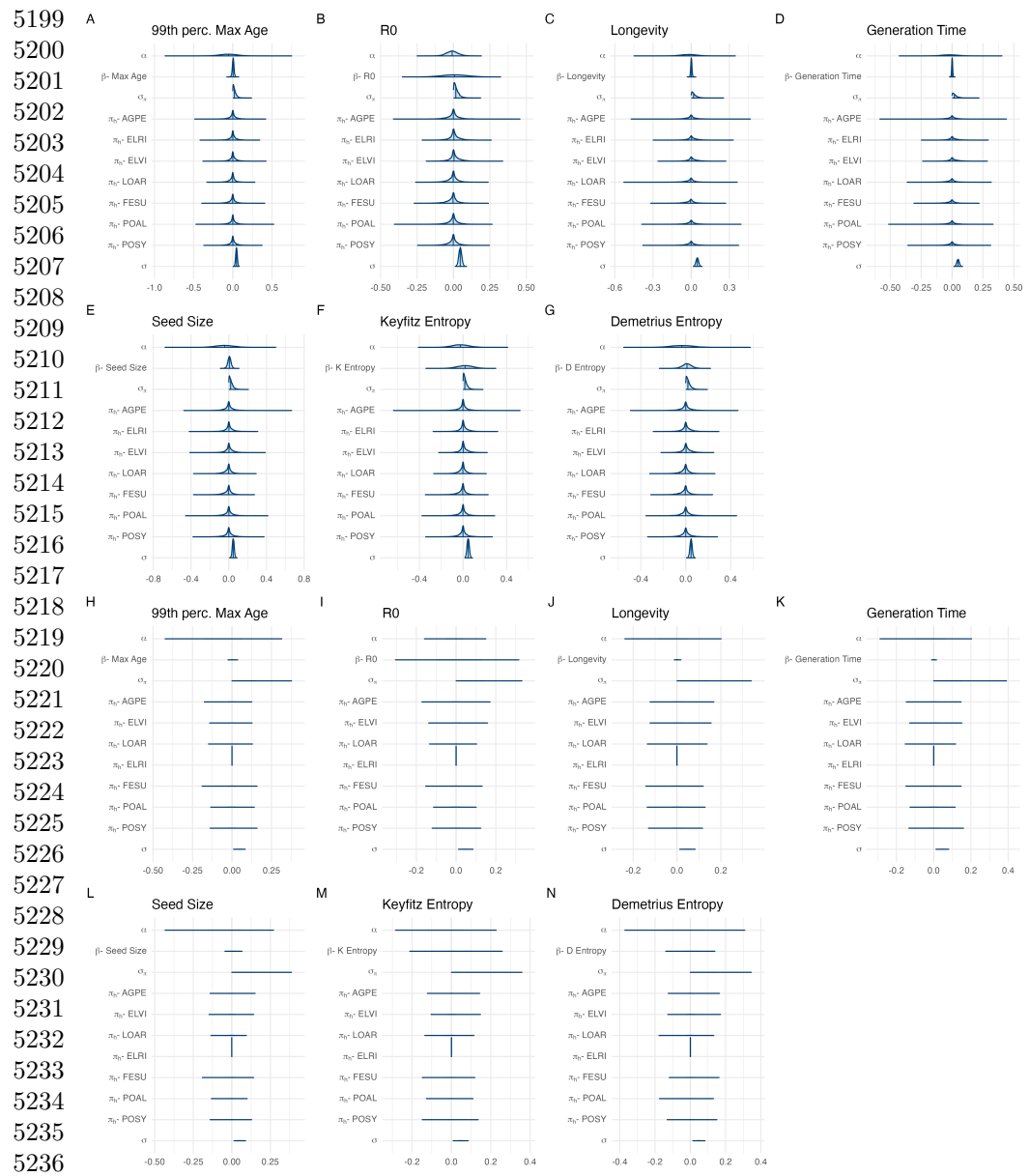


Figure 85: Posterior estimates of life history trait effects on variance buffering. Grey histograms show the posterior distribution of the slope parameter from models incorporating (A) host plant phylogenetic covariance and (B) symbiont phylogenetic covariance for each life history trait with blue bars showing the posterior mean.

5153
5154
5155
5156
5157
5158
5159
5160
5161
5162
5163
5164
5165
5166
5167
5168
5169
5170
5171
5172
5173
5174
5175
5176
5177
5178
5179
5180
5181
5182
5183
5184
5185
5186
5187
5188
5189
5190
5191
5192
5193
5194
5195
5196
5197
5198



5237 Figure 86: Posterior distributions of the life history trait regressions. Panels show
 5238 parameter estimates from phylogenetic models incorporating host phylogenetic covari-
 5239 ance (A-G) and for symbiont phylogenetic covariance (H-N). Density curves show 80%
 5240 credible interval along with the posterior mean.

5241
 5242
 5243
 5244

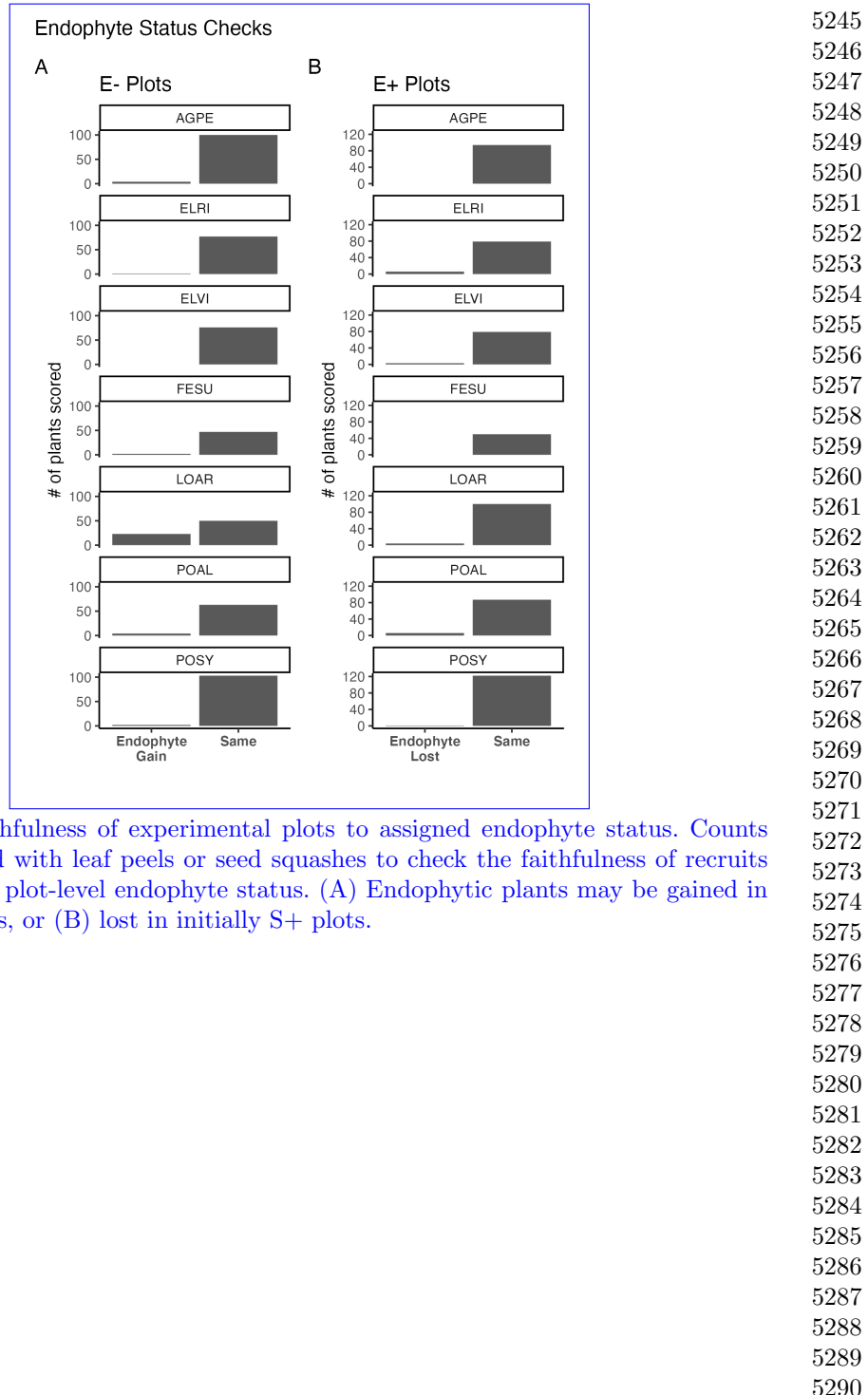
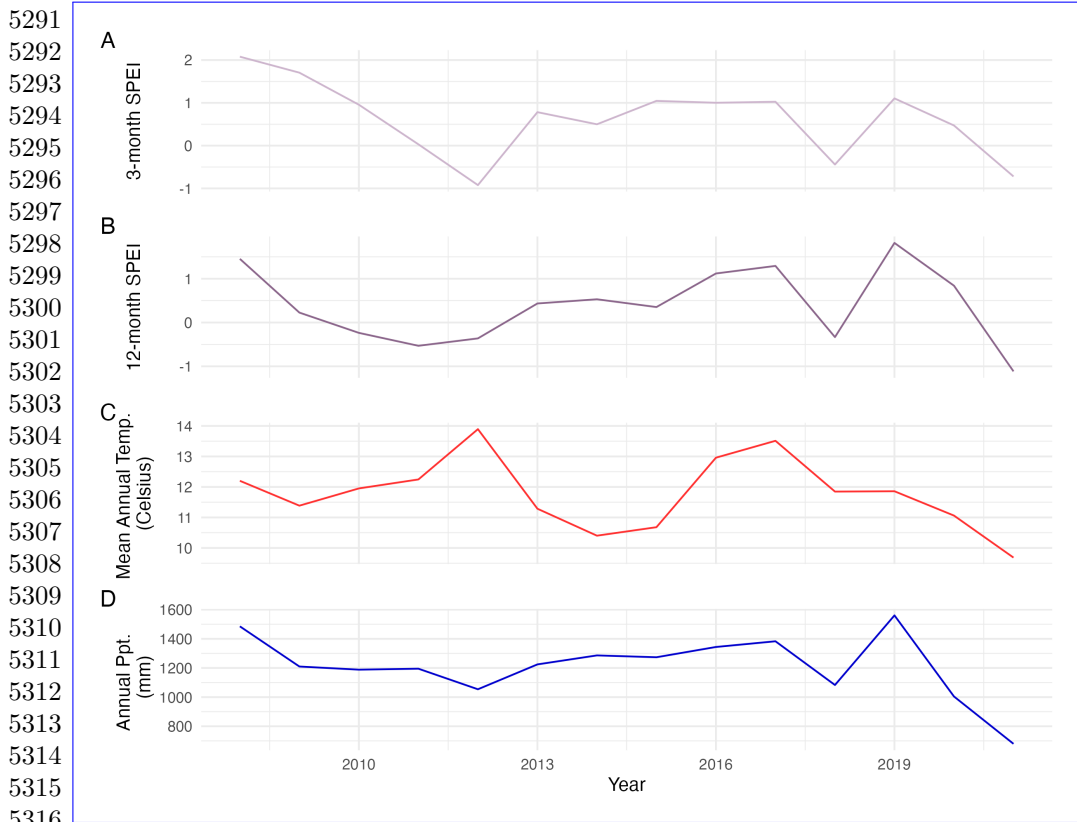


Figure 87: Faithfulness of experimental plots to assigned endophyte status. Counts of plants scored with leaf peels or seed squashes to check the faithfulness of recruits to the assigned plot-level endophyte status. (A) Endophytic plants may be gained in initially S- plots, or (B) lost in initially S+ plots.



5317 Figure 88: Weather station time-series for Bloomington, IN. The Seasonal
 5318 Precipitation-Evapotranspiration Index (SPEI) calculated for the (A) three month
 5319 growing season and (B) annually from daily weather station observations of (C)
 5320 average temperatures and (D) cumulative precipitation. Climatic data shown are
 5321 determined by the census year centered on the month of July.

5322
 5323
 5324
 5325
 5326
 5327
 5328
 5329
 5330
 5331
 5332
 5333
 5334
 5335
 5336

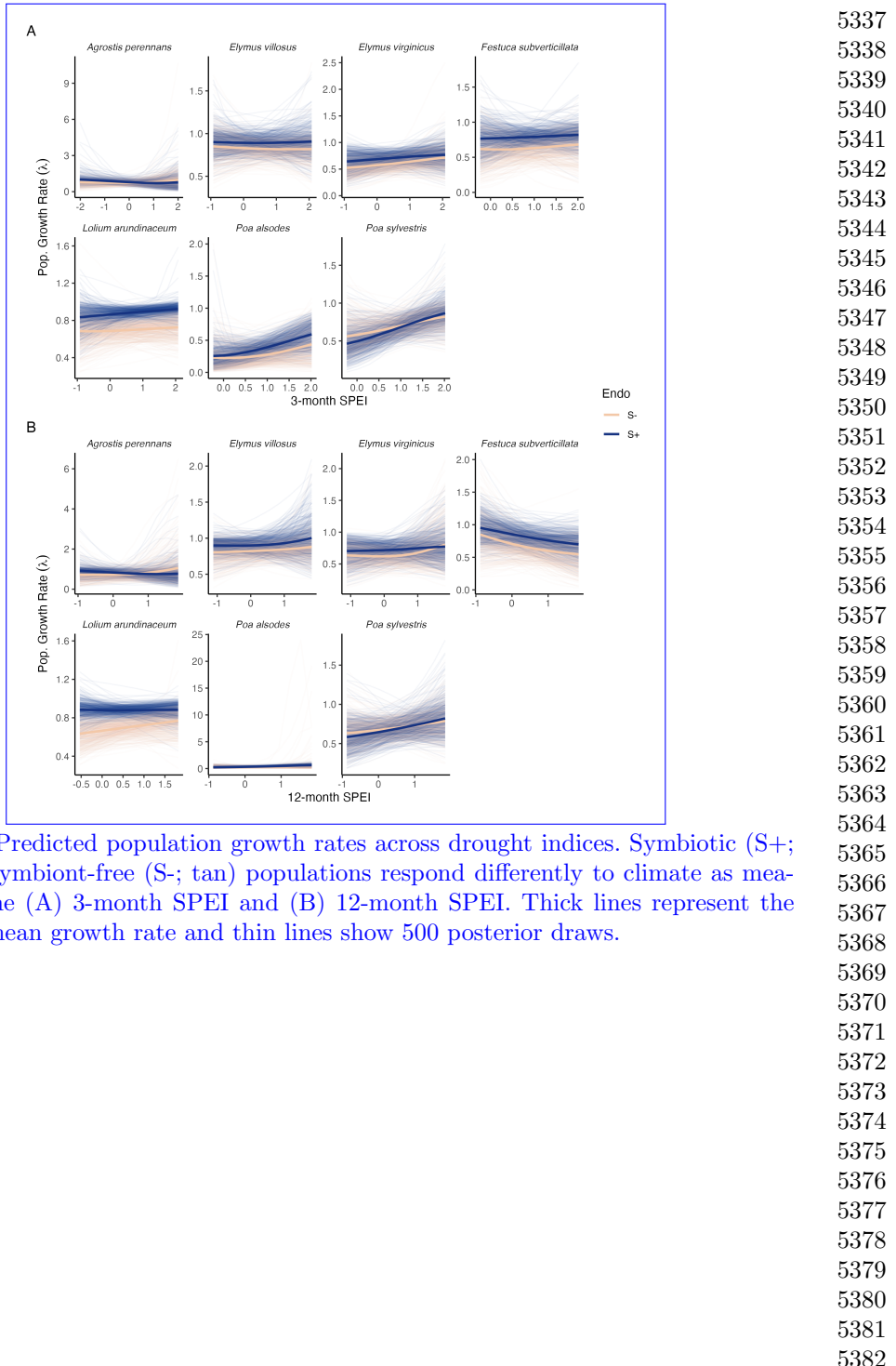


Figure 89: Predicted population growth rates across drought indices. Symbiotic (S+; blue) and symbiont-free (S-; tan) populations respond differently to climate as measured by the (A) 3-month SPEI and (B) 12-month SPEI. Thick lines represent the predicted mean growth rate and thin lines show 500 posterior draws.

5383 ~~Supplemental Tables S1-S3~~

5384 **Supplemental Tables S1-S3**

5386

5387

5388

5389

5390

5391

5392

5393

5394

5395

5396

5397

5398

5399

5400

5401

5402

5403

5404

5405

5406

5407

5408

5409

5410

5411

5412

5413

5414

5415

5416

5417

5418

5419

5420

5421

5422

5423

5424

5425

5426

5427

5428

Table S1: Summary of host-endophyte propositing and transplant methods

Host Species	Symbiont Species	Heat treatment duration (Temp.)	Transplant date
<i>Agrostis perennans</i>	<i>E. amarillans</i>	12 min. hot water bath (60 °C)	April 2008 (10 plots)
<i>Elymus villosus</i>	<i>E. elymi</i>	6 days drying oven (60 °C)	April 2008 (10 plots)
<i>Elymus virginicus</i>	<i>E. elymi</i> or <i>EviTG-1</i>	6 days drying oven (60 °C)	April 2008 (10 plots)
<i>Festuca subverticillata</i>	<i>E. starrii</i>	6 days drying oven (60 °C)	April 2008 (10 plots)
<i>Lolium arundinaceum</i>	<i>E. coenophiala</i>	6 days drying oven (60 °C)	Sept. 2007 (10 plots)
<i>Poa alsodes</i>	<i>E. alsodes</i>	7 days drying oven (60 °C)	Sept. 2007 (8 plots)/April 2008 (10 plots)
<i>Poa sylvestris</i>	<i>E. PsytG-1</i>	7 days drying oven (60 °C)	Sept. 2007 (8 plots)/April 2008 (10 plots)
			5429
			5430
			5431
			5432
			5433
			5434
			5435
			5436
			5437
			5438
			5439
			5440
			5441
			5442
			5443
			5444
			5445
			5446
			5447
			5448
			5449
			5450
			5451
			5452
			5453
			5454
			5455
			5456
			5457
			5458
			5459
			5460
			5461
			5462
			5463
			5464
			5465
			5466
			5467
			5468
			5469
			5470
			5471
			5472
			5473
			5474

5475
 5476
 5477
 5478
 5479
 5480
 5481
 5482
 5483
 5484
 5485
 5486
 5487
 5488
 5489
 5490
 5491
 5492
 5493
 5494
 5495
 5496
 5497
 5498
 5499
 5500
 5501
 5502
 5503
 5504
 5505
 5506
 5507
 5508
 5509
 5510
 5511
 5512
 5513
 5514
 5515
 5516
 5517
 5518
 5519
 5520

Table S2: Summary of focal life history traits

Host Species	Observed max age (years)	99th percentile max age (years)	Generation time (years)	R_0	Longevity (years)	Seed Length (mm)	Keyfitz Entropy	Demetrius Entropy	Imperfect transmission rate (%)	Stromata Observed (% of indiv. per species)
<i>Agrostis perennans</i>	11	7	7.6	0.58	6.4	1.75	0.9	2.1	69.8	0.0
<i>Elymus villosus</i>	14	14	20.7	0.35	9.8	7.25	1.3	2.9	100	4.6
<i>Elymus virginicus</i>	14	14	13.4	0.25	12.5	8	1.1	2.6	100	0.6
<i>Festuca subverticillata</i>	9	6	6.6	0.28	4.3	3.75	0.8	1.8	42.7	0.0
<i>Lolium arundinaceum</i>	12*	12*	27.4	0.08	21.3	7	1.1	3.1	100	0.0
<i>Poa alsodes</i>	8	6	9.2	0.003	2.6	3.45	0.5	1.2	99.9	0.0
<i>Poa sylvestris</i>	12	6	8.0	0.14	3.2	2.6	0.7	1.8	16.6	0.1
Page's λ(host)-host	—	0.270.23	0.280.22	0.19	0.23	0.280.23	0.270.19	0.250.22	0.25	—
Page's λ-host (90% CI)	—	(0-0.8)	(0-0.8)	(0-0.7)	(0-0.8)	(0-0.8)	(0-0.8)	(0-0.8)	—	—
Page's λ(symbiont)-symbiont	—	0.630.57	0.630.56	0.630.56	0.630.56	0.620.56	0.620.55	0.620.58	—	—
Page's λ-symbiont (90% CI)	—	(0-0.9)	(0-0.9)	(0-0.9)	(0-0.9)	(0-0.9)	(0-0.9)	(0-0.9)	—	—

*Censuses for *L. arundinaceum* plots stopped after year 12 of the experiment.

5521
5522
5523
5524
5525
5526
5527
5528
5529
5530
5531
5532
5533
5534
5535
5536
5537
5538
5539
5540
5541
5542
5543
5544
5545
5546
5547
5548
5549
5550
5551
5552
5553
5554
5555
5556
5557
5558
5559
5560
5561
5562
5563
5564
5565
5566

Table S3: Summary of host-endophyte drought sensitivities

Host Species	Effect on CV(λ)	Effect on Mean(λ)	$\frac{\Delta\lambda^-}{\Delta SPEI_3}$	$\frac{\Delta\lambda^+}{\Delta SPEI_3}$	3 month S- to S+ ratio	$\frac{\Delta\lambda^-}{\Delta SPEI_{12}}$	$\frac{\Delta\lambda^+}{\Delta SPEI_{12}}$	12 month S- to S+ ratio
<i>Agrostis perennans</i>	-0.02640.04750.04440.0513 0.03-0.06		-0.040.05	0.850.83	0.11-0.05	-0.060.119	4.822.34	
<i>Elymus villosus</i>	0.00030.0105 0.05090.0710 -0.030.00		0.01-0.01	0.955.89	0.05	0.03	0.040.700.74	
<i>Elymus virginicus</i>	0.01200.031 0.05780.0913 0.070.04		0.050.06	0.501.56	0.100.02	0.070.06	4.422.41	
<i>Festuca subverticillata</i>	-0.0622-0.1524	0.16390.1386 0.02	0.020.03	0.011.15	-0.13-0.09	1.43-0.11	1.20	
<i>Lolium arundinaceum</i>	-0.0118-0.0799	0.10220.1872 -0.010.02	0.01	1.320.47	0.03-0.00	-0.030.05	4.02111.	
<i>Poa alsodes</i>	-0.1179-0.6859	0.12820.1079 0.10	0.140.09	0.710.62	0.110.14	0.730.11	0.79	
<i>Poa sylvestris</i>	-0.0298-0.0164	-0.0055-0.0211	0.070.18	0.160.12	0.440.64	0.050.09	0.100.06	0.550.64

5567
5568
5569
5570
5571
5572
5573
5574
5575
5576
5577
5578
5579
5580
5581
5582
5583
5584
5585
5586
5587
5588
5589
5590
5591
5592
5593
5594
5595
5596
5597
5598
5599
5600
5601
5602
5603
5604
5605
5606
5607
5608
5609
5610
5611
5612